Development of an Effective Flared Guardrail Terminal

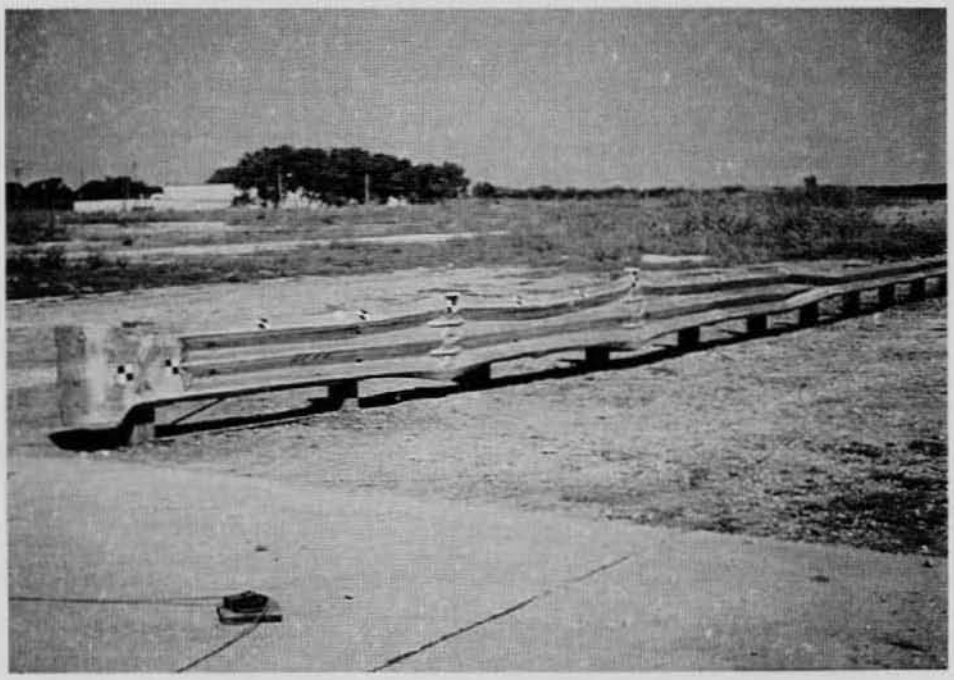

Prepared by:
Midwest Roadside Safety Facility (MwRSF)
Center for Infrastructure Research
Civil Engineering Department
University of Nebraska-Lincoln
1901 Y Street, Building C
Lincoln, Nebraska 68588-0601
(401) 472-9198

June 1997

1. Performing Organization Report No.	2. Report Date	3. Type of Report
TRP-03-56-96	June 1997	Final Report

4. Title and Subtitle

Development of an Effective Flared Guardrail Terminal

5. Author(s)

Pfeifer, B.G., J.D. Reid, and B.S. Brar

6. Performing Organization Name and Address

Midwest Roadside Safety Facility (MwRSF)
Civil Engineering Department
University of Nebraska - Lincoln
1901 Y St., Bldg C
Lincoln, Nebraska 68588-0601
(402) 472-9198

7. Sponsoring Agency Name and Address

Midwest States Regional Pooled Fund
Nebraska Department of Roads
1500 Nebraska Highway 2
Lincoln, Nebraska 68509-4567

8. Contract or Grand No.

FY-95 Midwest States Regional Pooled Fund Program (Year 5)

9. Abstract

The Breakaway Cable Terminal (BCT), which has been used for a number of years to terminate w-beam guardrail in Kansas and a number of other states, does not always perform adequately when impacted by small vehicles. As a result of this poor performance, it has recently been disallowed by the FHWA for use on high speed, high volume roads on the National Highway System. Several modifications have been made to improve the performance of this terminal over the years, but no non-proprietary system has met with much success. The Kansas Department of Transportation (KDOT), and other states, felt that there was a need for a non-proprietary end terminal which met the current crash test standards of Test Level 3 of NCHRP Report 350.

As a result of this interest, this study was initiated to develop a non-proprietary guardrail end treatment which would satisfy the current safety standards. Computer simulation and component testing was undertaken to evaluate the concept of flattening areas of the rail used in the terminal in order to reduce the force required to buckle the rail. Several dynamic bogie tests as well as one full-scale test were conducted. The design selected for evaluation under full scale crash test conditions consisted of a thrie beam flattened at two locations. The thrie beam was selected for testing because it had the best potential for successfully redirecting a pickup at 100 km/h and 20 degrees, as required by the new NCHRP Report 350 test criteria. Although the full-scale vehicle crash test failed to meet the required criteria, it was determined that this concept had the potential for success.

10. Keywords	11. Distribution Statement
Highway Safety, Crash Tests, Guardrail, W-Beam, Thrie Beam, Terminal, End-Treatment	No restrictions. This document is available to the public from the sponsoring agency.

12. Security Classification (of this report)	13. Security Classification (of this page)	14. No. of Pages
Unclassified	Unclassified	129

Disclaimer Statement

The contents of this report reflect the views of the authors who are responsible for the facts and the accuracy of the data presented herein. The contents do not necessarily reflect the official views or policies of the Kansas Department of Transportation or other members of the Midwest-States Regional Pooled Fund Program. This report does not constitute a standard, specification, or regulation.

Acknowledgements

The authors wish to express their appreciation and thanks to the Midwest Regional States Pooled Fund and the Center for Infrastructure Research for funding the research described herein. A special thanks is also given the following individuals who made a contribution to this research study.

Kansas Department of Transportation
Ron Seitz, P.E., Squad Leader

Nebraska Department of Roads
Leona Kolbet, Research Coordinator

Missouri Highway Transportation Department
Pat McDaniel, P.E., Special Assignments Design Engineer

Minnesota Department of Transportation
Khani Sahebjam, P.E., State Aid Bridge Engineer

Iowa Department of Transportation
Dave Little, P.E., Design Methods Engineer

Center for Infrastructure Research
Maher Tadros, Ph.D., P.E.,

Midwest Roadside Safety Facility
Ronald K. Faller, P.E., Research Associate Engineer
James C. Holloway, Research Associate Engineer
Dean L. Sicking, Ph.D., P.E., Director, Assistant Professor
John R. Rohde, Ph.D., P.E., Associate Professor
Barry T. Rosson, Ph.D., P.E., Assistant Professor
Kenneth L. Krenk, Field Operations Manager
Graduate and Undergraduate Assistants

Table of Contents

Page

Disclaimer Statement ii
Acknowledgements iii
Table of Contents iv
List of Figures vii
1 INTRODUCTION 1
1.1 Problem Statement 1
1.2 Background 1
1.3 Research Plan 3
2 TERMINAL CONCEPT 4
2.1 Computer Simulation of Flattened Rail Concept 5
2.1.1 W-Beam BCT Simulation 5
2.1.2 Flattened Rail W-Beam Simulation 5
2.1.3 Bogie Vehicle - Thrie Beam Simulation 6
2.1.4 Flattened Thrie Beam MELT/BCT Simulation 6
3 GUARDRAIL SHAPE MODIFICATION 13
3.1 Equipment Used 13
3.2 Background 14
3.3 Flattening Procedure 16
3.3.1 W-beam 16
3.3.2 Thrie Beam 16
4 STATIC TESTING 17
4.1 Preliminary Static Tests 18
4.1.1 Equipment 18
4.1.2 Results 19
4.1.3 Discussion of Results 21
4.1.4 Conclusion 22
4.2 Static Compressive Testing of 3810 mm (12 ft - 6 in.) Sections 22
4.2.1 Test Setup 22
4.2.2 Test Procedure 24
4.2.3 Results of Static Tests on 3810 mm Beams 25
4.2.4 Analysis of 3810 mm Buckling Tests 27
5 DYNAMIC BOGIE TESTS 28
5.1 Test Setup 28
5.1.1 Testing Configuration 28
5.1.2 Bogie Vehicle 29
5.1.3 Tow and Guidance System 29
5.1.4 Data Acquisition Systems 30
5.2 Test Results 30
5.2.1 KDW1 Series 30
5.2.2 KDW2 Series 39
5.2.3 KDW3 Series 44

Page
5.2.4 KDT5 Series 48
5.2.5 KDT6 Series 52
5.3 Bogie Testing Summary 57
6 GUARDRAIL MATERIAL TESTING 61
6.1 Objective 61
6.2 Test Procedure 61
6.2.1 Sample Preparation 62
6.2.2 Yield Stress 63
6.2.3 Engineering Stress Strain 63
6.2.4 True Stress Strain 64
6.2.5 Young's Modulus 65
6.2.6 Surface Hardness 65
6.3 Test Results 66
7 BASELINE MODEL SIMULATION 68
7.1 Preprocessing 68
7.1.1 Background 68
7.1.2 Geometry and Mesh Generation 68
7.2 Analysis 71
7.2.1 Contacts 71
7.2.2 Nodal Data 72
7.2.3 Initial Velocity 72
7.2.4 Shell Element Thickness 72
7.2.5 W-beam Material Properties 72
7.2.6 Bogie Vehicle Properties 72
7.2.7 Constraints 72
7.2.8 Stone Wall 73
7.3 Model Development 73
7.4 Final Baseline Model 75
7.5 Postprocessing 78
7.6 Comparison 78
7.7 Baseline Simulation Summary 83
8 MODIFIED GUARDRAIL IMPACT SIMULATION 83
8.1 Modeling and Meshing 83
8.1.1 50% Flattened W-Beam 83
8.1.2 100% Flattened W-Beams 84
8.2 Analysis 84
8.3 Results 84
8.3.1 50% Flattening 84
8.3.2 100% Flattening 86
9 FULL-SCALE CRASH TESTING 89
9.1 System Modifications 89
9.2 System Details 90

Page
9.3 Test Conditions 96
9.3.1 Test Site 96
9.3.2 Vehicle Guidance System 96
9.3.3 Test Vehicle 96
9.3.4 Data Acquisition Systems 97
9.4 Performance Evaluation Criteria 102
9.5 Test Results 104
10 ANALYSIS OF RESULTS 114
11 CONCLUSIONS AND RECOMMENDATIONS 115
12 REFERENCES 116

List of Figures

Page

Figure 1. W-Beam BCT LS-DYNA3D Simulation. 8
Figure 2. Flattened W-Beam. 9
Figure 3. Flattened W-Beam BCT Concept Simulation. 10
Figure 4. Bogie - Thrie Beam Velocity vs Time Simulation Results. 11
Figure 5. Flattened Thrie-Beam Simulation. 12
Figure 6. Flattening Setup. 13
Figure 7. Warped thrie beam guardrail. 15
Figure 8. Failure mode for static test on a short W-beam section. 19
Figure 9. Failure mode for static test on a short thrie beam section. 20
Figure 10. Setup for static tests on 3810 mm guardrail. 23
Figure 11. Hydraulic actuators and stress chairs for static buckling tests. 23
Figure 12. Thrie beam static buckling failure. 24
Figure 13. W-beam static buckling test results. 26
Figure 14. Thrie beam static buckling test results. 26
Figure 15. Test KDW1A before and after impact. 32
Figure 16. Test KDW1B before, during, and after impact. 34
Figure 17. Test KDW1C before, during, and after impact. 36
Figure 18. Test KDW1D before, during, and after impact. 38
Figure 19. Accelerations and change in velocity for standard W-beams. 39
Figure 20. Test KDW2A before, during, and after impact. 40
Figure 21. Test KDW2B before, during, and after impact. 42
Figure 22. Acceleration and change in velocity for 50% flattened W-beams. 43
Figure 23. Test KDW3A before, during, and after impact. 45
Figure 24. Test KDW3B before, during, and after impact. 47
Figure 25. Acceleration and change in velocity for 100% flattened W-beams. 48
Figure 26. Test KDT5A before and after impact. 49
Figure 27. Test KDT5B before, during, and after impact. 51
Figure 28. Accelerations and change in velocity for 50% flattened thrie beams. 52
Figure 29. Test KDT6A before, during, and after impact. 53
Figure 30. Test KDT6B before, during, and after impact. 55
Figure 31. Acceleration and change in velocity for 100% flattened thrie beams. 57
Figure 32. Material test coupon (all units in inches). 62
Figure 33. Coupon locations. 63
Figure 34. True stress/strain curves for the guardrail steel samples. 66
Figure 34. Meshed W-beam model. 69
Figure 35. Flared end, initial (left) and remeshed (right). 70
Figure 36. Bogie simulation model. 70
Figure 37. Results of first simulation run. 73
Figure 38. Baseline model with wood bumper. 74
Figure 39. Initial computer simulation run with flared end. 74
Figure 40. Buckle at front quarter point. 75

Page
Figure 41. Buckle in middle with imperfect buckle shape. 76
Figure 42. Top view of simulated crash. 77
Figure 43. Side view of simulated crash. 77
Figure 44. Velocity and acceleration time curves for simulation and actual test. 78
Figure 45. Crash test buckling failure. 80
Figure 46. Failure geometry from simulation. 80
Figure 47. Post impact buckled W-beam. 81
Figure 48. Post impact W-beam (simulated). 81
Figure 49. Front quarter kink. 82
Figure 50. Front quarter kink (simulated). 82
Figure 51. 50% flattening of guardrail. 83
Figure 52. 100% flattening of guardrail. 84
Figure 53. Accelerometer and velocity curves for 50% flattened W-beams. 85
Figure 54. Impact stages at 60 ms intervals. 85
Figure 55. Accelerometer and velocity comparisons for 100% flattened W-beam. 86
Figure 56. Simulated impact on 100% flattened beam. 87
Figure 57. Test KDW3B during impact. 88
Figure 58. Photographs of the FRT system for Test KBCT-1. 92
Figure 59. Photographs of the FRT system for Test KBCT-1 (continued). 93
Figure 60. Plan drawing of the FRT for Test KBCT-1. 94
Figure 61. Shelf bracket used to support rail at post nos. 2, 3, and 4. 95
Figure 62. Test vehicle for Test KBCT-1. 100
Figure 63. Vehicle dimensions, Test KBCT-1. 101
Figure 63. Vehicle and system prior to impact. 106
Figure 64. Summary of Test KBCT-1. 107
Figure 65. Overhead sequential photos, Test KBCT-1. 108
Figure 66. Perpendicular sequential photos, Test KBCT-1. 109
Figure 67. Vehicle trajectory, Test KBCT-1. 110
Figure 68. Vehicle damage, Test KBCT-1. 111
Figure 69. Failure of cable breakaway mechanism. 112

List of Tables

Page

Table 1. Short Specimen Static Buckling Results 21
Table 2. 3810 mm Static Buckling Results. 25
Table 3. 3810 mm Buckling Force Averages. 26
Table 4. Comparison of 3810 mm Sample Buckling Results. 27
Table 5. Dynamic Testing Summary 59
Table 6. Bogie Test Force Comparison 60
Table 7. Plastic Region Stress/Strain Values. 67
Table 8. Average Stress/Strain Values. 67
Table 9. Input Values for the LS-DYNA3D Deck. 67
Table 10. NCHRP 350 Test Level 3 Crash Test Conditions 102
Table 11. Relevant NCHRP 350 Evaluation Criteria. 103
Table 12. Summary of Evaluation Results. 113

1 INTRODUCTION

1.1 Problem Statement

The Breakaway Cable Terminal (BCT), which has been used for a number of years to terminate w-beam guardrail in Kansas and a number of other states, does not always perform adequately when impacted by small vehicles. As a result of this poor performance, it has recently been disallowed by the FHWA for use on high speed, high volume roads on the National Highway System. Current efforts to develop a replacement for this end terminal are being privately funded and will result, if successful, in terminals which are proprietary and require bidding of alternatives or justification for their use on federal aid projects. The Kansas Department of Transportation (KDOT) felt that there was a need for a non-proprietary end terminal which could be produced by a number of manufacturers. It was thought that this would result in greater economy through the competitive bidding process.

1.2 Background

Highway engineers have been searching for many years for a safe and economical means of terminating strong post W-beam systems. The first W-beam barriers were installed with an untreated stand-up end situated parallel to the roadway. It was soon realized that this configuration was very dangerous, as the guardrail had a tendency to pierce through vehicles that impacted the end of the guardrail system. One attempt at resolving this problem was to simply flare the end of the guardrail away from the highway. The concept behind this modification was that when the end of the guardrail is flared away from the roadway the likelihood of it being impacted decreases, and impacts that do occur will probably occur at an angle to the end. However, the stand-up end still proved to be a hazard to impacting vehicles, so alternative end

treatments were pursued.

Another attempt to resolve the spearing problem involved twisting the W-beam 90 degrees and fastening it to a ground anchor. Although this system, called a turned-down terminal, effectively prevented spearing, it had a tendency to cause small vehicles impacting the end of the rail to roll over (1,2). In order to alleviate this problem, the post to guardrail connections near turn downs were weakened to allow the guardrail to drop to the ground during end-on impacts. Although this "floppy end turn down terminal" reduced the magnitude of the rollover problem, it still had two major flaws. This terminal was found to create maintenance problems when the rail fell down due to freeze/thaw cycles, road vibration, and minor impacts with roadside mowers. Further, as the vehicle fleet downsized during the 1970's and 1980's, the floppy end terminal was found to represent a significant rollover problem for many of the smaller impacting vehicles. Several attempts were made to overcome the safety problems associated with the floppy end terminals (3,4,5,6), but none of the new systems were able to meet safety performance standards presented in NCHRP Report 230 (7).

The Breakaway Cable Terminal (BCT) was developed through the National Cooperative Highway Research Program (NCHRP) in the early 1970's (8). This system consisted of a parabolic flare over the last 11.3 m (37.22 ft) of the guardrail, terminated with a stand-up end and a wrap around buffer plate. The concept behind this system is that when the terminal is impacted from the end, the W-beam will buckle and allow the vehicle to pass behind the installation. Unfortunately, this system was found to be very sensitive to the flare configuration and field experience has shown that these systems are frequently installed improperly (9). Additionally, the BCT has been found to impart unacceptably high deceleration forces on small vehicles, even

when installed correctly (10), and has recently been disallowed by the FHWA for use on high speed, high volume roads on the National Highway System.

Improved BCT designs, the Eccentric Loader Terminal (ELT) (11) and Modified Eccentric Loader Terminal (MELT) (12), have been developed and successfully crash-tested to NCHRP Report 230 criteria (7). These systems utilize improved buffer mechanisms, and optimized post locations, to reduce the forces required to collapse the terminal. Although these systems should offer improved safety performance over the standard BCT, the flared barrier end remains a critical component of the design. Further, the ELT and MELT have several other important design details which may adversely affect end-treatment performance if not installed correctly. Although the MELT is beginning to be used widely, its field performance has not been monitored closely enough to be adequately evaluated.

Another modification to the BCT system is the Slotted Rail Breakaway Cable Terminal (SRBCT) (13). This proprietary system utilizes longitudinal slots in the W-beam to lower the dynamic buckling load. This system is based on the concept that thin slots along the peaks and valley of the W-beam greatly reduces the section modulus with only a small reduction in the tensile capacity of the rail. This system has recently been evaluated according to the Test Level 3 criteria in NCHRP Report 350 (14), but it has not been installed in the field for a long enough period of time to accurately assess its performance.

1.3 Research Plan

The objective of this research project was to develop a non-proprietary guardrail terminal which meets the current safety criteria in Test Level 3 of NCHRP Report 350 (14). It was also highly desirable to develop the system in such a way that it will be possible to retrofit existing

BCT systems with this new terminal. With these objectives in mind, brainstorming sessions were conducted to come up with alternative concepts for the new system. Static and dynamic component testing were then undertaken, in conjunction with computer simulation, to investigate the most promising of the concepts. Both W-beam and thrie beam rail elements were considered for use in the new terminal. Upon successful completion of the developmental work, full-scale crash testing was conducted to evaluate the performance of the system.

2 TERMINAL CONCEPT

The principal behind the operation of the Breakaway Cable Terminal (BCT) is that the W-beam rail is designed to buckle out of the way when the system is impacted on the end, thus eliminating the dangerous spearing action. This design works reasonably well for large vehicles, but the buckling of the rail subjects small vehicles to large deceleration forces, causing them to spin out. This can be a serious problem, as the vehicle is often spun into the buckled rail section which pierces through the side of the vehicle. In order to improve the performance of this system, one must decrease the force required to buckle the rail, while maintaining the tensile capacity for redirectional impacts downstream of the terminal.

The concept chosen for investigation in this study consisted of flattening sections of either W-beam or thrie beam in order to reduce the buckling strength of the rail. Although W-beam has historically been the section of choice for terminals, recent testing (15) has shown that there are problems associated with this rail redirecting 3/4 ton pickup trucks. Since the current safety criteria specified in NCHRP Report 350 (14) requires that terminals be capable of redirecting 3/4 ton pickups, it was decided to investigate the behavior of both W-beam and thrie beam. The thrie beam is a much deeper section, which should be capable of redirecting a pickup.

2.1 Computer Simulation of Flattened Rail Concept

Nonlinear, large deformation finite element analysis was used to simulate the initial concepts of the flattened rail. LS-DYNA3D from Livermore Software Technologies Corporation was the FEA code used for the simulation.

2.1.1 W-Beam BCT Simulation

The initial simulation performed was that of the existing W-Beam BCT model being impacted by an 820-kg vehicle. This baseline model, with known results, gives confidence in subsequent models when results are not known. The vehicle model was obtained from Dr. Malcolm Ray (University of Iowa) and modified to fit our needs. The rail model was developed according to standard BCT plans. The impact condition was 100 km/hr, 0 degree, 1/4 car offset. Figure 1 shows the results of the simulation. As observed in published test results, the vehicle impacts the rail, forms a hinge, and the vehicle yaws causing a side impact of the vehicle into the hinge of the rail. This side impact is very dangerous as the W-beam is forced into the occupant compartment, and is the reason that the flattened rail concept is being pursued.

2.1.2 Flattened Rail W-Beam Simulation

The next simulation performed is shown in Figure 2. This model consisted of the W-Beam BCT model with flattened portions of the rail. For convenience, the rail was flattened at the posts in this model. The flattening of the rail provides a weaker bending moment, allowing the rail to bend easily and reduce the amount of yaw in the vehicle. The results of this simulation, shown in Figure 3, indicate the feasibility of the concept. The rail buckles at the flattened sections without inducing a large yaw on the vehicle. The vehicle is then capable of passing safely behind the rail.

2.1.3 Bogie Vehicle - Thrie Beam Simulation

With confidence in the W-Beam simulation, it was decided to investigate the thrie beam. The first thrie beam simulation was a straight thrie beam BCT system. Of course, this system does not really exist because it is far too stiff of a system for a terminal. However, by comparing the stiffness of this system to that of a flattened thrie beam system, the behavior of the flattened thrie beam system under consideration can be better understood.

The first thrie beam simulation used a bogie vehicle, rather than the 820-kg vehicle. The bogie vehicle was a rigid, rounded block of 820 kg. The bogie provides a significantly reduced computational model, allowing multiple runs in a fraction of the time. The second thrie beam simulation was similar to the first with the exception of the thrie beam being flattened at post nos. 2, 3 and 4.

Velocity vs. time curves for the two bogie - thrie beam simulations are shown in Figure 4. The straight thrie beam results show the "stiffness" of the thrie beam. As expected, the initial hit on the thrie beam (0 to 50 ms) shows a steep decline in velocity. From 50 to 130 ms the rail is imparting almost no forces on the bogie. At about 130 ms another impact between the bogie and thrie beam occurs. This impact causes the bogie to come to an abrupt stop, as it is an extremely stiff system.

With the flattened rail, the bogie vehicle is shown to decrease in velocity at a much more controllable level until about 250 ms when the bogie passes safely behind the thrie beam rail.

2.1.4 Flattened Thrie Beam MELT/BCT Simulation

With encouraging results from the bogie - thrie beam simulations, the next concept investigated was the 820 kg vehicle impacting a flattened thrie beam MELT/BCT system. The MELT/BCT system was made by combining the MELT head with the BCT post spacing. The reason for the combination was two fold:

- The MELT head provides a stiffer load path between the vehicle and the rail. The stiffer load path was thought to provide a better buckling force on the flattened sections.
- It was felt that the BCT post spacing was slightly more tolerable to installation error. It was desired that the final system be able to function properly with the posts installed within a reasonable tolerance level.

The results of the flattened thrie beam MELT/BCT simulation are shown in Figure 5. With encouraging simulation results, the details of the system and testing were then undertaken.

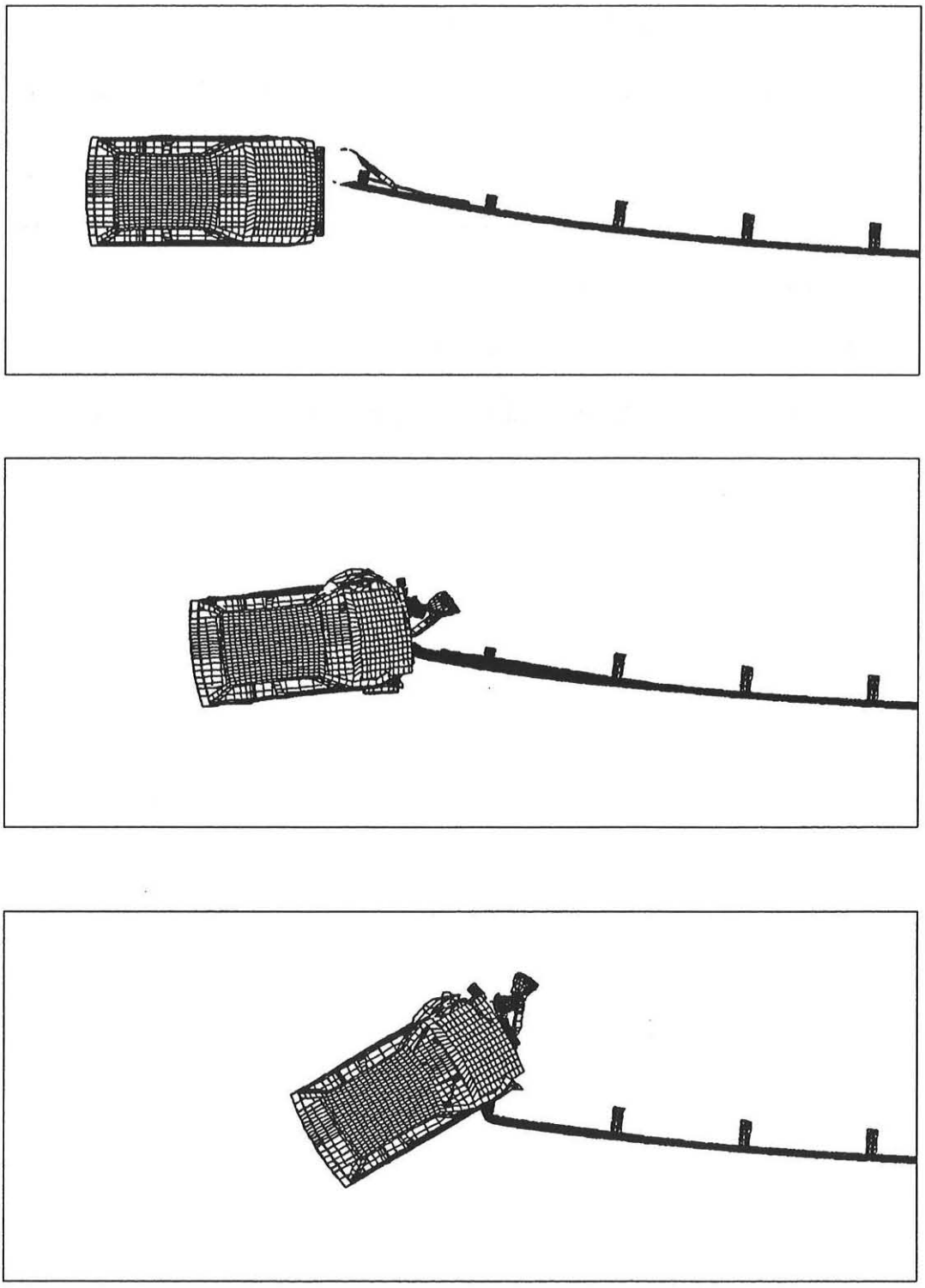

Figure 1. W-Beam BCT LS-DYNA3D Simulation.

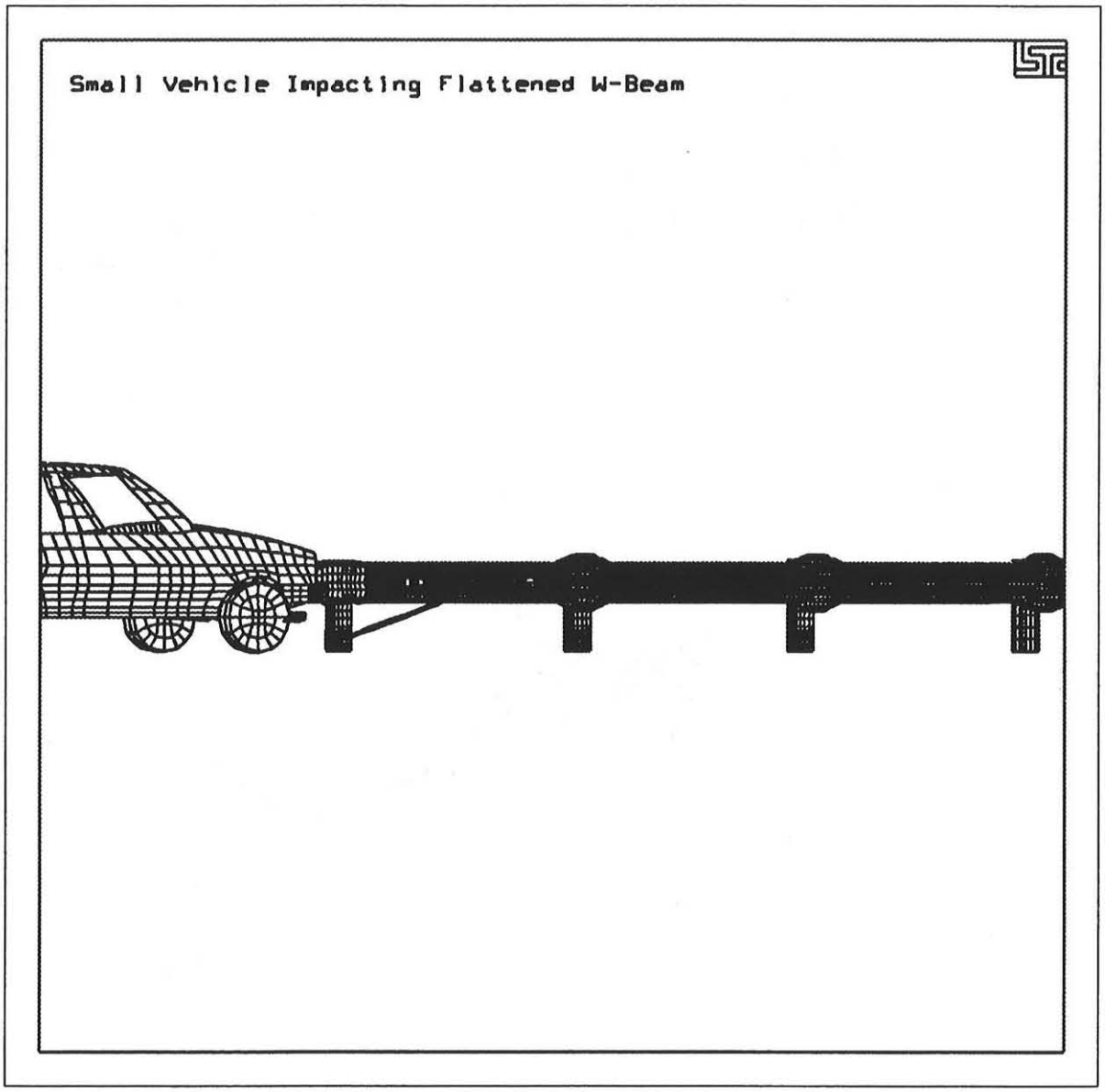

Figure 2. Flattened W-Beam.

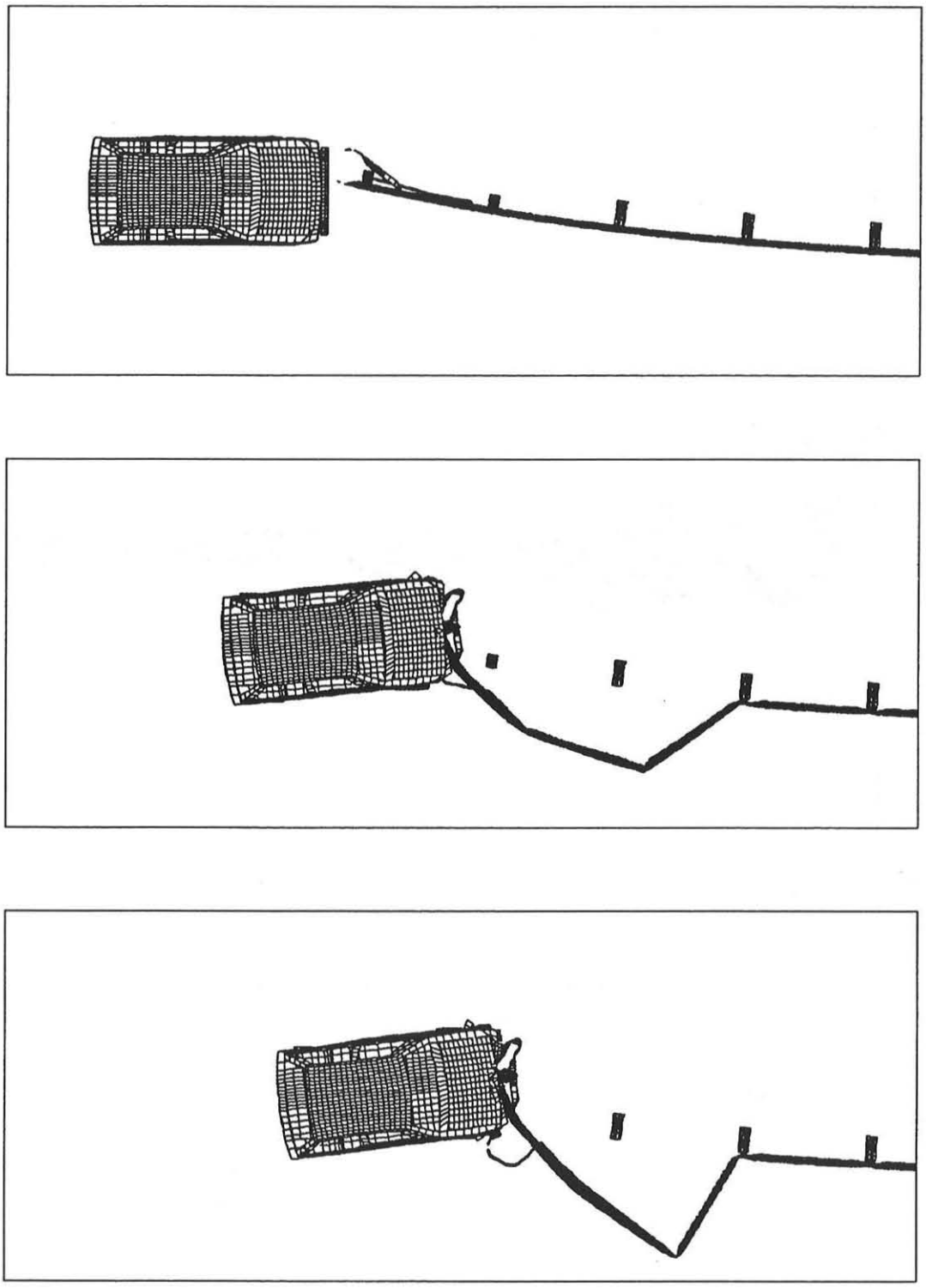

Figure 3. Flattened W-Beam BCT Concept Simulation.

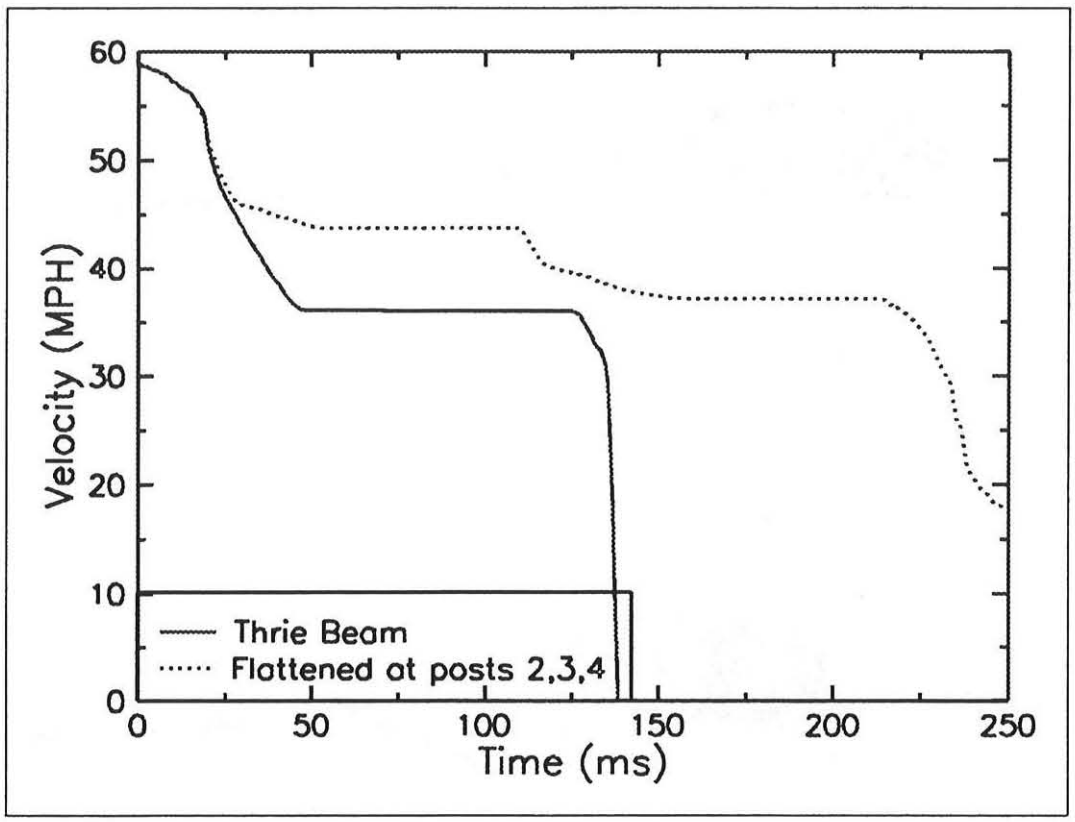

Figure 4. Bogie - Thrie Beam Velocity vs Time Simulation Results.

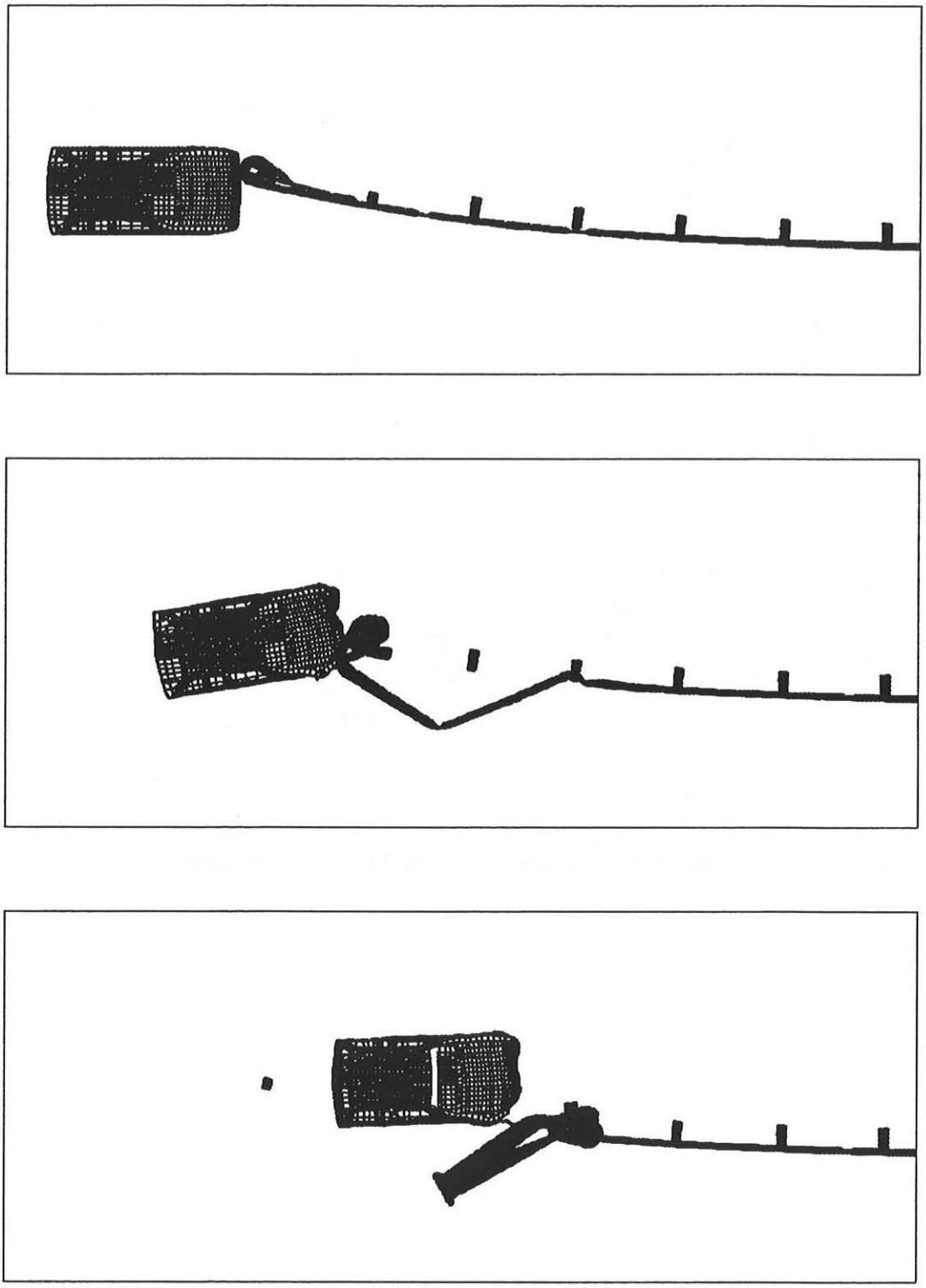

Figure 5. Flattened Thrie-Beam Simulation.

3 GUARDRAIL SHAPE MODIFICATION

In order to reduce the buckling strength of the guardrail beams, the section modulus was reduced at strategic locations throughout the system. This was accomplished by flattening sections of the beams to reduce the moment of inertia. In order to evaluate this concept, W-beam and thrie beam guardrail test specimen were flattened at the middle 305 mm (12 in.) section by pressing the beam in the center with a flat metal plate. This section describes the process of shape modification on the guardrail beams.

3.1 Equipment Used

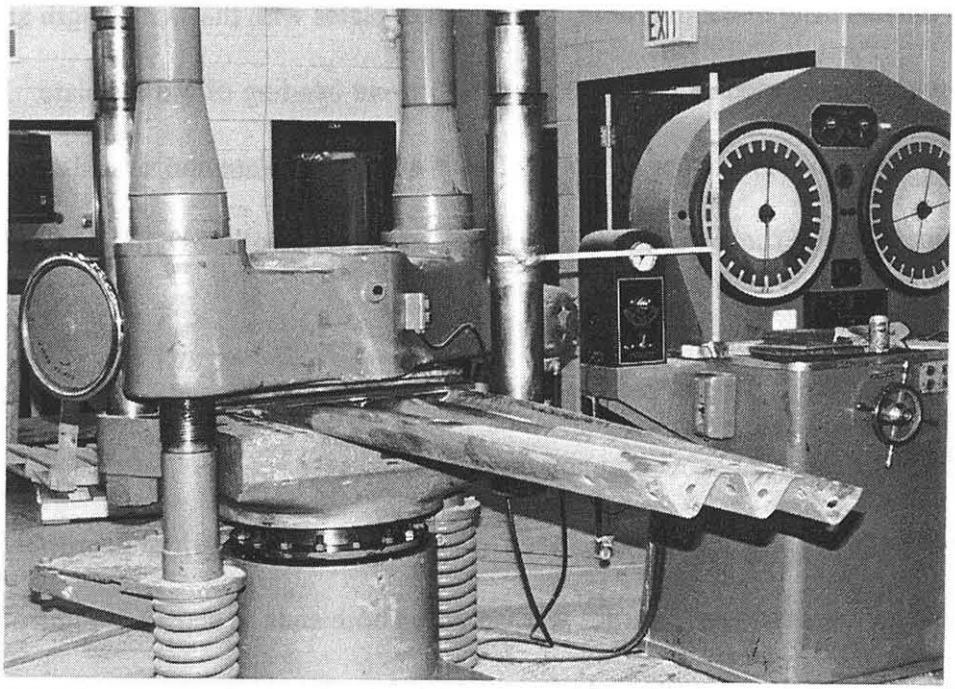

Figure 6. Flattening Setup.

Figure 6 shows the equipment setup used to flatten the W-beam and thrie beam. Details on the description of the equipment used follow.

Hydraulic Press.

The unflattened specimen was placed in a 1958 kN (440 kip) hydraulic press, which provided the flattening force. The swivelling head was removed so that there would be minimal rotation of the dies during the pressing operation. A pointer attached to the moving platform, in conjunction with a scale held fixed in the vertical direction, was used to measure the movement of the platform and control the extent of deformation of the rail.

Die.

A 305 mm x 864 mm x 19 mm (12 in. x 34 in. x ¾ in.) rectangular metal plate was used as a die to aid in the flattening of the guardrail. Two smaller plates with the same length and thickness, but half the width, were used as reinforcements to prevent bending of the die plate. For the thrie beams a smaller 305 mm x 152 mm x 19 mm (12 in. x 6 in. x ¾ in.) plate and a number of shims were used in combination with the die in order to get the desired shape of the flattened portion.

3.2 Background

In order to arrive at the die configuration discussed above, preliminary testing was done using a variety of shapes. These have been summarized as follows

a) A 152 mm (6 in.) wide plate was used initially to flatten this length of guardrail. During the pressing action, however, the rails warped up on both ends as shown in Figure 7. With the existing setup on the press, this led to contact between the regular shaped sections of the rails and the press head. As a result of this problem, as well as concerns about such a narrow flattened area, it was decided to pursue a wider flattened area in subsequent trials.

b) A cylindrical die was used in this trial instead of a flat plate in an effort to prevent the warping which occurred in the previous trial. This did not help the problem, and it led to

nonsymmetrical spreading and formation of a localized deformity closely approximating a channel section. This concept was thus dropped, as the section modulus of a channel section is much higher than that of a flat plate.

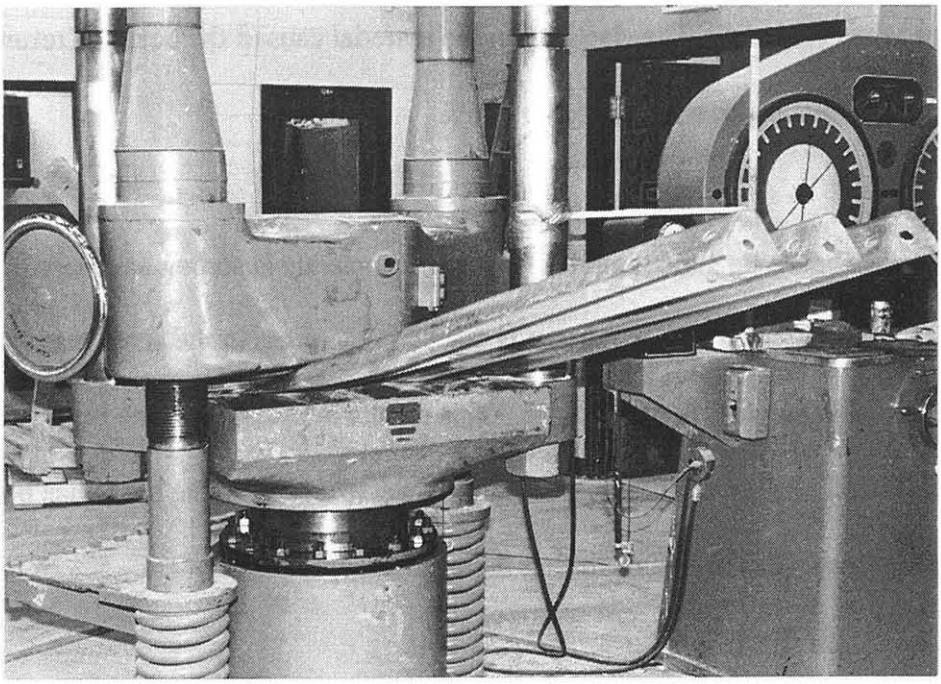

Figure 7. Warped thrie beam guardrail.

c) In this trial, the width of the die plate was increased to 305 mm (12 in.) and, in order to prevent the plate from bending, two additional 152 mm (6 in.) wide plates were stacked on top of it, thus increasing its bending strength. This resulted in reasonable flattening of the rail. Further refinements were then made in the actual flattening procedure for W-beam as well as thrie beam.

3.3 Flattening Procedure

3.3.1 W-beam

50% Flattening.

In order to flatten the W-beam to 50 % of its original depth, the beam was situated in the press and its initial depth was measured. The beam was crushed until the depth was 35% of the original, and then released. The elasticity in the material caused the beam to return approximately 15% so that the final depth was reduced by 50%.

100% Flattening.

The procedure for flattening the W-beam completely is somewhat more involved than that required for 50% flattening. The W-beam is placed in the press in the same manner as for the 50% flattening, and the guardrail is pressed flat. This results in the ends of the beam warping upwards. The beam is then flipped over and pressed on the reverse side until the beam has been straightened. This procedure results in a W-beam which is flattened to approximately 2% - 5% of its original depth.

3.3.2 Thrie Beam

Initial trial crushes indicated that thrie beams tend to form channel sections on the middle corrugation when crushed with the same dies and procedure as used for W-beams. Thus, it was necessary to develop a different crushing sequence for the thrie beam, and additional shims were used to obtain the desired results.

50% Flattening.

In order to obtain a 50% flattened section in the thrie beam, it was necessary to begin by flattening only the center corrugation. The center corrugation was pressed to 50% of the initial depth of the beam by using the smaller 305 mm x 152 mm x 19 mm (12 in. x 6 in. x ¾ in.) plate shimmed

down 127 mm (5 in.) from the upper section of the press. This prevented the channel formation by flaring the center corrugation out before the outer corrugations were crushed. The next step was to take the top shims out, leaving the smaller die plate on the deformed center corrugation. The larger die and the two reinforcing metal plates (used for W-beams previously) were then put on top of these, and the entire thrie beam was crushed to 30% of the initial height. The smaller die plate was then removed and the beam was pressed to 40% of its original depth. The thrie beam was then flipped over and pressed from the other side with the same die configuration, in order to remove the resultant warp. This procedure of flipping and pressing was conducted until the beam was flattened to 50% of the original depth, which was normally accomplished after 2 or 3 iterations.

100% Flattening.

The initial steps followed for the full flattening of thrie beams were similar to those for the 50% flattening. However, after the smaller die on the middle hump is removed, the beam is pressed all of the way down, instead of pressing to 40% of the initial height. The beam is then flipped over only once, and pressed in the other direction until the beam is straight.

4 STATIC TESTING

Preliminary static buckling tests were performed on standard sections of both W-beam and thrie beam with a length of 1676 mm (5 ft - 6 in.). This preliminary testing was conducted on short beam segments due to the size limitations of the hydraulic press. Upon completion of this preliminary testing, a test fixture was constructed consisting of a frame and hydraulic actuators. This fixture was used to test modified and unmodified specimens of both W-beam and thrie beam. The modified beams were 3810 mm (12 ft - 6 in.) in length and had the center 305 mm (12 in.) flattened by 50%

and 100% of the original depth.

The objective of this series of tests was to evaluate the effect of changing the section modulus to obtain reduced buckling properties in terms of strength and failure mode.

4.1 Preliminary Static Tests

The length capacity of the conventional tensile/compressive testing machine being used for this testing was not large enough to accommodate testing of the standard 3810 mm (12 ft - 6 in.) length of guardrail. Hence, shorter 1676 mm (5 ft - 6 in.) unmodified sections of 10 gauge thrie and 12 gauge W-beams were used. A special fixture was used for holding one end of the beam fixed in the press, thus resulting in fixed-pinned end conditions. The procedure used in this preliminary testing is outlined below.

4.1.1 Equipment

Hydraulic Press.

These tests were conducted on the 1958 kN (440 kip) capacity hydraulic testing machine which was described previously and shown in Figure 6.

Fixtures.

The fixtures used for this testing were fabricated to hold the guardrail vertically on the press platform. This fixture consisted of a 337 mm (13.25 in.) length of guardrail welded to a 10 gage rectangular metal base plate reinforced with angle iron. This short section of guardrail contained bolt holes so that the test specimen could be bolted to it.

4.1.2 Results

W-Beam.

The failure load of the W-beam was 243 kN (54.6 kips). As can be seen in Figure 8, the mode of failure was local buckling concentrated on the upper one-quarter of the beam.

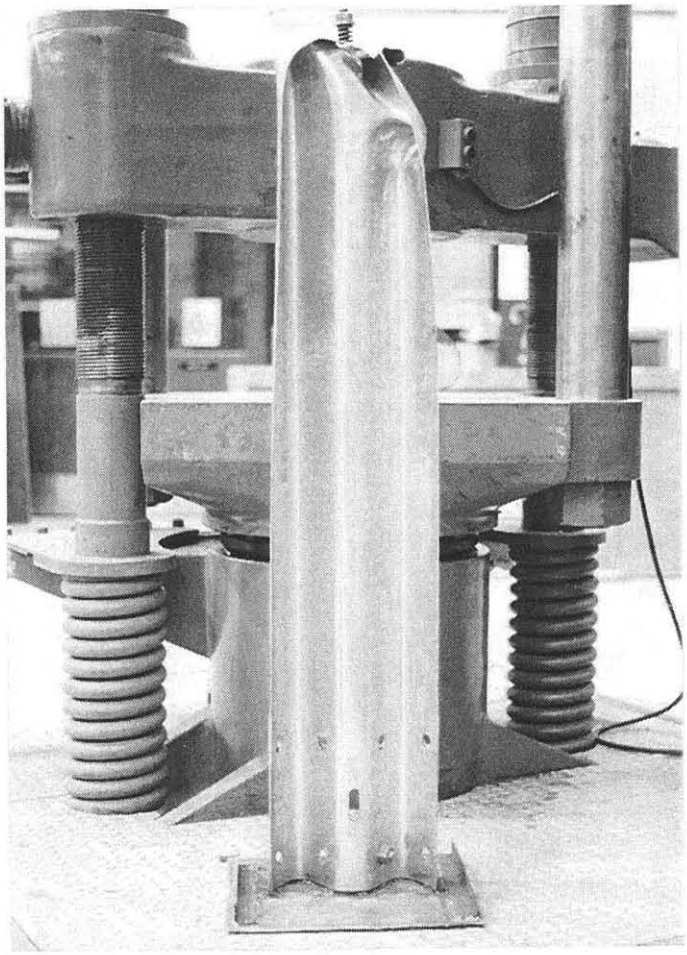

Figure 8. Failure mode for static test on a short W-beam section.

Thrie Beam.

The failure load of the thrie beam was 656 kN (147 kips). As can be seen in Figure 9, the failure mode in this case was mainly local buckling, but there was also noticeable compressive bearing failure at the fixture bolts. Overall the local buckling was very uniform.

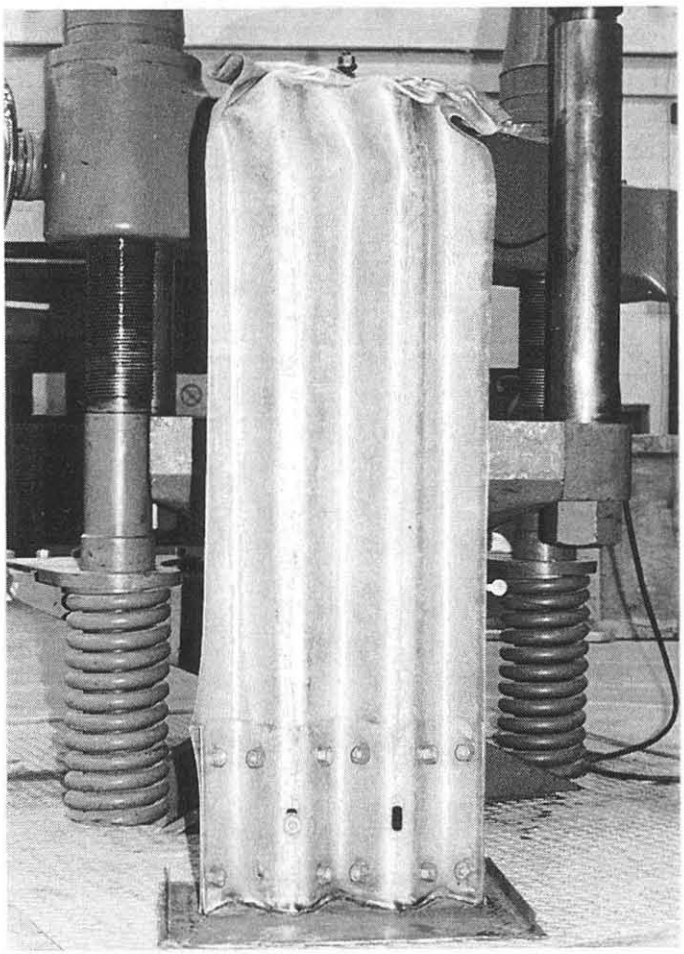

Figure 9. Failure mode for static test on a short thrie beam section.

4.1.3 Discussion of Results

Numerical calculations were performed to investigate possible modes of failure and to compare with the experimental results. These calculations are shown in Appendix A, and summarized in Table 1.

Table 1. Short Specimen Static Buckling Results.

Guardrail Type	Test Failure Load	Calculated Global Buckling Failure	Calculated Material Failure	Calculated Bearing Failure
W-beam (12 gauge)	243 kN	447 kN	527 kN	138 kN
Thrie beam (10 gauge)	656 kN	895 kN	1054 kN	265 kN.

Conversion factor: 1 kip = 4.448 kN

W-Beam.

Even though the calculated critical load for compressive bearing failure was 138 kN (31 kips), there was no indication of this type of failure at the maximum load of 243 kN (55 kips). It is thought that this behavior was a result of the contribution from the clamping force, which was not considered in the calculation. The experimental critical load of 243 kN (55 kips) is significantly less than the calculated global buckling load of 447 kN (100 kips). The most likely reason for this difference in force is that the actual mode of failure was local buckling, which in this case occurred at a lower load level than was required for global buckling.

Thrie beam.

The experimental failure load of 656 kN (147 kips) for the thrie beam was less than the calculated buckling load of 895 kN (201 kips). This load, however, is greater than the predicted

compressive bearing failure at the bolts of 265 kN (60 kips). The beam failed as a result of local buckling, similar to the previous test on the W-beam.

4.1.4 Conclusion

Results from crushing of the 1676 mm (5 ft - 6 in.) sections were not conclusive since they failed in local buckling instead of global buckling which is expected to occur in actual field installation. It is likely that the cause of this local buckling can be attributed to a combination of partially eccentric loading and the fact that it was a relatively short specimen. These conditions could result in local buckling on the outer edges of the beam which, once initiated, continue through the cross section of the beam. Therefore, static tests on longer 3810 mm (12 ft - 6 in.) sections were conducted next.

4.2 Static Compressive Testing of 3810 mm (12 ft - 6 in.) Sections

Static crushing tests were carried out for modified and unmodified 12 gage, 3810 mm (12 ft - 6 in.) length, W-beams and thrie beams. Unmodified beams were standard sections currently being used as roadside safety guardrail. The modified beams had the center 305 mm (12 in.) section flattened 50% and 100% as described previously.

4.2.1 Test Setup

The apparatus used for this testing is shown in Figure 10. This setup consisted of three spreader beams, one for each of the ends and one acting as the moving head powered by actuators. Two single acting 534 kN (120 kip) hydraulic actuators with a stroke of 152 mm (6 in.) were installed on the loading frame to push the head spreader beam. Two 'Dwydag' bars were used to connect the main spreader beams. Two stress chairs, shown in Figure 11, were located between the actuators and the head spreader beams to double the stroke of the apparatus if required.

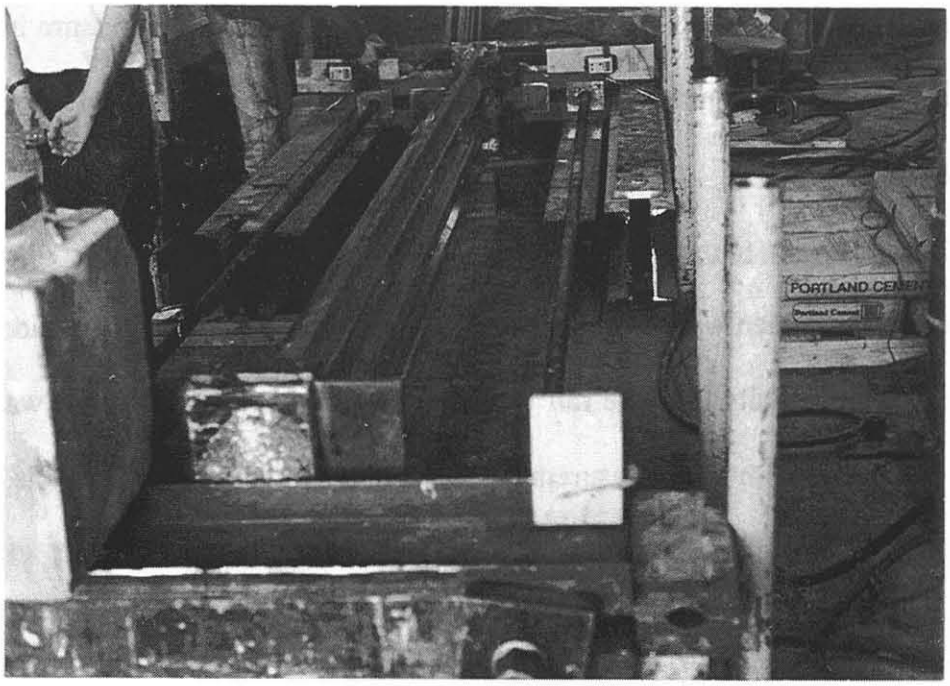

Figure 10. Setup for static tests on 3810 mm guardrail.

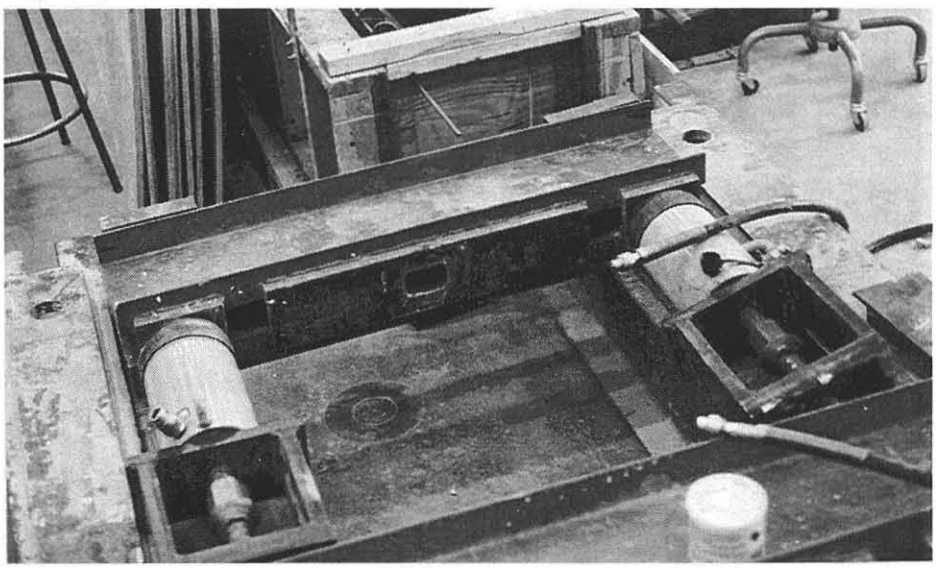

Figure 11. Hydraulic actuators and stress chairs for static buckling tests.

The data acquisition for this testing consisted of two string potentiometers to measure the displacement of the head, as well as a pressure transducer to measure the pressure in the actuators. The voltage from this instrumentation was read directly from a voltmeter, and recorded as the test progressed.

4.2.2 Test Procedure

Each test specimen was placed between the fixed end and the head spreader beam, and a load was applied gradually until the rail was held snugly in between. A load was then steadily applied to the beam, with data measurements being taken at prescribed intervals. This process was carried out until the beam buckled, as can be seen in Figure 12.

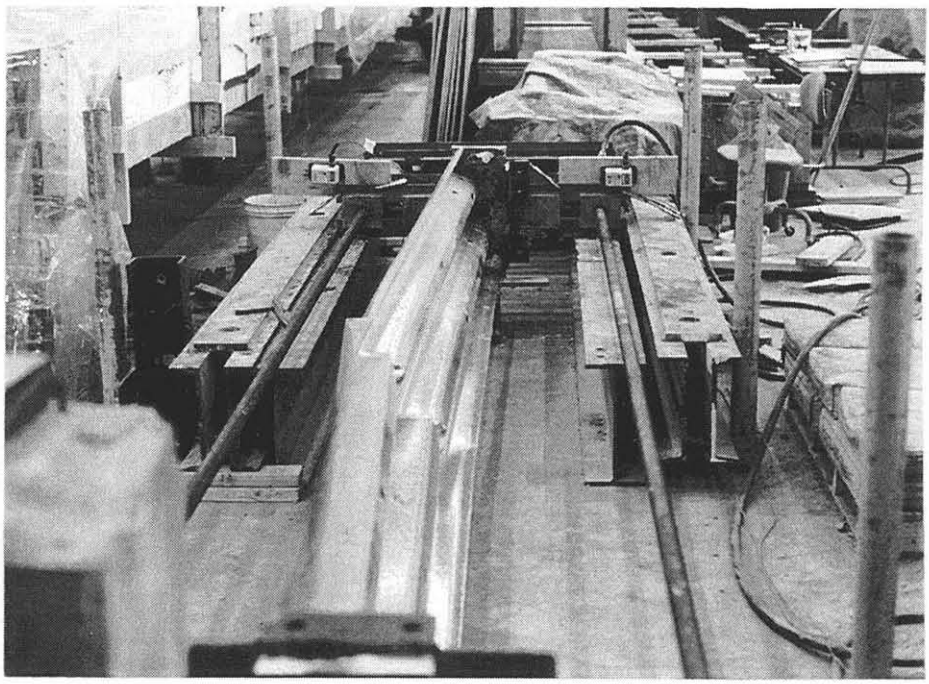

Figure 12. Thrie beam static buckling failure.

4.2.3 Results of Static Tests on 3810 mm Beams

Only the standard beam sections and those that had been flattened 50% were tested. The 100% flattened beams could not be tested because the stiffness at the flattened section was decreased so significantly that they could not be placed in the fixture without being supported in the center.

As expected, significant reduction in the buckling forces were found on the beams with flattening, as can be seen in Tables 2 and 3. The force deflection characteristics of these tests are reported in Figures 13 and 14. At this point it was decided to initiate the next phase of the development which consisted of dynamic bogie testing.

Table 2. 3810 mm Static Buckling Results.

Test Sample	Beam Type	Flattening	Buckling Load
KSW1A	W	0 %	197 kN
KSW1B	W	0 %	238 kN
KSW1C	W	0 %	277 kN
KSW2A	W	50 %	22 kN
KSW2B	W	50 %	88 kN
KSW2C	W	50 %	75 kN
KST4A	Thrie	0 %	433 kN
KST4B	Thrie	0 %	430 kN
KST5A	Thrie	50 %	125 kN
KST5B	Thrie	50 %	41 kN

Table 3. 3810 mm Buckling Force Averages.

Flattening	W-beam Avg. Buckling Force	Thrie Beam Avg. Buckling Force
0 %	237 kN	431 kN
50 %	62 kN	83 kN

Conversion factor: 1 kip = 4.448 kN

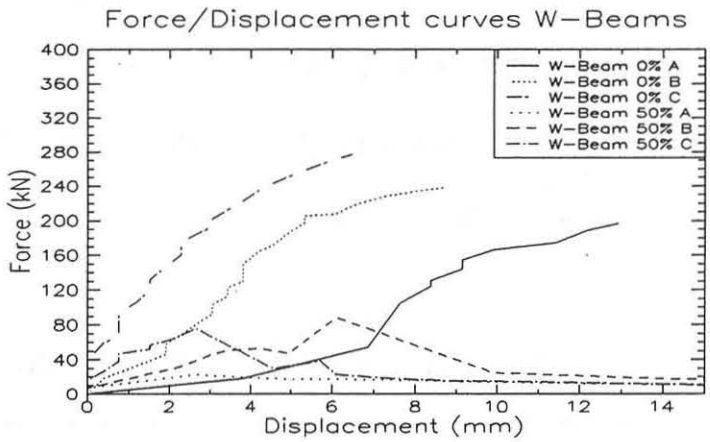

Figure 13. W-beam static buckling test results.

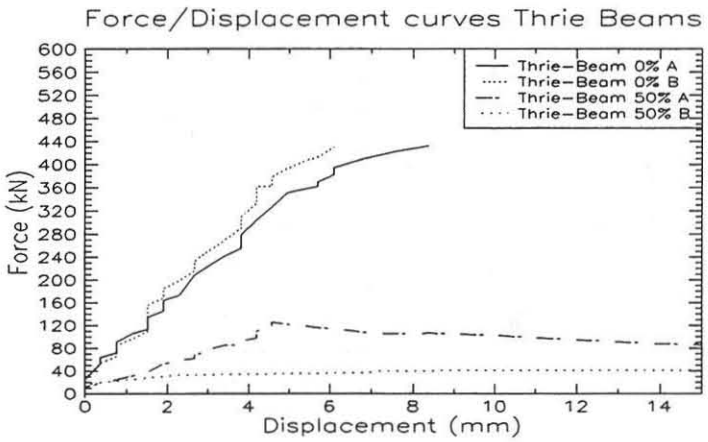

Figure 14. Thrie beam static buckling test results.

4.2.4 Analysis of 3810 mm Buckling Tests

To obtain the theoretical buckling load, Euler's buckling formula was used considering the beam to be a long slender column with central loading. According to Euler's equation the critical buckling load P_{cr} is given by

$$\frac{P_{cr}}{A} = \frac{C\pi^2 E}{[\frac{l}{k}]^2}$$

Using this formula, the buckling load for the unmodified W-beam was calculated to be 169 kN (38 kips), while the critical buckling load for the unmodified thrie beam was found to be 338 kN (76 kips). These numbers are compared to the average of the experimental results in Table 4.

Table 4. Comparison of 3810 mm Sample Buckling Results.

Guard Rail Type	Theoretical Buckling Loads	Average of Experimental Buckling Loads
W-beam	169 kN	237 kN
Thrie Beam	338 kN	432 kN

These results are considered to be reasonable, as the end condition constant C used in the theoretical calculation is difficult to determine, and therefore lacks accuracy.

5 DYNAMIC BOGIE TESTS

As the next step in the development of this system, dynamic bogie testing was initiated to evaluate the behavior of the modified guardrail shapes under dynamic loading conditions. The 12 gage modified and unmodified W-beam and thrie beam sections were installed horizontally and impacted with a bogie vehicle at a predesignated speed. The guardrail failure modes were noted and the decelerations of the bogie were recorded to be analyzed for a better understanding of the dynamic buckling behavior.

The objective of this phase was to investigate the dynamic buckling behavior of the modified W-beams and thrie beams. The main items of interest included the mode of failure, the peak forces, and the energy absorbed.

5.1 Test Setup

5.1.1 Testing Configuration

The bogie tests were conducted at the Midwest Roadside Safety Facility outdoor test site, located at the Lincoln Municipal Airport. As shown in Figure 15, the test configuration consisted of placing the non-impacted end of the guardrail against a rigid concrete block, while supporting the specimen at the center with the aid of a post. The attachment to the concrete block consisted of a rectangular shaped steel box anchored to the block, into which the beam was placed. This effectively provided a pinned type connection, because the end of the beam was allowed to rotate, but it was restrained from translation.

A 140 mm x 190 mm (5 ½ in. x 7 ½ in.) post was inserted into a steel fixture which was fixed to a hole in the concrete apron. Varying sizes of blockouts were used to account for the different amounts of crush in the center portion in order to assure that the beam was situated perpendicular

to the concrete block. In all tests except for the first, an angle bracket with a 76 mm (3 in.) ledge was attached to the post, which supported the center of the beam. This held the beam in place while allowing it to buckle away from the post. It is anticipated that brackets similar to this will be used in the final design. Tires were placed in front of the concrete block to protect the bogie in the event that it impacted the rigid structure.

5.1.2 Bogie Vehicle

The bogie vehicle consists of a fabricated chassis with wheels, having the desired mass of 810 kg (1785 lbs). A platform for attaching the accelerometer package is located at the center of gravity of the bogie vehicle. A remote control breaking system is utilized, which uses compressed nitrogen to activate the brakes at each of the four wheels. The bogie impact head consists of five 19 mm (¾ in.) sheets of plywood attached to the front of a steel plate connected to the chassis with two cylindrical tubes. The wood surface is intended to prevent the end of the beam from sliding off the impact head and to aid in distributing the load evenly over the end of the beam.

5.1.3 Tow and Guidance System

A reverse cable tow system was used to propel the bogie. The bogie is released from the tow cable before impact with the beam. A fifth wheel was used in conjunction with a digital speedometer on the tow car to increase the accuracy of the bogie impact speed.

The guidance system for the bogie consisted of guide roller bearings attached under the front and the rear axle of the bogie and a pipe rail guidance system. The rail guidance system consisted of 51 mm (2 in.) diameter pipes fixed 102 mm (4 in.) above the concrete apron. The roller bearings on the bogie vehicle straddled the pipe, ensuring the proper direction and position of the bogie prior to impact.

5.1.4 Data Acquisition Systems

The bogie and beam reactions upon impact were monitored with SVHS video, accelerometers, and tape pressure switches. These systems are described in the following subsections.

Accelerometers.

A triaxial piezoresistive accelerometer system with a range of ± 200 g's was used to measure the acceleration in the longitudinal, lateral, and the vertical direction at a sample rate of 3200 Hz. The environmental shock and vibration sensor/recorder system, Model EDR-3, was developed by Instrumented Sensor Technology (IST) of Okemos, Michigan. The EDR-3 was configured with 256 Kb of RAM memory and a 180 Hz filter. Computer software, "DynaMax 1 (DM-1)" and "DADiSP" were used to digitize, filter, analyze, and plot the accelerometer data.

Speed Trap.

Five tape pressure switches spaced at 1.52-m (5-ft) intervals were used to determine the speed of the vehicle before impact. Each tape switch fired a strobe light and sent an electronic timing mark to the data acquisition system as the left front tire of the bogie passed over it. Test vehicle speeds were determined from these timing marks by the software "Enhanced Graphics Acquisition and Analysis" (EGAA).

5.2 Test Results

5.2.1 KDW1 Series

This first series consisted of four tests on unmodified 12 gauge W-beam. The first of these tests was considered to be the worst case for buckling, as it was bolted to the post in the center, and there was no flared section on the end of the rail to keep it from digging into the impact head. After

this test, the test conditions were changed for the remaining three tests, which were performed under identical conditions to establish the repeatability of the results.

Test KDW1A.

This test consisted of a standard 12 gauge W-beam fixed to the post with a bolt at the center location, as can be seen in Figure 15. When the Bogie Vehicle impacted the end of this beam at 9.45 m/s (21.1 mph), it dug into the wood on the front of the bogie, in effect providing a fixed end condition. The combination of the fixed end condition and the reduced effective buckling length raised the critical global buckling force enough that the failure mode in the beam was a local buckling on the end that the impact took place. The force from the impact caused the welds connecting the impact head to the bogie to fail.

The bogie was subsequently repaired and steps were taken to reduce the severity of the impact conditions for future tests. This included supporting the beam at the post with an angled bracket which provided a 76 mm (3 in.) shelf on which the beam could rest. This resulted in the doubling of the effective buckling length in the direction which the failure occurs. A flared end was also attached to the end of all subsequent test specimens, as shown in Figure 16. This prevented the end of the beam from gouging into the wood as was witnessed in this test.

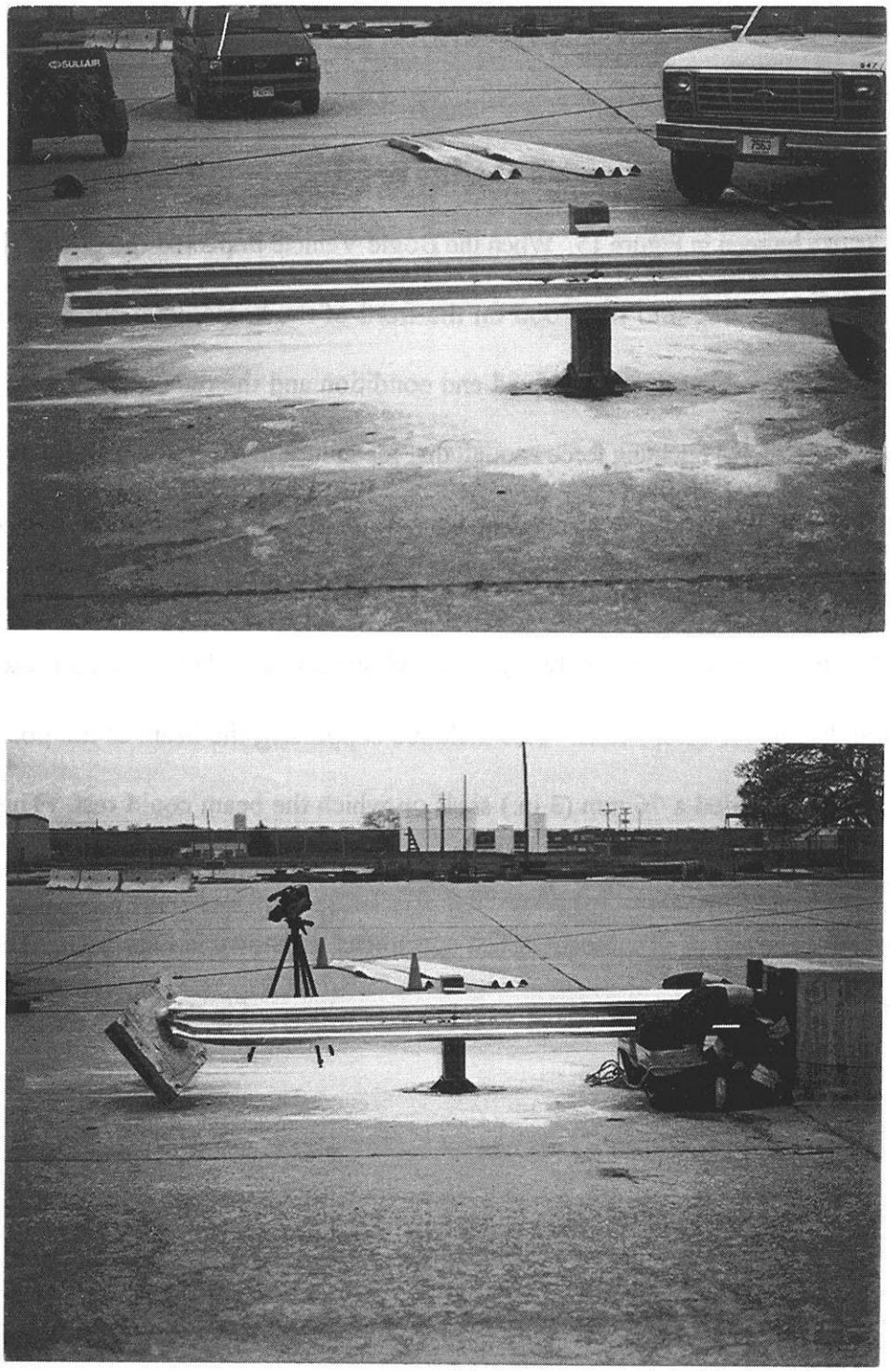

Figure 15. Test KDW1A before and after impact.

Test KDW1B.

This test was performed with a standard 12 gauge W-beam with a flared end as shown in Figure 16. The rail was supported vertically in the center with an angle bracket. The bogie impacted the system head on at a speed of 8.5 m/s (19.0 mph).

Immediately after being impacted by the bogie, the flared end on the beam curled up. Shortly after this, three kinks appeared on the outer edges of the beam near the quarter point closest to the bogie. Two of these occurred on the upper edge and one occurred between the two on the lower edge. The two deformities on the upper edge of the beam were in the elastic region, so they disappeared after the load was released. The deformation on the lower edge was clearly in the plastic region and left a permanent deformation in the beam.

Shortly after this, similar kinks started to form in the middle of the beam. One of these started on the upper edge, and the other started diagonally across the bolt slot on the lower side. The forward half of the beam crushed slightly into the rear half at this point, and the middle of the beam started to fold up and away from the post. The buckle progressed into a more prominent fold, and the end of the beam lost contact with the bogie as it was pushed to the side.

The acceleration and change in velocity plots for this test are presented in Figure 19. The accelerometer plot represents the deceleration of the center of mass of the bogie vehicle. This curve is integrated to obtain the change in velocity curve.

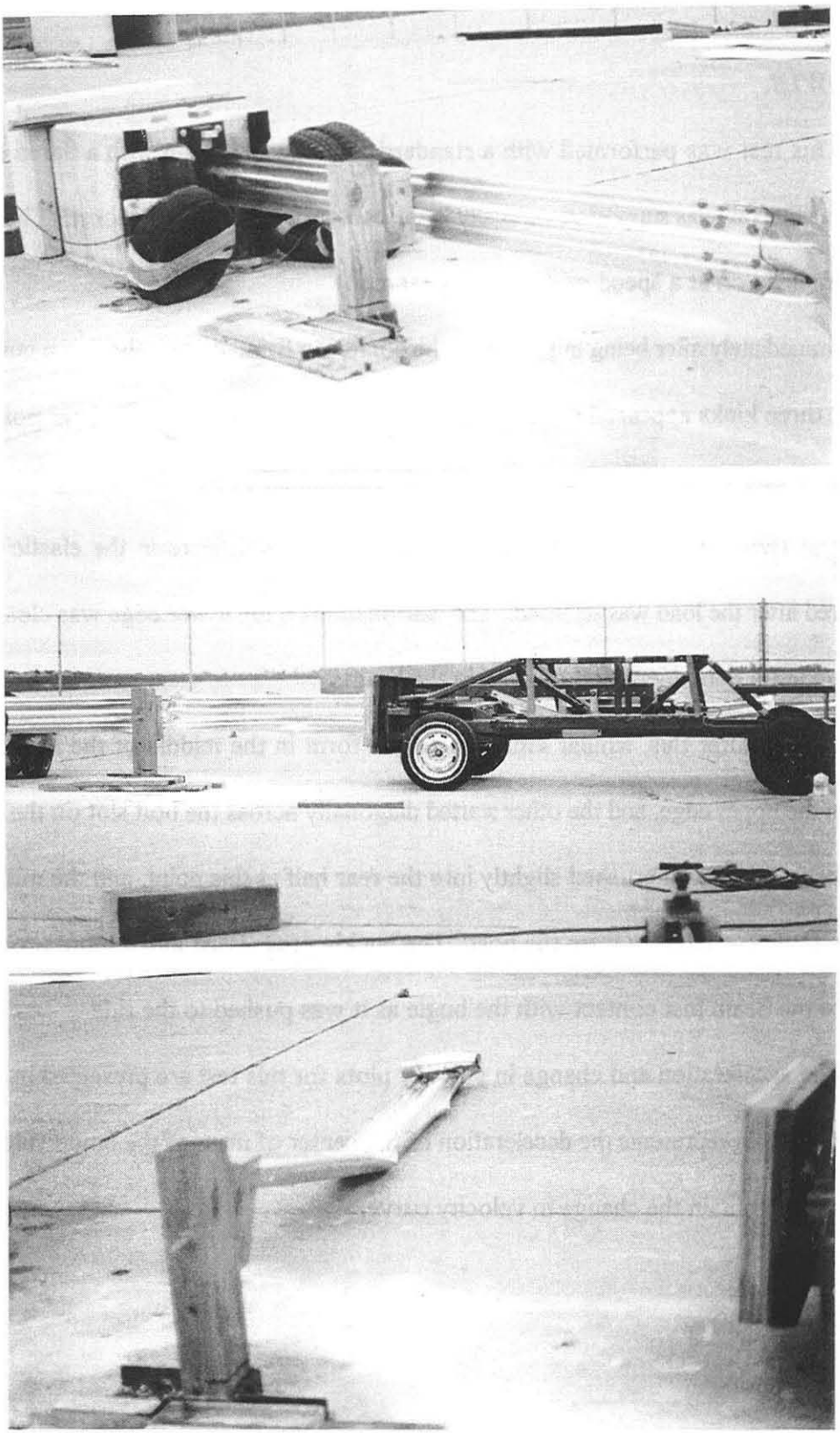

Figure 16. Test KDW1B before, during, and after impact.

Test KDW1C.

The configuration for this test was identical to that of KDW1B, as can be seen in Figure 12. The standard 12 gauge W-beam was supported in the center by an angle bracket attached to a post, and a flared end was attached to the W-beam on the impacted end.

The bogie vehicle impacted the end of the W-beam at 9.1 m/s (20.3 mph). Immediately after impact, two kinks started to form at the quarter point of the beam closest to impact. One of these deformations was on the top edge of the beam, and the other was located diagonally across from it on the bottom edge, similar to the behavior witnessed in the previous test. However, unlike Test KDW1B, the beam continued to buckle at this quarter point and was subsequently pushed to the side.

The acceleration and change in velocity plots for this test are presented in Figure 19.

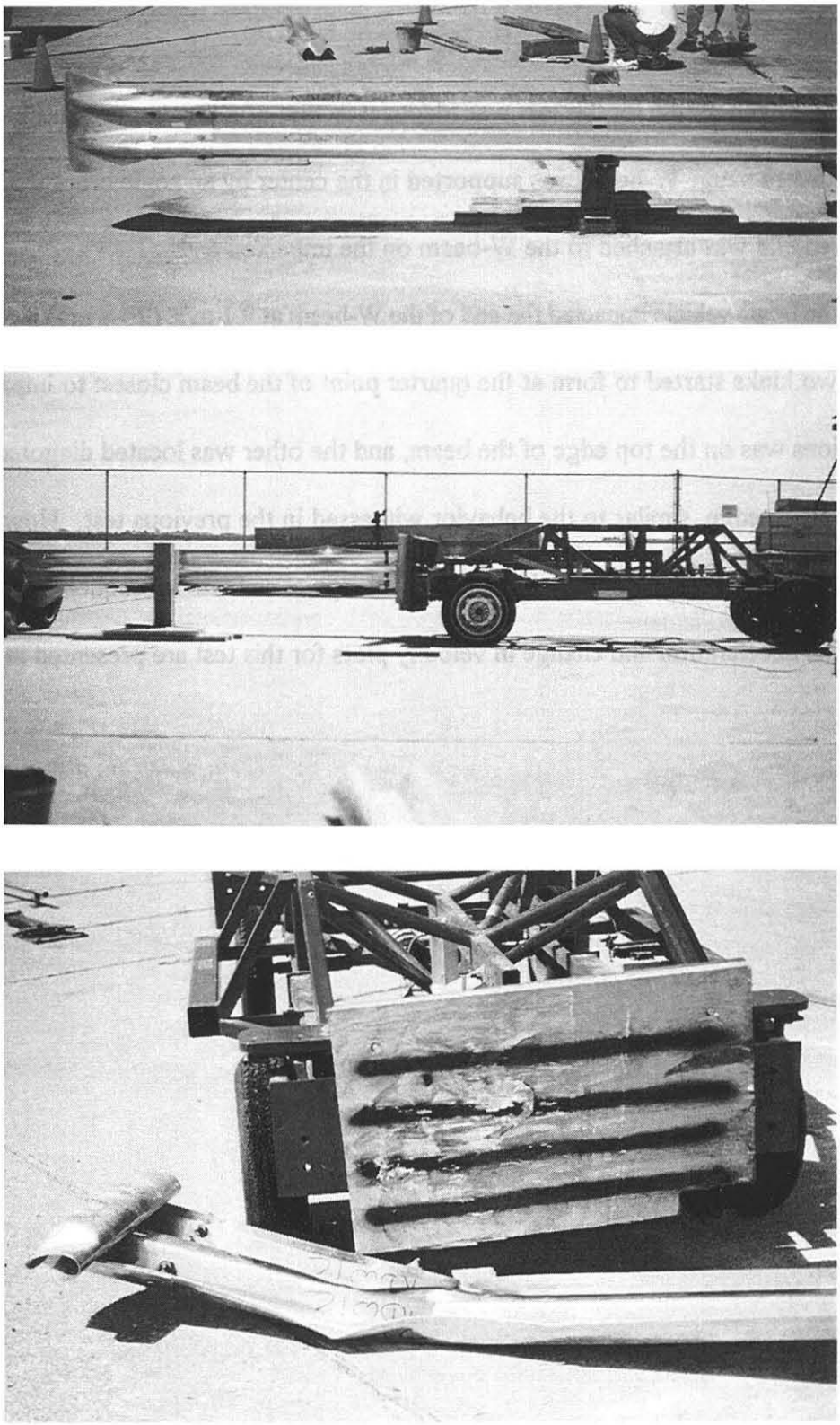

Figure 17. Test KDW1C before, during, and after impact.

Test KDW1D.

The configuration for this test was identical to that of the previous two. The standard 12 gauge W-beam was supported in the center by an angle bracket attached to a post, and a flared end was attached to the end which was to be impacted, as can be seen in Figure 18.

The bogie impacted the end of the W-beam at 9.2 m/s (20.5 mph) and a kink appeared on the lower side of the beam at the quarter point, similar to the previous two tests. There was no deformation on the top of the rail at this point, however. The beam then buckled at its center, and folded away from the post. The beam was subsequently projected in an upward direction away from the post. The brakes were applied to the bogie and it came to rest touching the post, without breaking it. The bogie vehicle yawed approximately 10 to 15 degrees during this impact event.

The acceleration and change in velocity plots for this test are presented in Figure 19. The results from the unmodified W-beam tests were not uniform in these last three cases involving unflattened W-beams, despite having similar initial conditions. The differences are attributed to the unpredictability of sudden dynamic buckling process. The remainder of the tests with the modified W-beams and the thrie beams gave similar results for each individual set of test specimen.

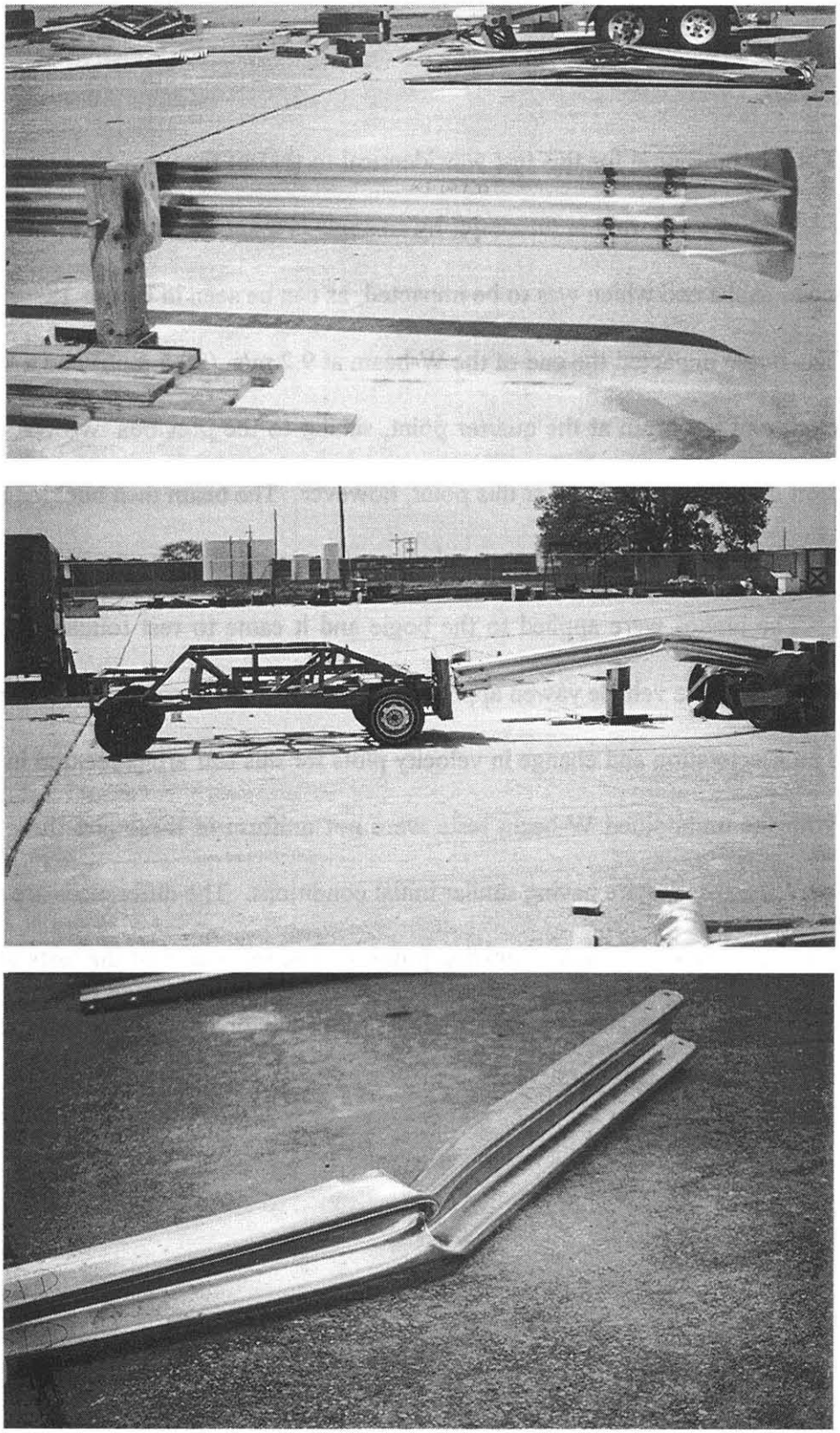

Figure 18. Test KDW1D before, during, and after impact.

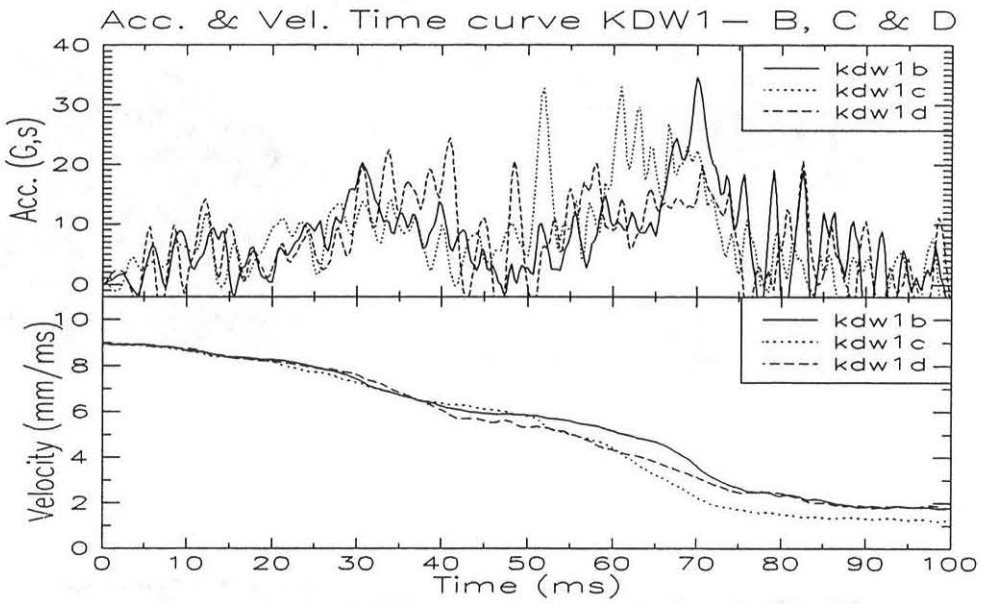

Figure 19. Accelerations and change in velocity for standard W-beams.

5.2.2 KDW2 Series

This series involved bogie tests on 3 samples of 50 % flattened W-beams. All three test configurations were identical so that the repeatability of the performance could be judged.

Test KDW2A.

This test was conducted with a W-beam which had been flattened 50% in the center, as described previously. There was no flared end placed on the W-beam for this test. The bogie impacted the system head-on at 8.6 m/s (19.2 mph). The half-flattened W-beam was supported on an angled bracket attached to the post. During the impact, the beam buckled away from the post in the center of the beam, forming a kink at the rear portion of the 305 mm (12 in.) flattened section. Photographs of this test are presented in Figure 20, and plots of the accelerometer and change in velocity data are shown in Figure 22.

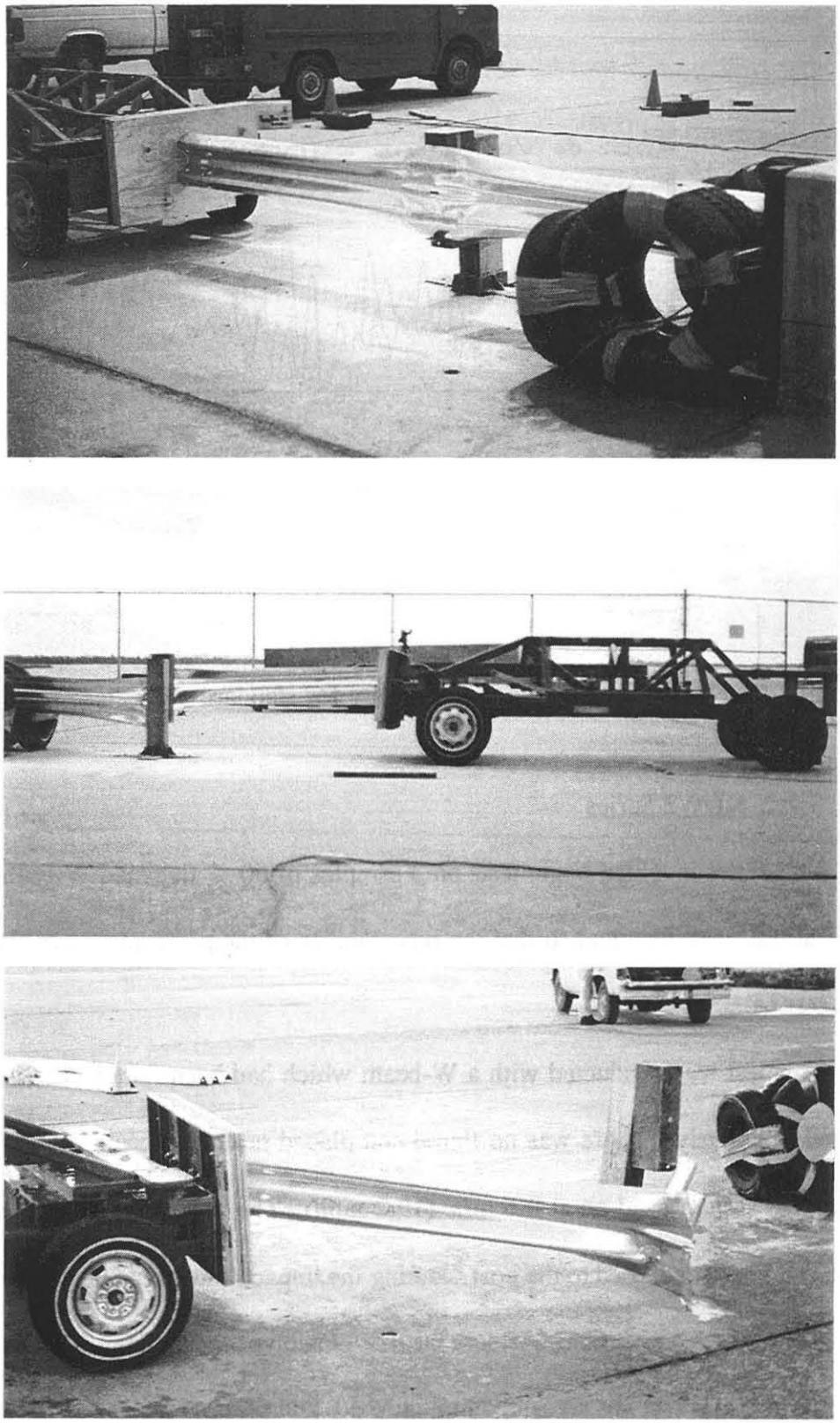

Figure 20. Test KDW2A before, during, and after impact.

Test KDW2B .

During this test the bogie vehicle impacted the end of the 50% flattened W-beam at 9.0 m/s (20.2 mph). There was a flare end present on this test. The beam buckled in the middle and was ejected to the side. The bogie impacted and broke off the half sawn post. The bogie then impacted the tire cushions before rebounding. Photographs of this test are presented in Figure 21, and plots of the accelerometer and change in velocity data are shown in Figure 22.

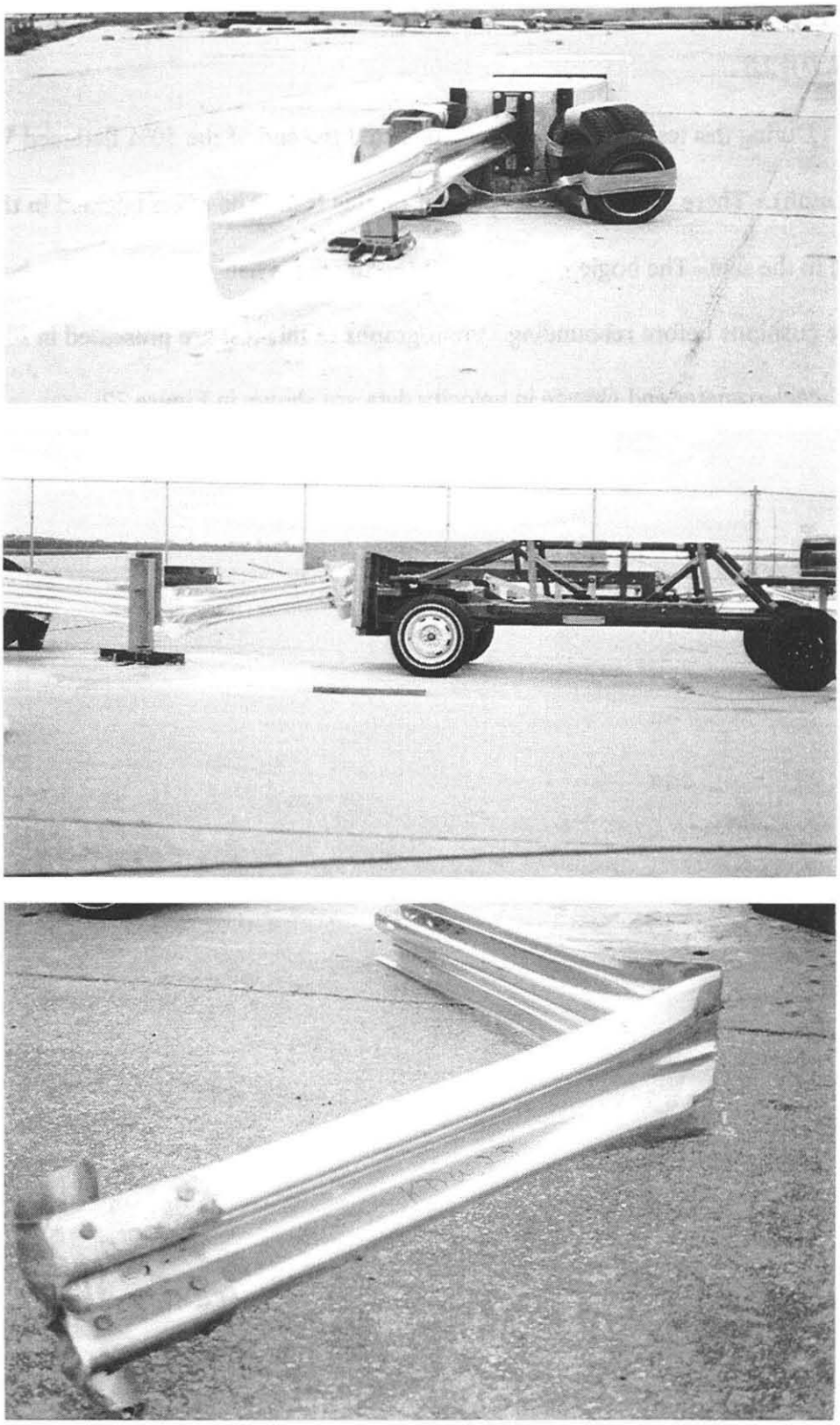

Figure 21. Test KDW2B before, during, and after impact.

Test KDW2C.

During this test the bogie vehicle impacted the end of the 50% flattened W-beam at 8.5 m/s (19.0 mph). There was a flare end present on this test. As a result of warping in the beam which led to misalignment, the beam started to buckle toward the post, instead of away from it. This resulted in a testing configuration which was uncharacteristic of that found in the system. This test was therefore considered to be invalid, and the accelerometer data is not reported.

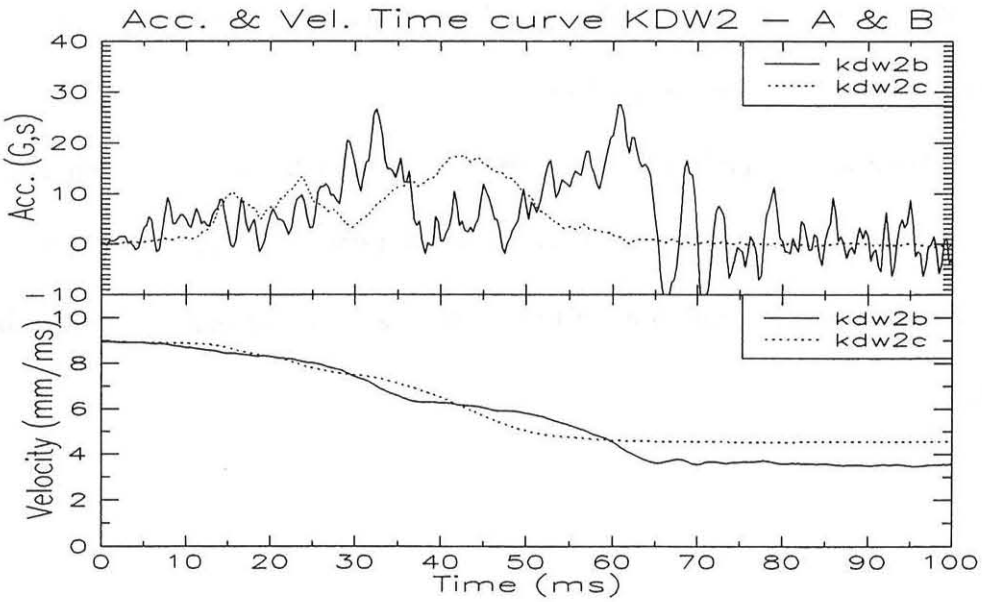

Figure 22. Acceleration and change in velocity for 50% flattened W-beams.

5.2.3 KDW3 Series

The KDW3 series consisted of dynamic bogie tests on W-beams with a 305 mm (12 in.) long section in the center which was flattened 100%. The test configuration for each of the tests in this series were identical so that the repeatability of the performance could be estimated.

Test KDW3A.

In this test the 100% flattened W-beam was impacted by the bogie vehicle traveling at 8.9 m/s (19.8 mph). The center of the beam was supported on a metal ledge bolted to the post. The flattened section had a width of 483 mm (19 in.), hence a longer 559 mm (22 in.) blockout was required to attach the shelf bracket to.

The beam folded into a 'Z' shape with the folds being on the front and the rear sides of the flattened section only and the section itself remaining flat. Photographs of this test are presented in Figure 23, and plots of the accelerometer and change in velocity data are shown in Figure 25.

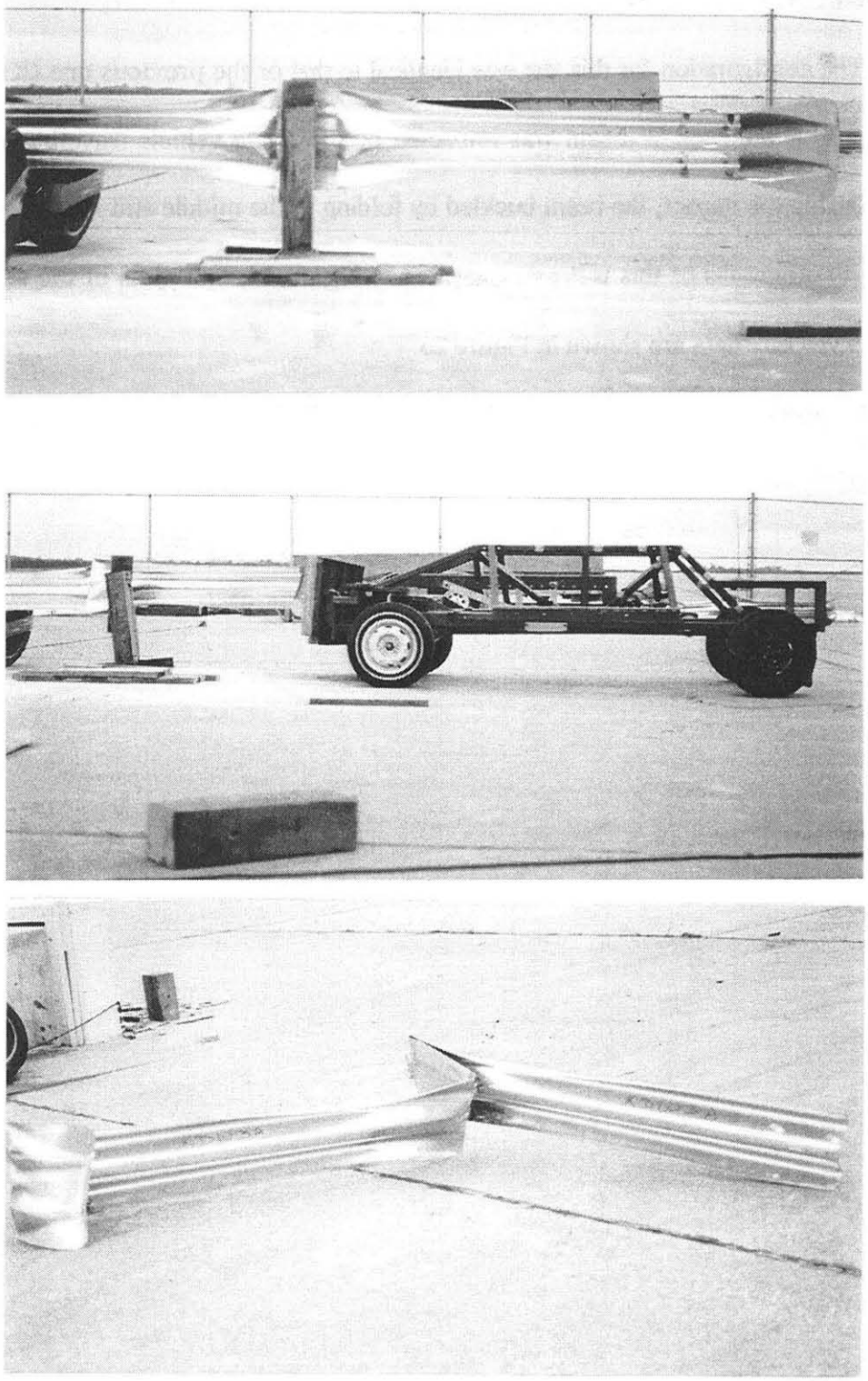

Figure 23. Test KDW3A before, during, and after impact.

Test KDW3B.

The configuration for this test was identical to that of the previous one (KDW3A). In this test the 100% flattened W-beam was impacted by the bogie vehicle traveling at 9.1 m/s (20.3 mph). During the impact, the beam buckled by folding in the middle and rear end of the flattened section. Photographs of this test are presented in Figure 24, and plots of the accelerometer and change in velocity data are shown in Figure 25.

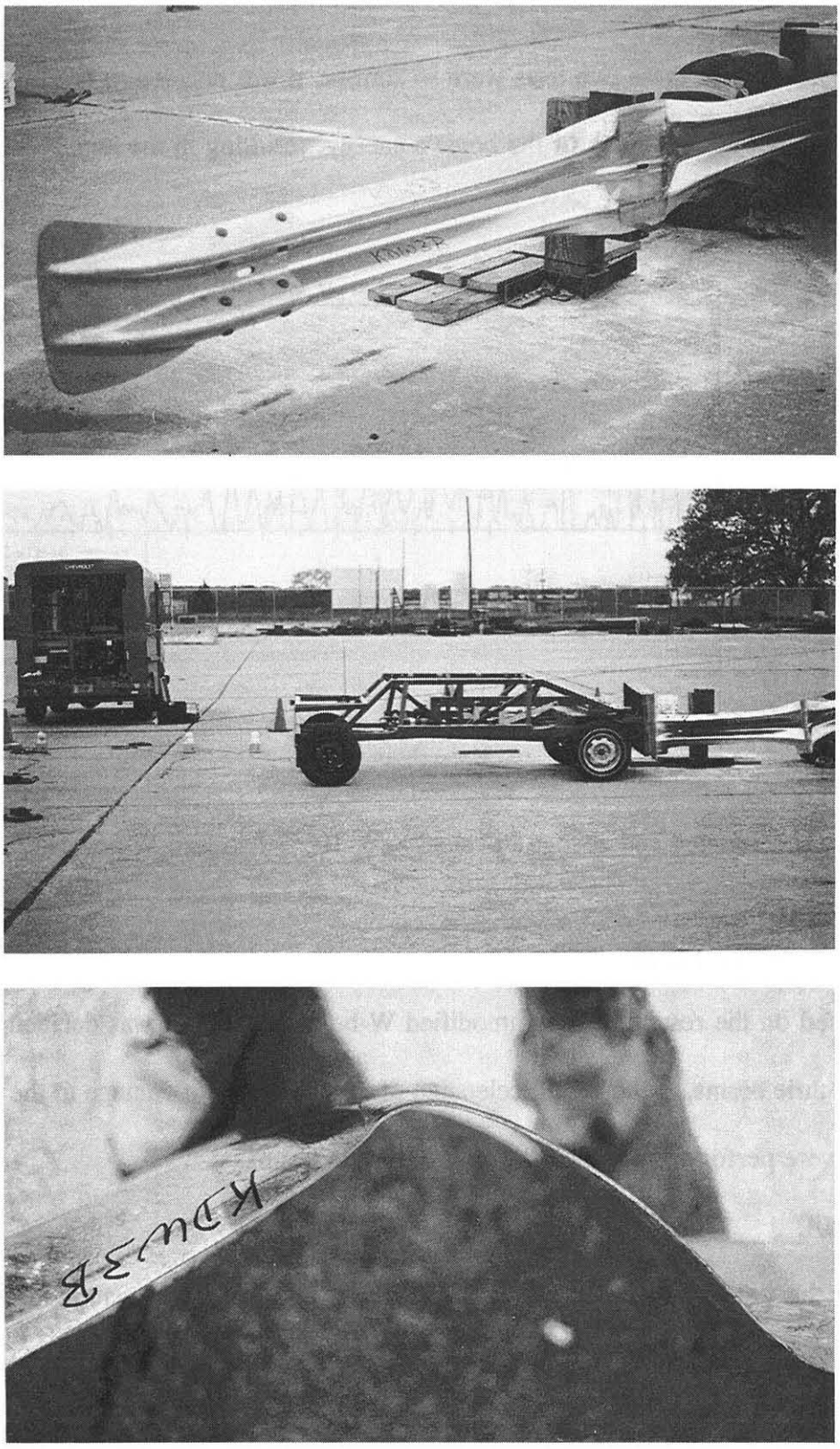

Figure 24. Test KDW3B before, during, and after impact.

Since the results from these two tests were so similar, it was decided to test only two samples. The beam did not absorb much of the bogie's energy, resulting in the impact with the post and the concrete block in these tests.

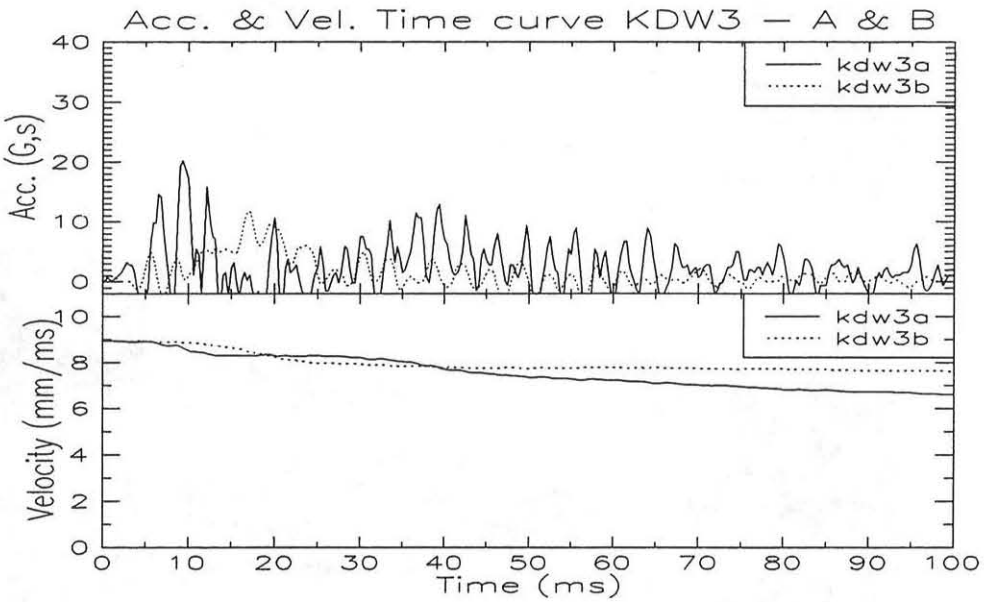

Figure 25. Acceleration and change in velocity for 100% flattened W-beams.

5.2.4 KDT5 Series

Based on the results of the unmodified W-beam impacts, it was decided not to test the unmodified thrie beams, as the high deceleration rates could result in damage to the bogie vehicle. Two tests were performed for the 50% flattened thrie beams.

Test KDT5A.

For this test a W-beam flared end was attached to the lower corrugation to prevent the end of the thrie beam from gouging into the plywood on the bogie impact head. 711 mm (28 in.) long blockouts were used, with the beam being simply supported on a shelf bracket bolted to it. During this test the bogie impacted the 50% flattened beam at 9.0 m/s (20.1 mph). Upon impact

the bogie yawed 70 degrees and stopped without hitting the post. Photographs of this test are presented in Figure 26, and plots of the accelerometer and change in velocity data are shown in Figure 28.

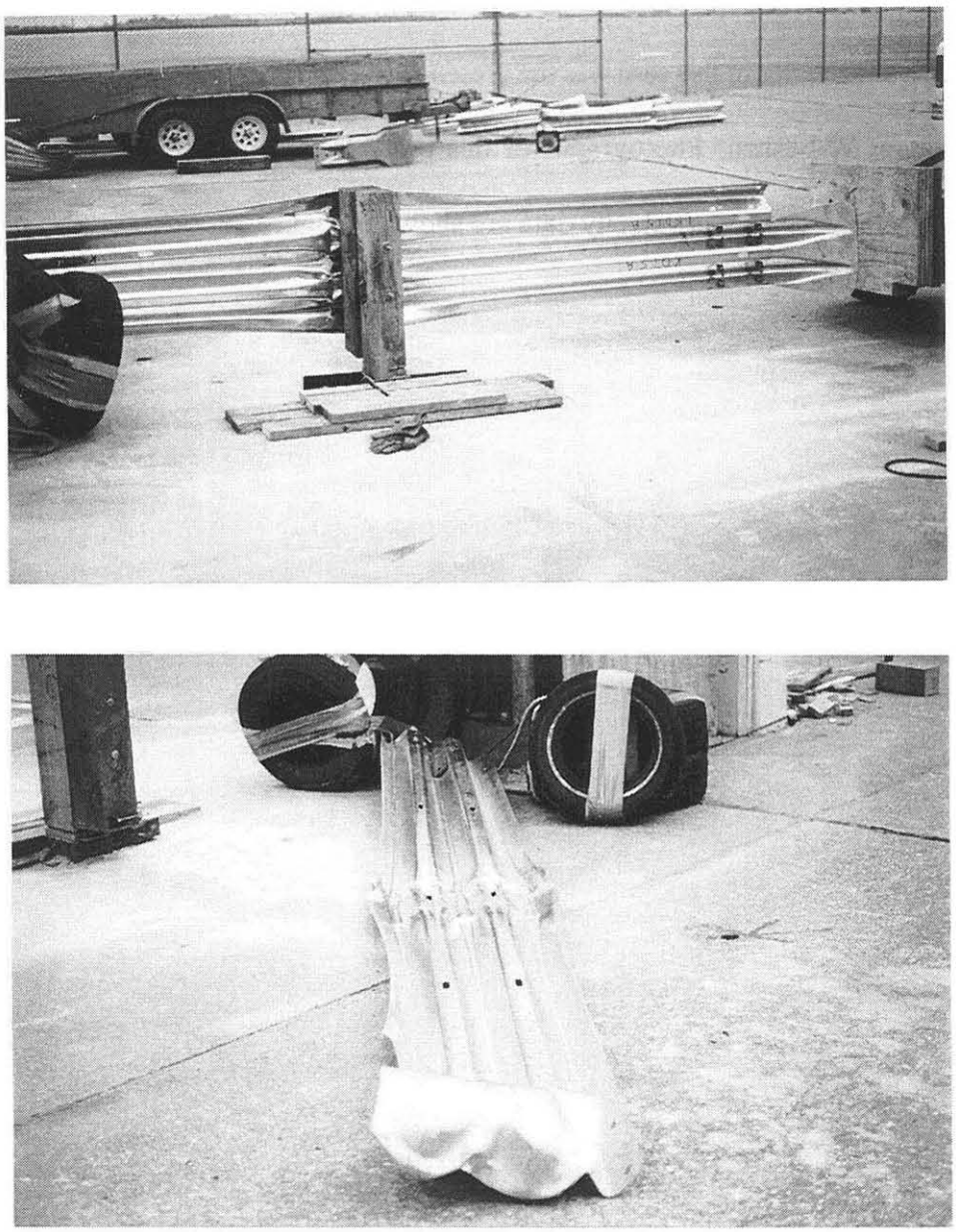

Figure 26. Test KDT5A before and after impact.

Test KDT5B.

The configuration for this test was similar to that of Test KDT5A except that its end was fitted with a thrie beam flare end instead of a W-beam end. The impact speed for this test was 8.9 m/s (20.0 mph). The mode of failure was similar to that of KDT5A. The acceleration curves had the first peak more prominent than in the previous case. The noticeable difference in the acceleration time curves in this case was the presence of a third peak instead of the usual two as seen in the case of W-beams. Photographs of this test are presented in Figure 27, and plots of the accelerometer and change in velocity data are shown in Figure 28.

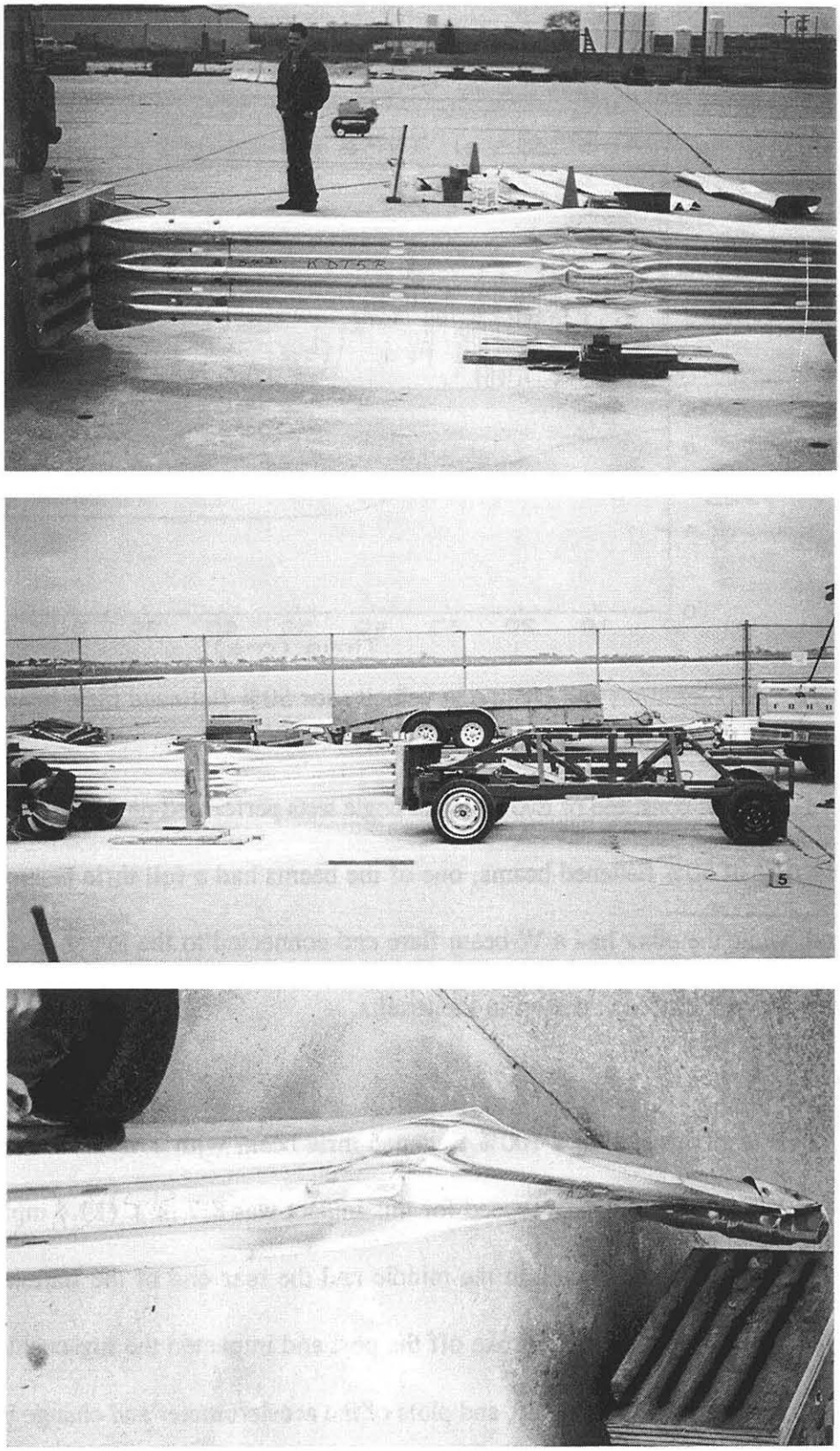

Figure 27. Test KDT5B before, during, and after impact.

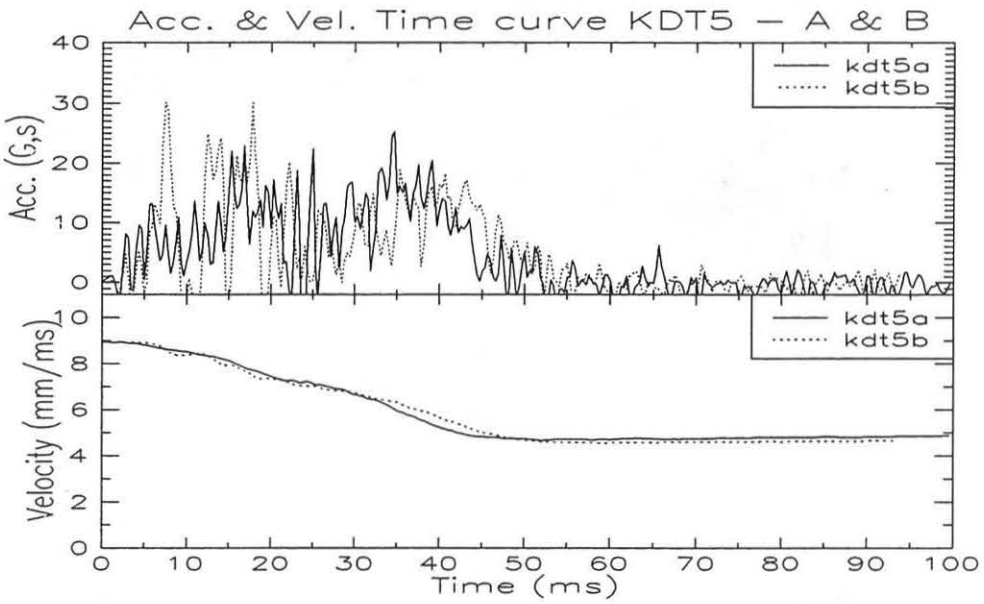

Figure 28. Accelerations and change in velocity for 50% flattened thrie beams.

5.2.5 KDT6 Series

This series consisted of two dynamic bogie tests performed on 100% flattened thrie beams. As in the case of 50% flattened beams, one of the beams had a full thrie beam flare end attached to its end, while the other had a W-beam flare end connected to the lower corrugation. This did not cause any noticeable variation in the results.

Test KDT6A.

This test consisted of a 100% flattened thrie beam with a W-beam flare end attached to the lower corrugation. The bogie speed for this impact was 8.7 m/s (19.4 mph). Upon impact, the thrie beam failed by folding in the middle and the rear end of the flattened section. After failing the thrie beam, the bogie broke off the post and impacted the tire cushions. Photographs of this test are presented in Figure 29, and plots of the accelerometer and change in velocity data are shown in Figure 31.

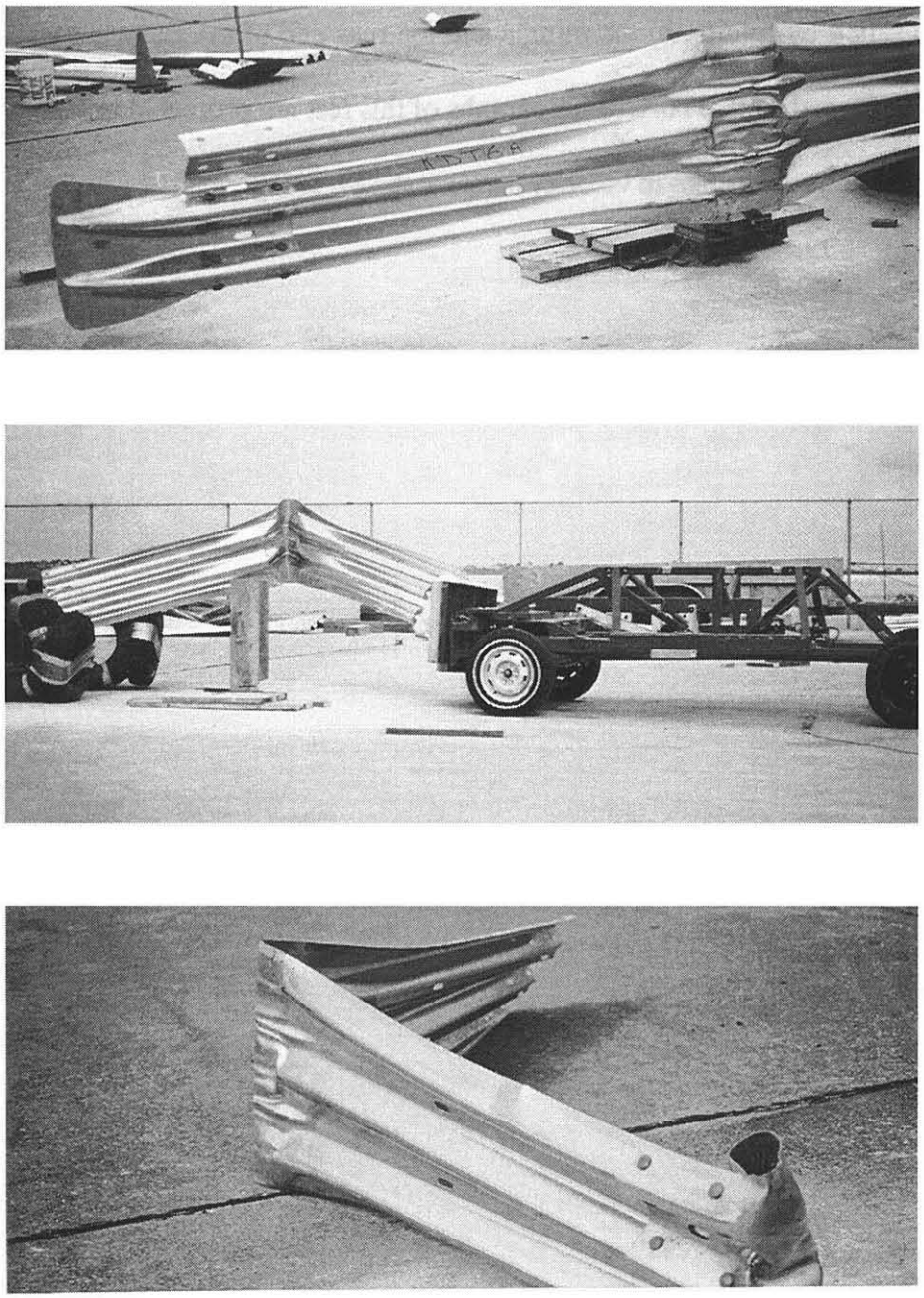

Figure 29. Test KDT6A before, during, and after impact.

Test KDT6B.

This test was similar to Test KDT6A except that a thrie beam flare end was attached to the end of the rail. The bogie speed for this impact was 9.0 m/s (20.1 mph). Upon impact, The thrie beam failed by folding in the middle and the rear end of the flattened section. The results were similar to that of KDT6A. Photographs of this test are presented in Figure 30, and plots of the accelerometer and change in velocity data are shown in Figure 31.

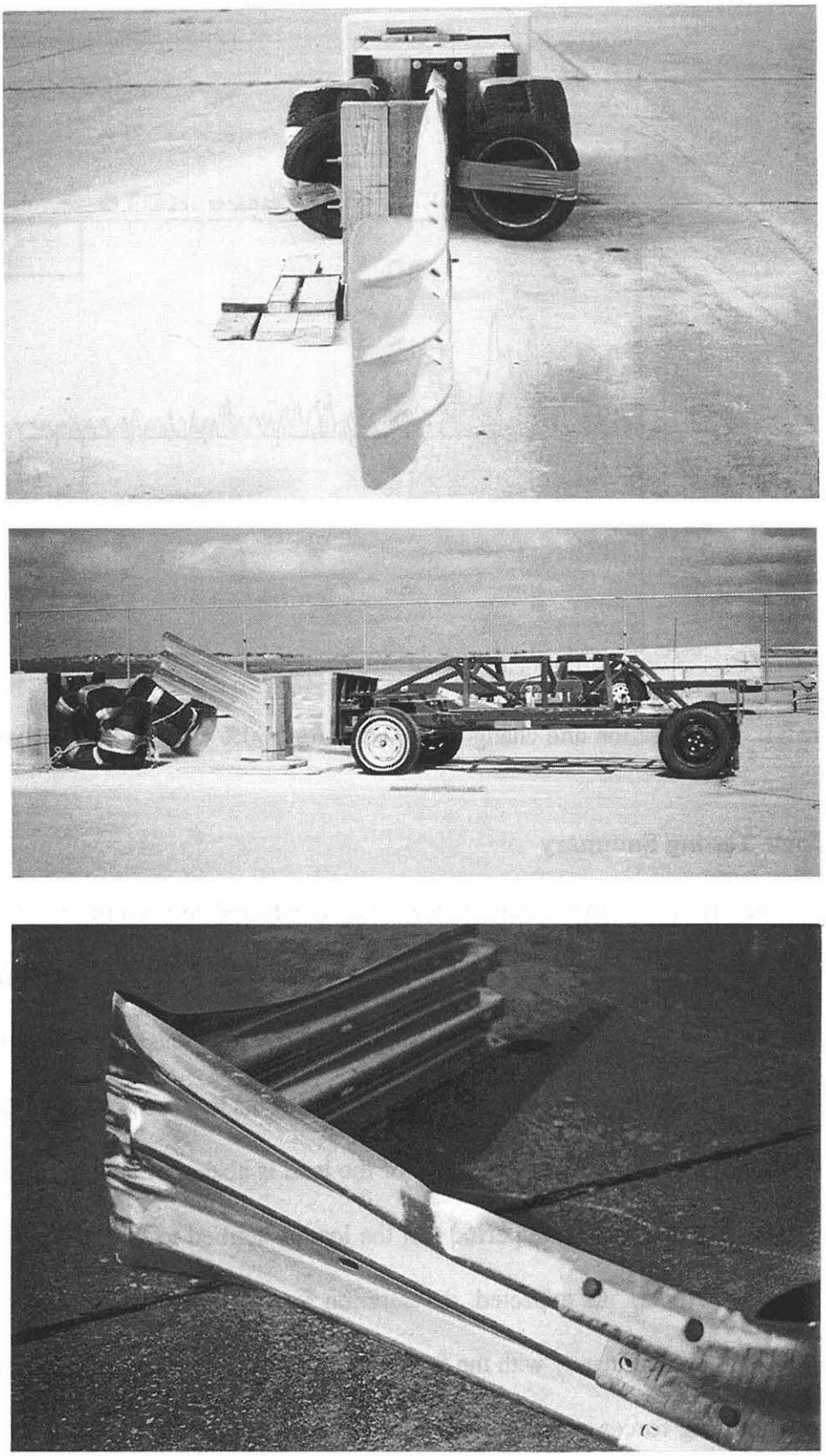

Figure 30. Test KDT6B before, during, and after impact.

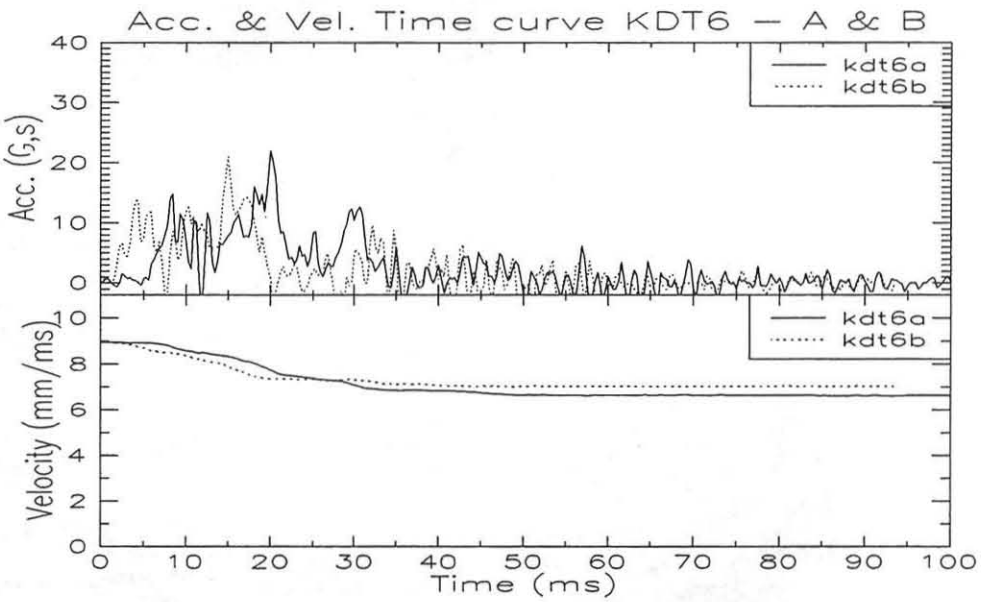

Figure 31. Acceleration and change in velocity for 100% flattened thrie beams.

5.3 Bogie Testing Summary

The dynamic bogie tests which were conducted are summarized in Table 5. The accelerometer data was filtered with a 180 Hz low pass filter, and the force values obtained from this data are presented in Table 6. The first peak referred to in the table corresponds to the failure of the flared end section, and the second peak represents the buckling of the beam. In addition to comparing the peak forces, the duration of the load is also an indicator of how the system will perform. The shorter the time period that the load is applied to the vehicle, the less yaw it will induce in the vehicle. As expected, the duration for which a 45 kN (10 kip) force lasted in the impact decreased significantly with the flattening of the rail. It was evident from these test results that the buckling forces of the 100% flattened W-beam and thrie beam samples were greatly reduced from the standard specimen. Even though it was anticipated that the 100% flattened W-

beam would perform better for end on impacts, it was decided to pursue the 100% flattened thrie beam system because of its anticipated improved redirectional performance. As discussed previously, the redirectional performance is a concern because the new criteria which the system will be tested to, NCHRP Report 350 (14), requires that the terminal be capable of redirecting a 3/4 ton pickup impacting the beginning of the length of need at 100 km/h and 20 degrees. Previous testing (15) has shown that the performance of standard W-beam system is questionable under these impact conditions because of the high center of gravity and bumper mounting height of the 3/4 ton pickup.

The most critical test for this system was thought to be the head on test with an 820 kg (1800 lb) small car. The system was constructed and subjected to this test in order to evaluate the effectiveness of this system.

Table 5. Dynamic Testing Summary

Test	Bogie Speed (mph)	Rail Type	Percent Flat (%)	Comments
KDW1A	21.1	W	0	Local buckling occurred at the impacted end of the sample, which became embedded in the wood on the impact head. The beam was bolted to post, and there was no flared end.
KDW1B	18.9	W	0	Beam buckled in the center with the bogie stopping before post.
KDW1C	20.3	W	0	In plane and out of plane buckle at the first quarter point of the beam.
KDW1D	20.5	W	0	The outer flanges warped inside, while buckling in the center of the beam.
KDW2A	19.2	W	50	Folded in the middle and at the far end of the flattened section while buckling.
KDW2B	20.2	W	50	Buckled in the center.
KDW2C	19.0	W	50	Results not appropriate. The rail started to buckle toward the post because of the initial shape of the rail.
KDW3A	19.8	W	100	Flattened section folded into a 'Z' shape.
KDW3B	20.3	W	100	Buckled by folds in the middle & end of the flattened section.
KDT5A	20.1	T	50	Bogie yawed 70 deg. Beam with very slight buckle in the center.
KDT5B	20.0	T	50	Test results similar to KDT5A.
KDT6A	19.4	T	100	Buckled by folding in the middle and end of the flattened section.
KDT6B	20.1	T	100	Similar results to KDT6A with the buckle by folding.

Table 6. Bogie Test Force Comparison

Beam Type & Flattening	Peak 1 (kN)	Peak 2 (kN)	Duration (ms) At 45 kN
W 0%	143	232	55
W 50%	168	185	42
W 100%	72	NA	6
Thrie 50%	165	121	43
Thrie 100%	89	117	17

6 GUARDRAIL MATERIAL TESTING

One of the most important factors in obtaining realistic finite element simulation results is the use of correct material properties for the model. Absence of relevant material property data is one of the leading causes of incorrect modeling. Material testing was performed on guardrail material to obtain the required properties since the existing data was not only insufficient but its accuracy was questionable. This section describes the procedure followed for material testing and presents the results.

6.1 Objective

The objective of performing these tests was to get authentic information on the mechanical properties of guardrail steel, as well as to investigate the variations of the properties along the curves of the rail. The properties were expected to vary slightly across the surface of the rail because of the variation in the hardness. Cold rolling of rails during manufacture changes hardness and consequently the strength. This change depends on the extent of cold working which occurs more on curves than on the straight portions of the rails. The investigated properties were:

1. Yield Stress
2. Plastic Strain at Failure
3. Effective Plastic Strain Values
4. Corresponding Yield Stress Values
5. Young's Modulus
6. Surface Hardness

6.2 Test Procedure

An Instron mechanical screw drive machine was used to pull the samples to failure. The

testing procedure as well as the methods used to obtain the desired values are discussed below.

6.2.1 Sample Preparation

1. The test coupons were cut out of the guardrail material according to the shape and the dimensions specified by ASTM E8-90A standard test methods for tension testing of metallic materials as shown in Figure 32 (16). This was performed in a machine shop with the pattern being cut on the beam section both longitudinally and laterally, as shown in Figure 33. Seven coupons were cut using a band saw, and the samples cut from curved sections were flattened out mechanically.

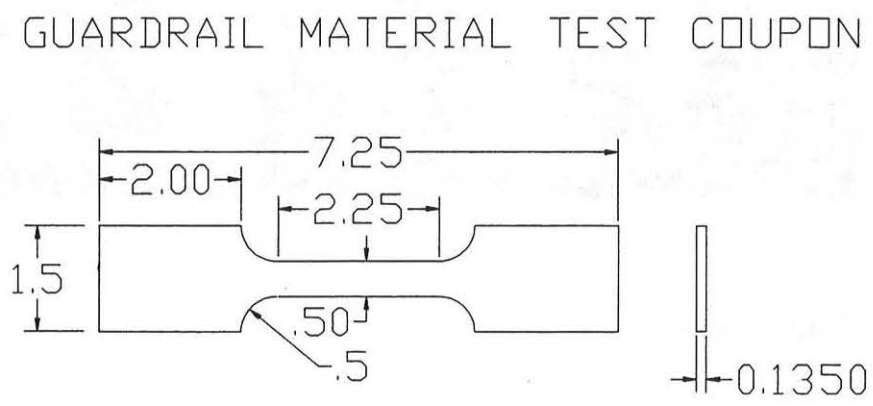

Figure 32. Material test coupon (all units in inches).

2. Sample width, thickness, and length between the gage marks were then measured and recorded for each individual specimen in accordance with ASTM specifications. Galvanized platting thickness was measured using a Fisher DALTASCOPE.

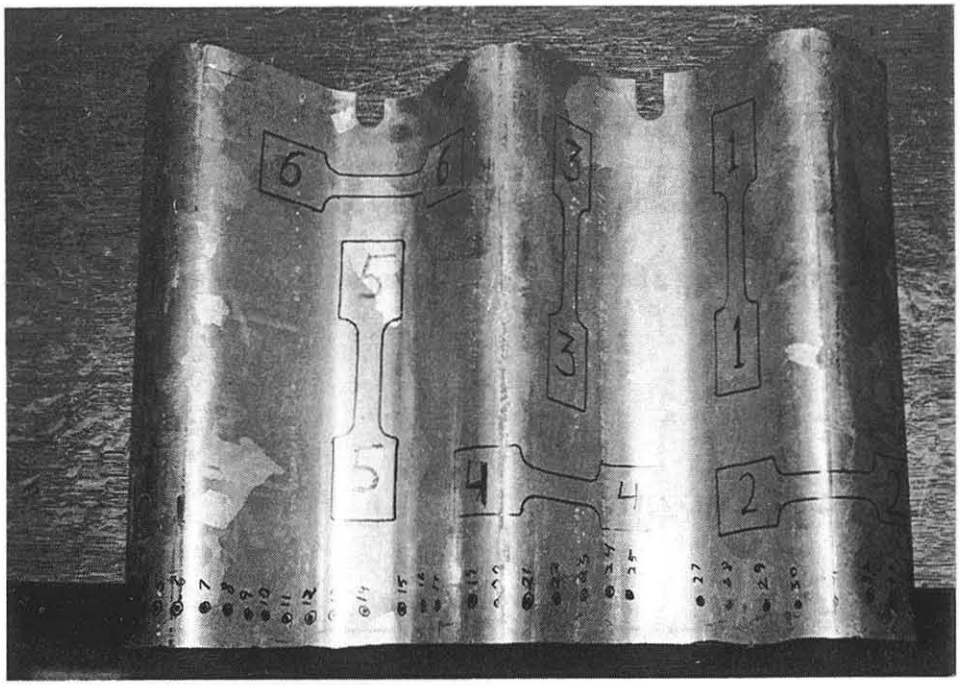

Figure 33. Coupon locations.

6.2.2 Yield Stress

The yield force, found using the 0.2% offset method, is divided by the original cross-sectional area to give the yield stress.

6.2.3 Engineering Stress Strain

Ten points were selected manually on the vertical axis of the plotter charts at equal intervals. A line with a slope equal to that of the elastic region of the curve was drawn at each of the 10 deflection points. The force 'F' for each point was given by the chart load reading at the intersection

of these lines with the plotted curve in the plastic region. Engineering stress 'S' was then calculated using the formula

$$S=\frac{F}{A_O}$$

for each of the ten points. F being the tensile force and A_0 the initial cross-sectional area of the specimen. This was done for each sample, except for some samples which failed before reaching sufficient strain values to obtain 10 sample points.

The engineering strain was determined by dividing the change in length Δl by the initial length, l_0.

$$\epsilon=\frac{\Delta l}{l_0}$$

6.2.4 True Stress Strain

True stress strain curves refer to the actual stress and strain based on the instantaneous cross-sectional area as the sample is being pulled, as opposed to engineering strain curves which are obtained using the initial cross-sectional area of the sample. It is very difficult to obtain the instantaneous cross-sectional area directly, so these values are obtained by assuming constant volume of the material until the point of necking which gives

$$\sigma_{true}=S(1+\epsilon)$$

where σ_{true} is the true stress, S the engineering stress and ϵ is the engineering strain (16).

True strain ϵ_{true} assuming a constant volume is given by

$$\epsilon_{true}=\ln(1+\epsilon)$$

The true fracture stress is obtained by dividing the load at fracture by the cross-sectional area

at fracture. True fracture strain ϵ_f is given by the relation

$$\epsilon_f = \ln \frac{A_o}{A_f}$$

This gives the value of plastic strain at failure (17). Eight points were then selected from the true stress/strain curve to obtain effective plastic stress/strain values. The effective plastic strain is calculated by subtracting the true strain at yield from the true strain at that particular point. Hence, the first point would have an effective plastic strain of 0.0 and the corresponding stress equals the yield stress.

6.2.5 Young's Modulus

Machine compliance prevented the accurate measurement of Young's modulus. Therefore, this value as well as that of the density and Poisson's ratio were taken from the standard values in literature (17).

6.2.6 Surface Hardness

Hardness was measured using a Wilson Rockwell Hardness Testing machine along the curves of the beam at intervals of 10 cm (4 in.) from one end to the other. The galvanized coating was first chemically removed from the test sample. Rockwell 'B' hardness was then measured using a 100 kg (220 lb) mass with a 1.6 mm (1/16 in.) diameter penetration ball. The readings were then correlated with the strength from Hardness Relationship Scales. The correlated variation for the bends and the straight portions of the guardrail was calculated. The percentage variation was used to obtain the effective plastic stress of the material at the curves from the experimentally measured values from the straight portions.

6.3 Test Results

The results of these tests are presented in Figure 34, and Tables 7 and 8. From the hardness tests at various points across the surface of the W-beam it was found that the yield stress of the guardrail material increased by approximately 6.6% at the bends as opposed to the straight portions, hence these values were increased by 6.6% to obtain the effective stresses at the curved portions of the beams. The effective strain and corresponding stresses used in the simulation are presented in Table 9.

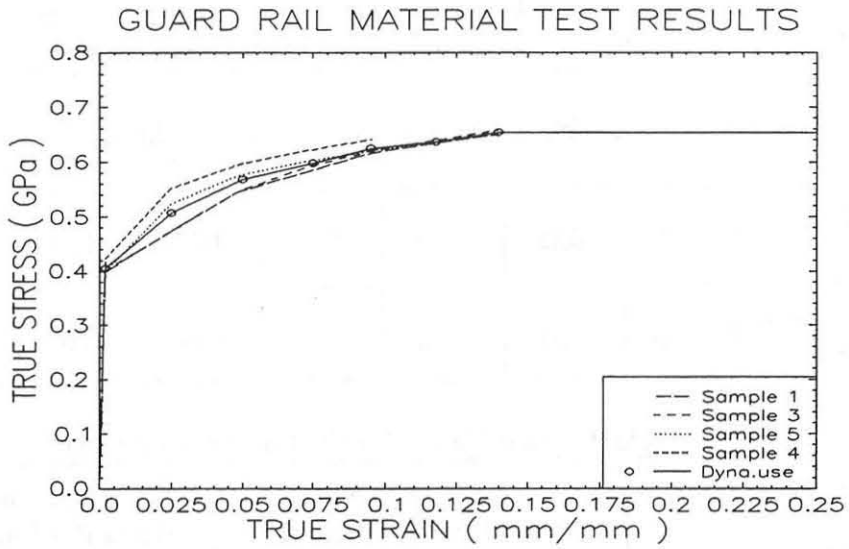

Figure 34. True stress/strain curves for the guardrail steel samples.

Table 7. Plastic Region Stress/Strain Values.

True Strain (mm/mm)	Stress Sample 1 (GPa.)	Stress Sample 3 (GPa.)	Stress Sample 4 (GPa.)	Stress Sample 5 (GPa.)
0.002	0.398	0.401	0.399	0.423
0.025	0.474	0.473	0.523	0.551
0.050	0.546	0.547	0.576	0.595
0.072	0.581	0.589	0.600	0.620
0.095	0.616	0.620	0.620	0.640
0.118	0.634	0.639	0.635	NA
0.140	0.650	0.658	NA	NA

Table 8. Average Stress/Strain Values.

True Strain (mm/mm)	.002	.025	.049	.072	.095	.118	.140	1.0
Average Stress (GPa.)	.405	.507	.568	.597	.624	.636	.654	.654

Table 9. Input Values for the LS-DYNA3D Deck.

Effective Plastic Strain	Corresponding Stress (Flat Portion of Beam)	Corresponding Stress (Bent Portion of Beam)
0.000	0.405 GPa.	0.432 GPa.
0.023	0.507 GPa.	0.541 GPa.
0.047	0.568 GPa.	0.606 GPa.
0.070	0.597 GPa.	0.637 GPa.
0.093	0.624 GPa.	0.665 GPa.
0.116	0.636 GPa.	0.678 GPa.
0.138	0.654 GPa.	0.697 GPa.
0.998	0.654 GPa.	0.697 GPa.

7 BASELINE MODEL SIMULATION

The baseline model for simulation refers to the master model of the unflattened W-beam which was dynamically buckled in the field bogie tests. After obtaining accurate simulations on the master model the parameters such as the shape and the impact conditions can then be altered to predict results on the modified versions of the design. This is the essence of design development using finite element modeling and simulation. This section describes the three main steps of nonlinear explicit finite element analysis in the component testing of this guardrail terminal. These steps are preprocessing, analysis, and postprocessing. The last section compares the baseline model results with the actual crash test.

7.1 Preprocessing

7.1.1 Background

The preprocessing of this model involved drawing and mesh generation of the complete field setup. This included representation of the bogie and the W-beam, as well as the post and the flared end fixed to the impacted end of the rail. The concrete block with the fixture for the beam was also simulated in the model. Subsequent sections describe the complete process. Iterative changes in meshing and drawing of the baseline model with the progress of FE analysis on the W-beam impact buckling have been documented in the last section.

7.1.2 Geometry and Mesh Generation

The software used for preprocessing the mesh for the DYNA deck was HyperMesh. HyperMesh is a preprocessing software suitable for drawing, as well as mesh generation of models. It is marketed by Altair Computing, Inc. based in Troy, Michigan (19).

The first step in creating the model was to import an ACAD drawing of the W-beam profile

into HyperMesh. The dimensions of the beam were taken from the standard specifications for Corrugated Sheet Steel Beams for Highway Guardrail AASHTO Designation: M 180-78. Meshing was done by extension of the W-shape to a length of 4128 mm (162.5 in.) initially with an asymmetrical mesh of 19 four node shell elements across and 164 elements along the length of the beam. The resulting mesh is shown below in Figure 34. After completion of W-beam mesh, its elements at the straight and the bent portions were divided into different components to give different material properties to these sections of the beam.

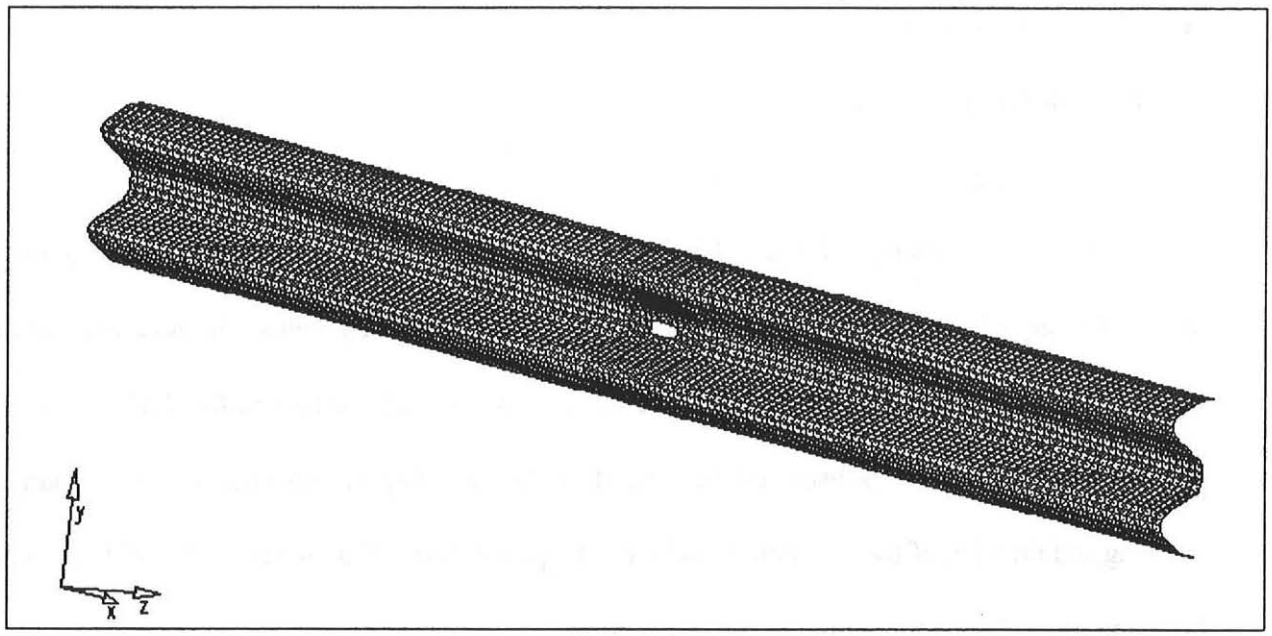

Figure 34. Meshed W-beam model.

The meshing of the flared end was drawn in HyperMesh manually. Coordinates of strategic points were taken from a flared end. The nodes resulting from these coordinates formed the flare geometry. Initial analysis resulted in incorrect spoon shape deformation, requiring the spoon to be redrawn and remeshed as shown in Figure 35.

The bogie vehicle was modeled into a simple cuboid with eight node solid elements, as shown in Figure 36. This was done to reduce the CPU time since the post impact bogie analysis was not the focus of the study. The post and the blockout were constructed from solid elements. A shell element open box was used to represent the fixture holding the end of the beam in place. Nodes at the bottom of the post had fixed boundary conditions to simulate a rigid attachment to the concrete.

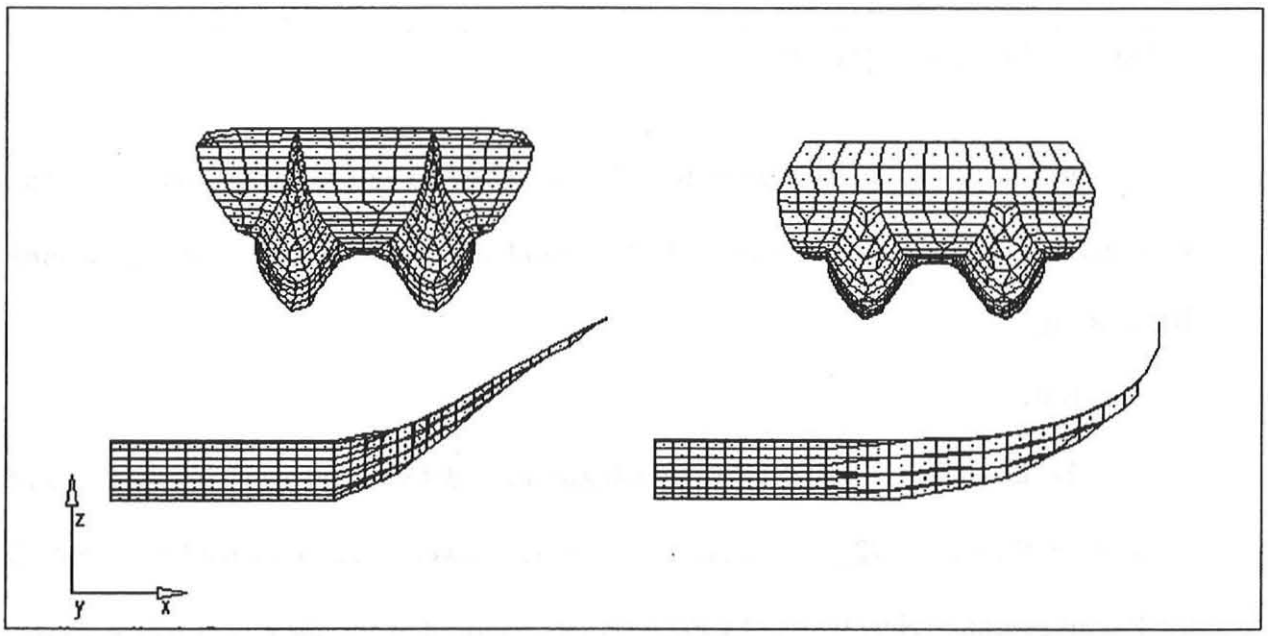

Figure 35. Flared end, initial (left) and remeshed (right).

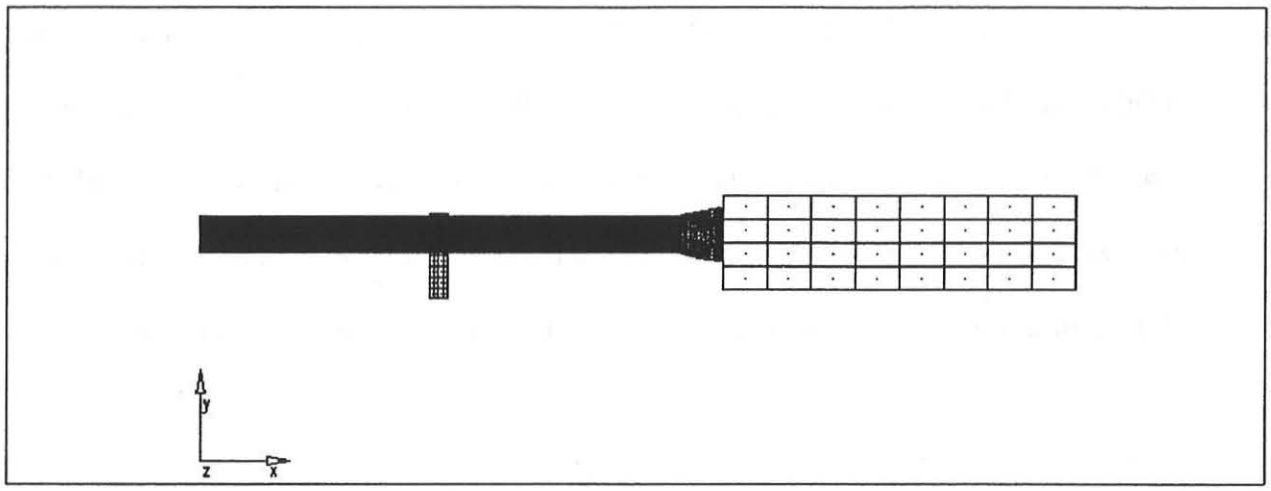

Figure 36. Bogie simulation model.

Once this model has been generated, all the duplicate nodes and elements were equivalenced. Preprocessed FE output in the form of an LS-DYNA3D input deck was then generated from HyperMesh.

7.2 Analysis

The three dimensional, dynamic, non-linear, large deformation explicit code LS-DYNA3D was used for the analyses (20). Sun Sparc 20 workstations were used to run the LS-DYNA3D deck for 150 ms of time. Nine hours of CPU time was required to run the model which consisted of 6869 shell and 272 solid elements with total 7611 nodes. The default Belytschko-Tsay shell formulation was used for all shells. The finite element entities which were specified for this model are described below.

7.2.1 Contacts

Contacts refer to the type of interaction between model surfaces. Automatic single surface contact was used for all the components of this model. This contact prevents penetration of one component into another. The coefficients of friction, both static and dynamic, were declared as 0.15.

The flared end, initially attached to the beam with spot welds, was subsequently attached with the TIED_NODES_TO_SURFACE contact. The nodes on the rail section of the flare were tied to the front rail portion of the beam.

7.2.2 Nodal Data

Nodal time histories of the node on the center of gravity of the bogie cube were read out in a file. This was done to obtain the acceleration time data from the model corresponding to the accelerometer data from the bogie vehicle.

7.2.3 Initial Velocity

The initial velocity of 8.94 mm/ms (29.4 fps) was declared on the nodes of the bogie block.

7.2.4 Shell Element Thickness

The shell element thickness was set at 2.67 mm (0.105 in.), the standard thickness for 12 gage W-beam guardrail.

7.2.5 W-beam Material Properties

The material properties of the W-beam were represented with eight effective stress-strain points from the material tests described previously. Piecewise linear plasticity properties were used to represent the material behavior.

7.2.6 Bogie Vehicle Properties

The bogie vehicle was declared as a rigid body to reduce CPU usage. This was logical since the actual behavior of the bogie was not the focal point of this research. The density of the rigid material was calculated to give the bogie a total mass of 810 kg (1786 lb).

7.2.7 Constraints

Initial runs resulted in excessive yawing of the bogie vehicle. This resulted from the absence

of ground friction present in the actual test. Rigid body rotational constraints in the 'y' direction were imposed on the bogie to prevent this yawing.

7.2.8 Stone Wall

In the initial runs, a rigid (stone) wall was used to represent the concrete backup block. However, it was determined that a rigid box made of shell elements and constrained in all directions produced better results.

7.3 Model Development

The baseline model was developed in steps. It took 44 runs and approximately 250 hours of CPU time to evolve the simulated model from the initial runs which did not match with the test results in terms of failure mode and acceleration time curves to an acceptable match for failure mode and a close similarity with the crash test acceleration curves. Description of this evolution is described in the following paragraphs.

The first crude model, shown in Figure 37, consisted of a simple W-beam backed up to a stationary wall. The impacting bogie was modeled by a moving wall. This model resulted in a deceleration curve peaking at 90 g's, with the mode of failure being a crush at the middle of the rail instead of the buckling which was seen in the test.

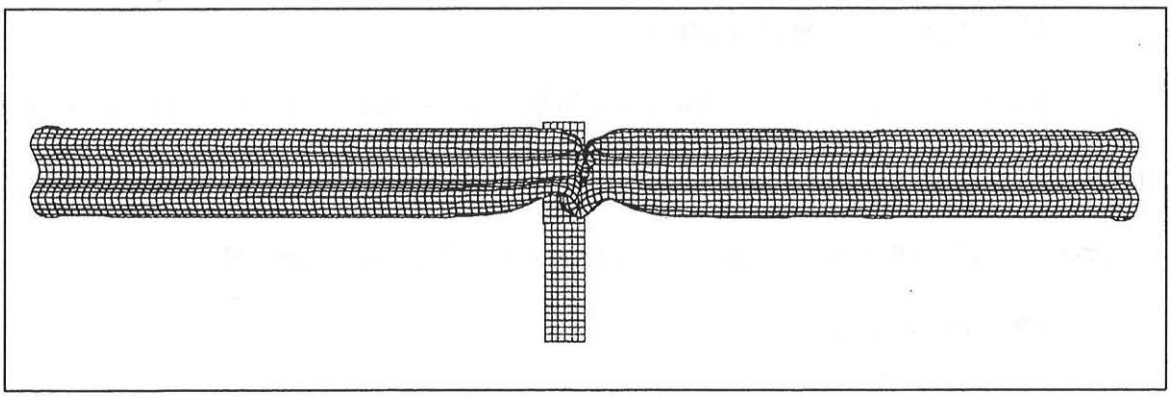

Figure 37. Results of first simulation run.

The next step was to replace the moving wall with a cuboid block representing the bogie vehicle, as shown in Figure 38. The front impact head of the bogie was represented with solid elements having material properties of wood. Contact problems resulted between the rail and the bogie. These problems could not be resolved, so it was decided to eliminated the solid elements on the front of the bogie.

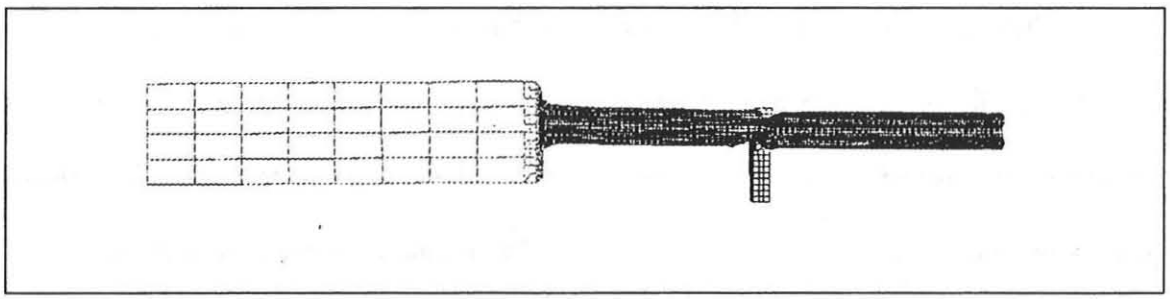

Figure 38. Baseline model with wood bumper.

In the next run, shown in Figure 39, a flared end was attached to the front of the rail with spotwelds. This resulted in localized buckling next to the edge of attached flared end. The decelerations were reduced to 36 g's, but neither the failure mode nor the velocity curve matched the physical test results.

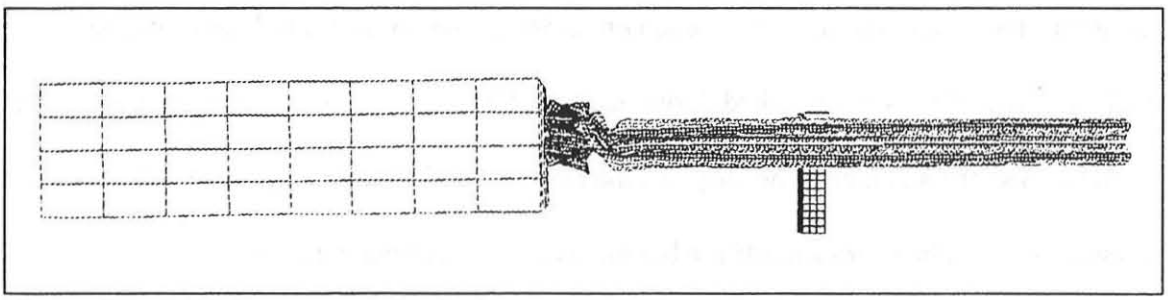

Figure 39. Initial computer simulation run with flared end.

The next iteration of the model included connecting the flared end to the end of the beam

using tied nodes to surface contact. The bogie vehicle was also given rotational constraints in the 'y' direction to prevent it from yawing. This was considered to be acceptable since it was the behavior of the W-beam which was of interest, not that of the bogie. This resulted in the buckle location being moved farther down to the quarter point closest to the bogie vehicle, as shown in Figure 40. The flared end did not collapse and roll up as was seen in the physical testing.

These problems resulted in the redrawing and remeshing of the flared end. The material tests described earlier were then conducted to obtain more accurate material properties for both the straight and the curved portions of the rail. Eight effective strain and corresponding effective stress points, obtained from material tests, were used. The automatic single surface coefficient of friction was declared to be 0.5.

The next step was to add four finite walls to represent the fixture supporting the W-beam at the far end. The W-beam rail was remeshed with a finer and symmetric (even number of elements across) mesh. This resulted in the deformed geometry shown in Figure 41.

7.4 Final Baseline Model

The final model consisted of the remeshed guardrail with ten elements in the center deleted to represent the bolt hole. The box fixture on the far guardrail end was made from rigid fixed shell elements. This provided the correct end conditions for the W-beam to behave properly. As shown in Figures 42 and 43, the remeshed flared end rolled into a cylinder as was seen in the tests, and the beam buckled at its center. The shape of the buckling deformation was identical to that seen in the physical tests. The beam slid off the bumper sideways as seen in the tests.

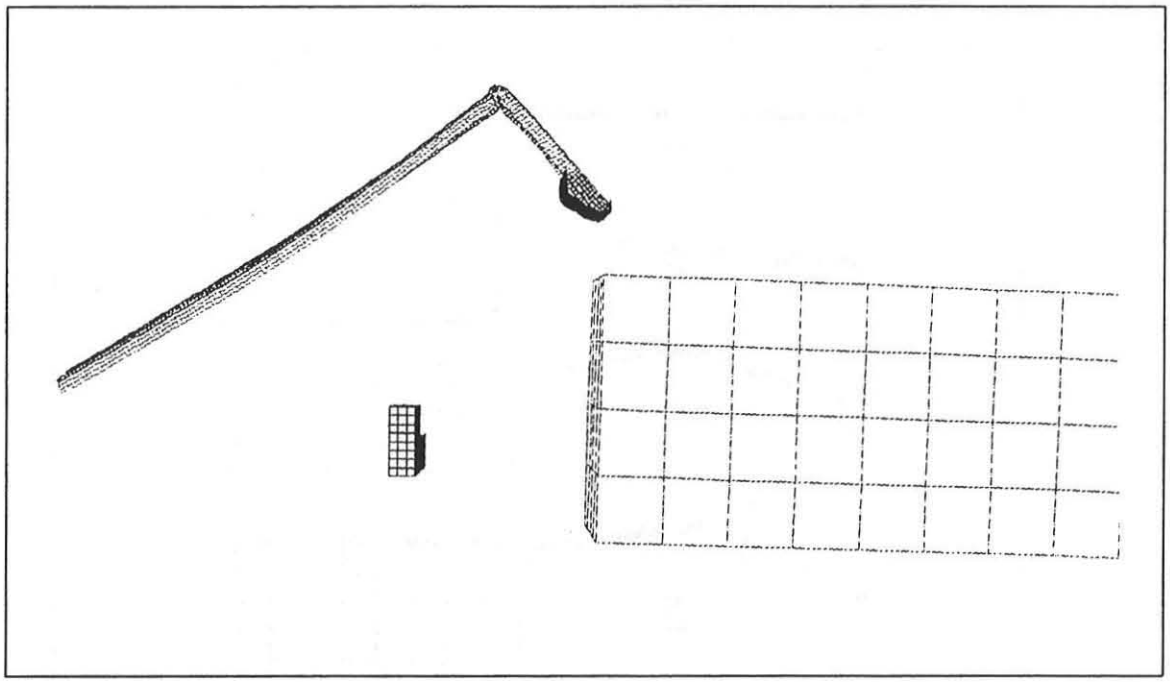

Figure 40. Buckle at front quarter point.

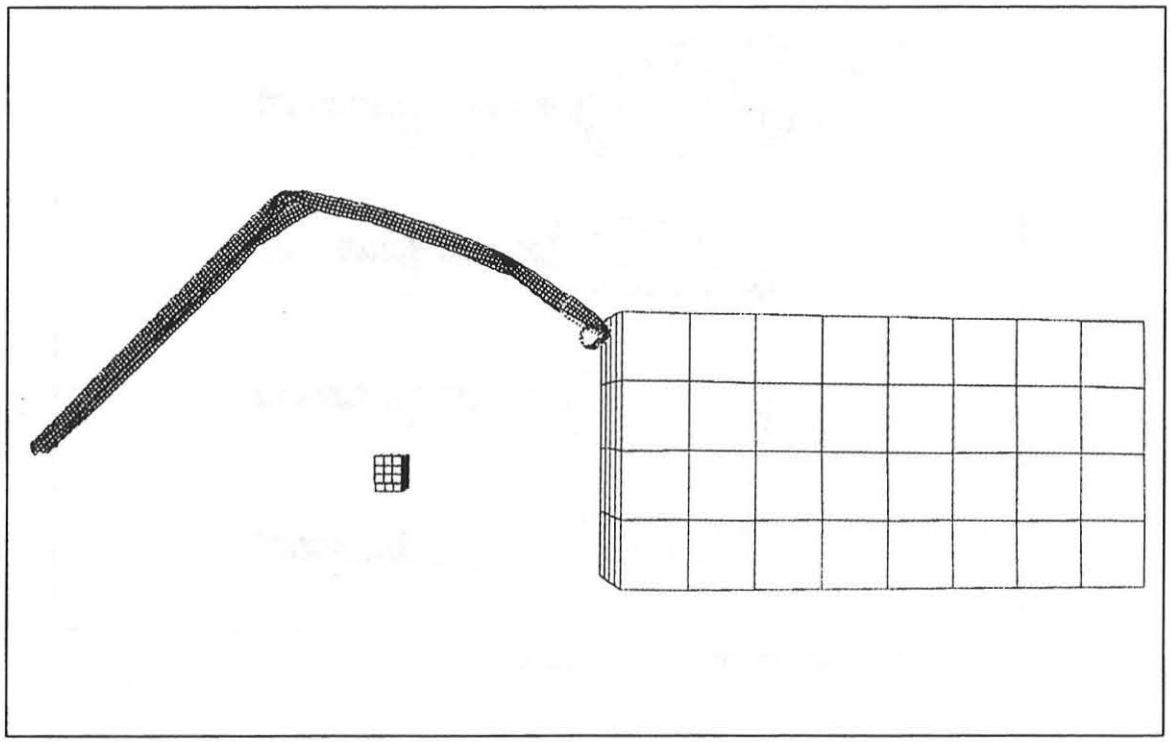

Figure 41. Buckle in middle with imperfect buckle shape.

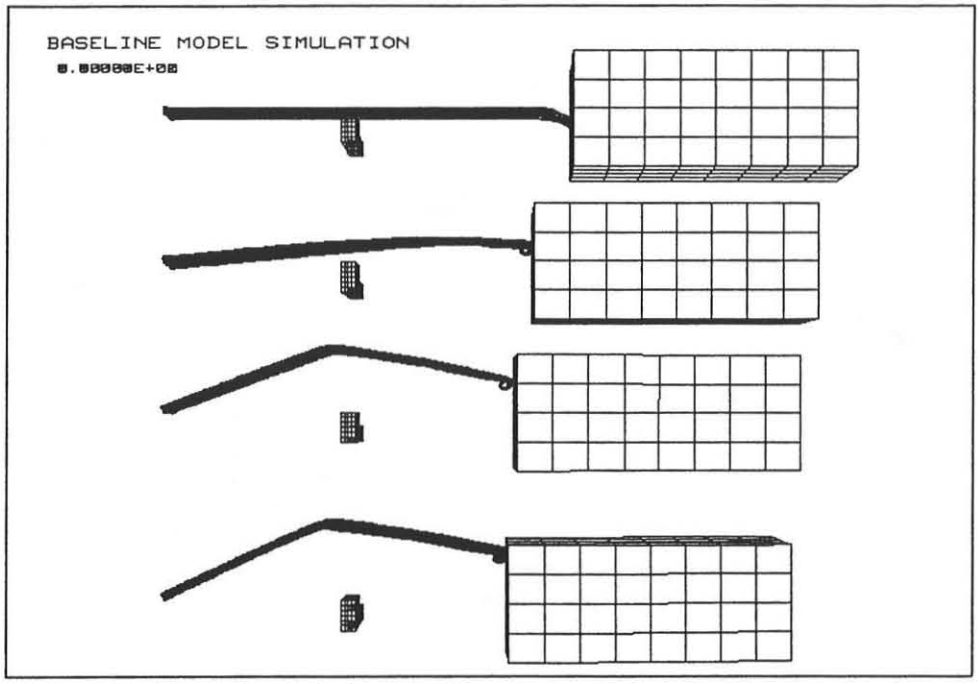

Figure 42. Top view of simulated crash.

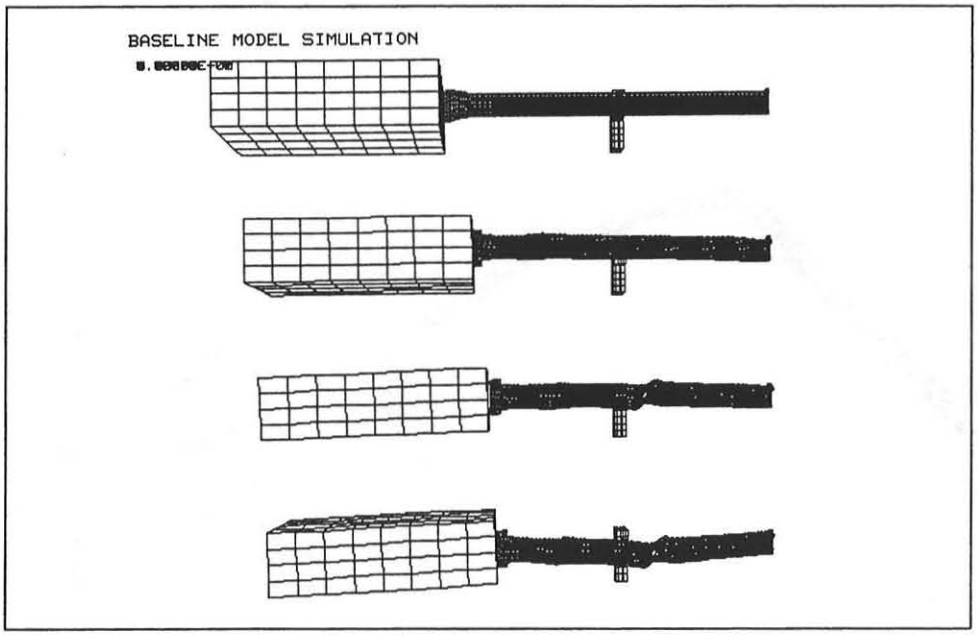

Figure 43. Side view of simulated crash.

7.5 Postprocessing

The software used for postprocessing was LS-TAURUS, an interactive post-processor developed by the Livermore Software Technology Corporation (21). This software was used to analyze the results of each run. It provided graphical output of the deformed geometries, as well as stress contours and other data.

7.6 Comparison

Figures 45 through 50 compare the post impact deformed shapes of the W-beam obtained from the actual crash tests to the simulation results. The specific geometrical deformities compared were the shape at buckling cross-section, the kink at the front quarter, and the shape of the flared end (cylindrical).

The velocity curve, shown in Figure 44, shows the same change in velocity during the first 50 ms into the impact, after which it differs by around ten percent. The acceleration curves peak at slightly different values. This is partially due to the data collection and processing methods (such as sampling rate, filtering, moving averages etc.) used while collecting the crash test data.

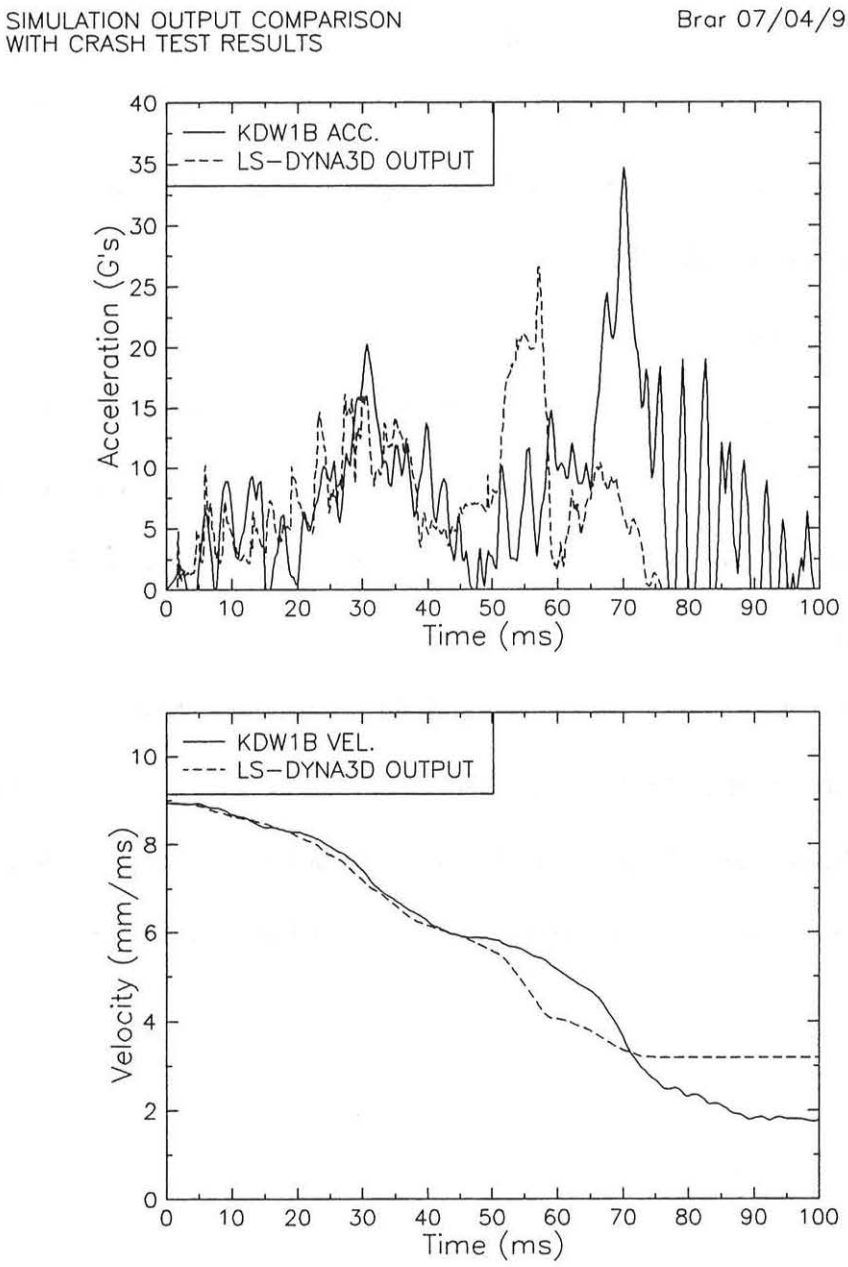

Figure 44. Velocity and acceleration time curves for simulation and actual test.

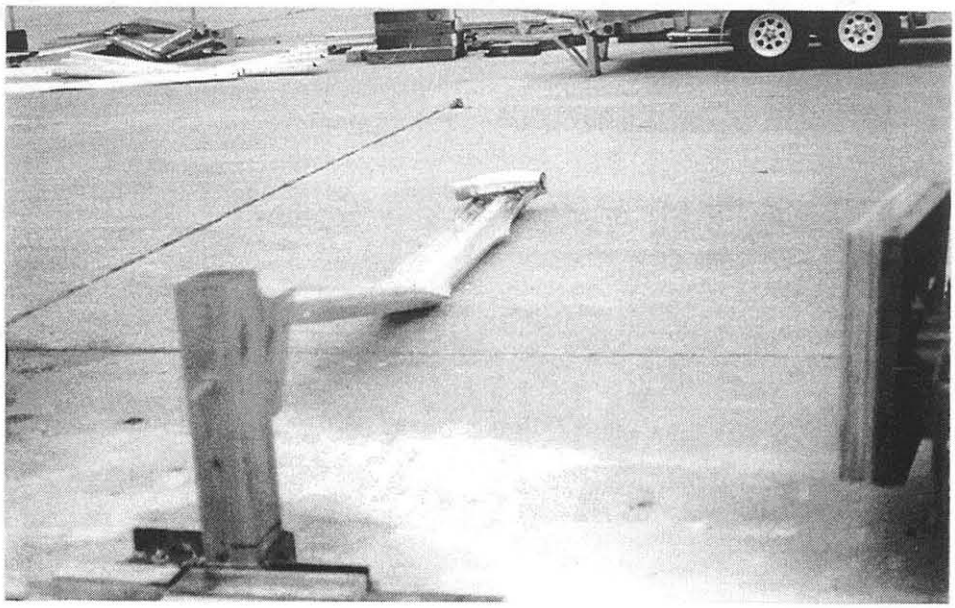

Figure 45. Crash test buckling failure.

Figure 46. Failure geometry from simulation.

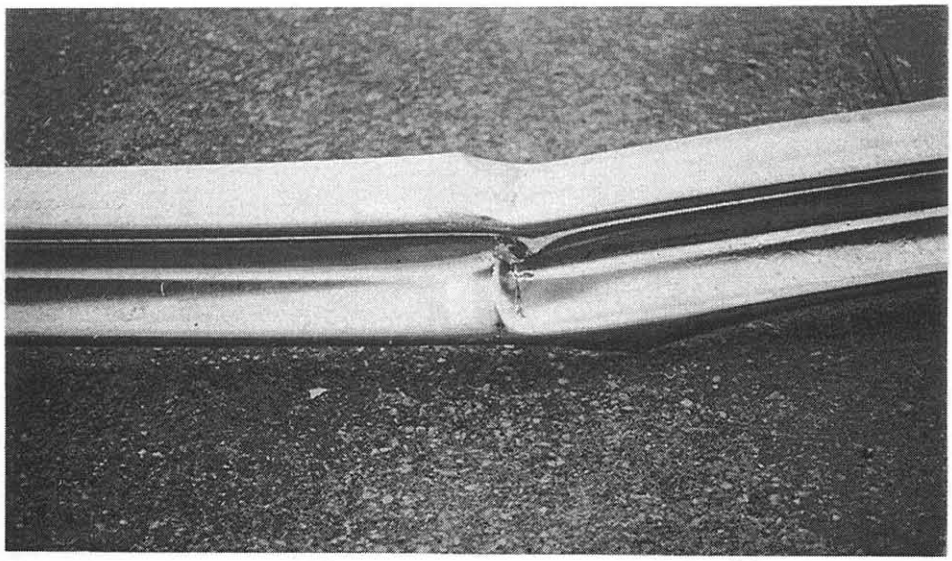

Figure 47. Post impact buckled W-beam.

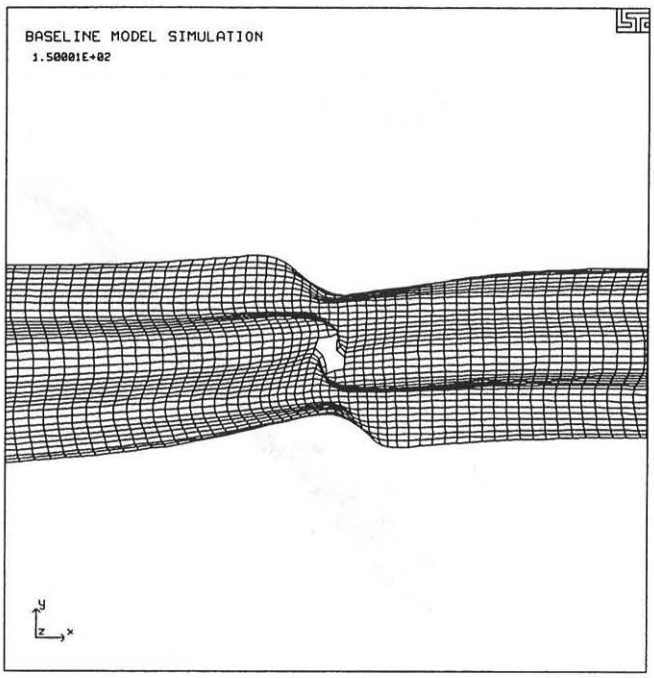

Figure 48. Post impact W-beam (simulated).

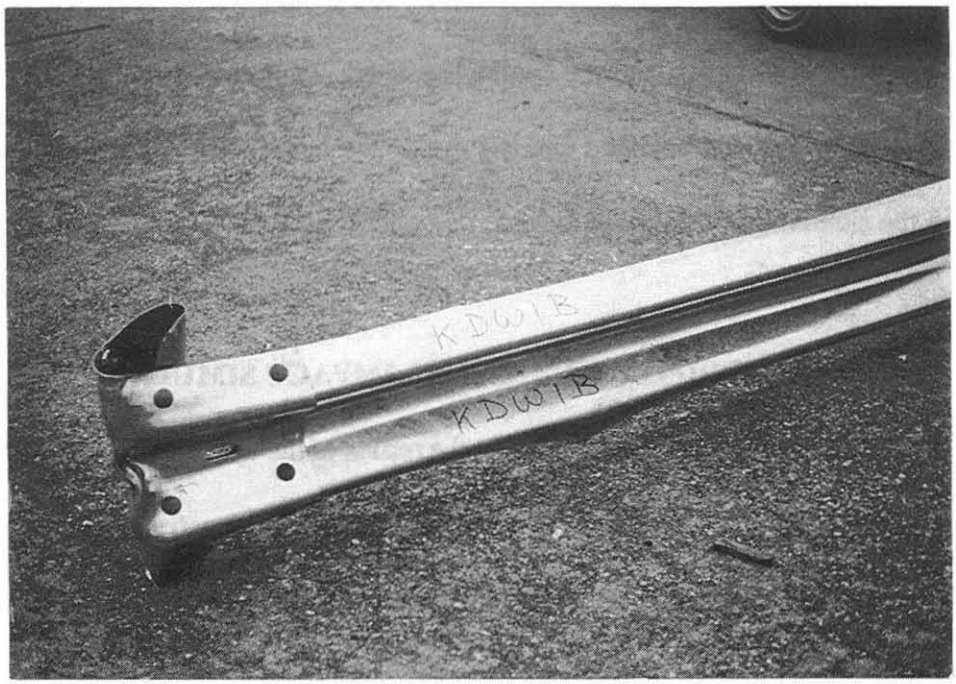

Figure 49. Front quarter kink.

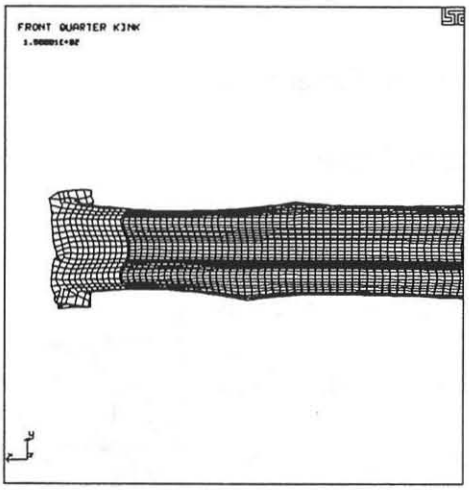

Figure 50. Front quarter kink (simulated).

7.7 Baseline Simulation Summary

With the baseline simulation model closely resembling the actual bogie testing, the impact conditions could now be varied and the results predicted. Guardrail shape (section modulus) is one of the properties which was changed and the results predicted. This effort is described in the next section on the simulation of flattened beams.

8 MODIFIED GUARDRAIL IMPACT SIMULATION

The baseline model was used to predict the results of the dynamic buckling of 50% and 100% flattened guardrail. This was accomplished by changing the geometry at the flattened section, by flattening the W-beam over the center 305 mm (12 in.). The transition from the regular shape to the flattened section was modeled similarly.

8.1 Modeling and Meshing

Geometrical modeling of the flattened beams required a close approximation with the test cases. These test specimen were not uniform and had surface imperfections at the flattened sections, particularly in the case of the 50% flattened beam.

8.1.1 50% Flattened W-Beam

In the case of 50% flattened beams, shown in Figure 51, a third corrugation is developed during the process of shape modification which needs to be modeled accordingly. The flattened section tends to curve instead of being straight.

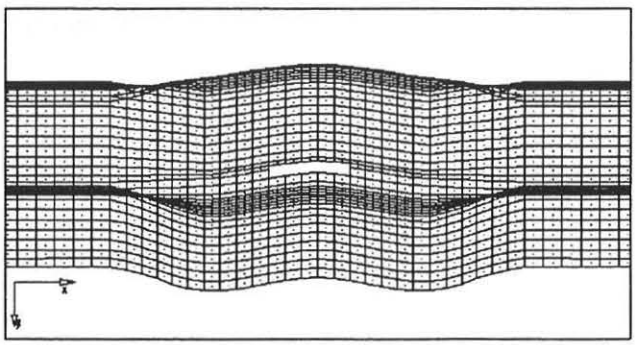

Figure 51. 50% flattening of guardrail.

8.1.2 100% Flattened W-Beams

For this case the transition zone from the regular W-shape to flat shape started at 300 mm (12 in.) on either side of the flattened middle part, as shown in Figure 52.

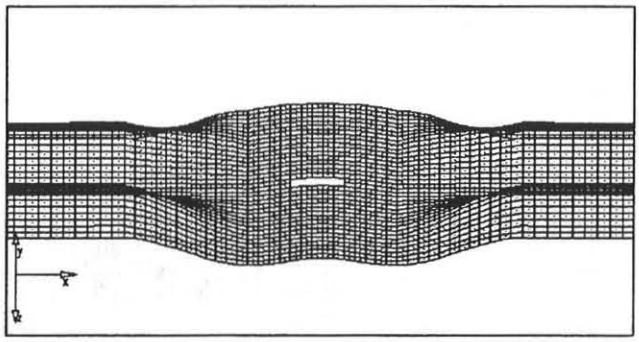

Figure 52. 100% flattening of guardrail.

8.2 Analysis

Input deck for LS-DYNA3D had the same modifications used for the baseline model. Analysis was performed on Sun Sparc 20 workstation running on SunOS version 5.3 and Solaris 3.3. It took approximately ten hours to complete both cases.

8.3 Results

The actual field tests on the modified beams had been performed previous to this simulation work, which allowed the simulation results to be matched and their accuracy judged.

8.3.1 50% Flattening

Results of this case as seen from the velocity and acceleration curves in Figure 53 match fairly accurately. The actual complex irregularities could not be matched in the model. This may have prevented the simulated decelerations to be the same in the time period from 30 to 40 ms. The net decrease in the velocity of the bogie is the same for both cases. Figure 54 shows the actual progress of the simulated impact at regular intervals of 60 ms.

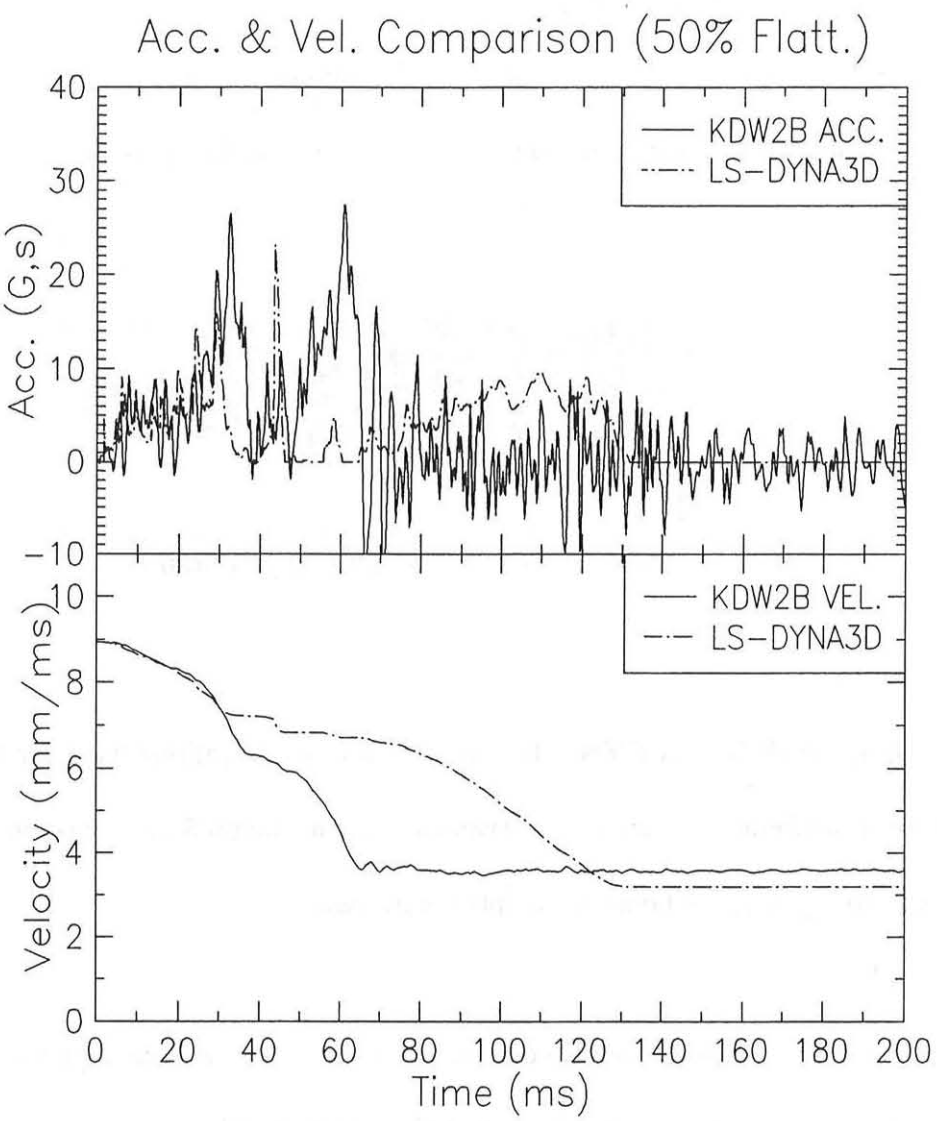

Figure 53. Accelerometer and velocity curves for 50% flattened W-beams.

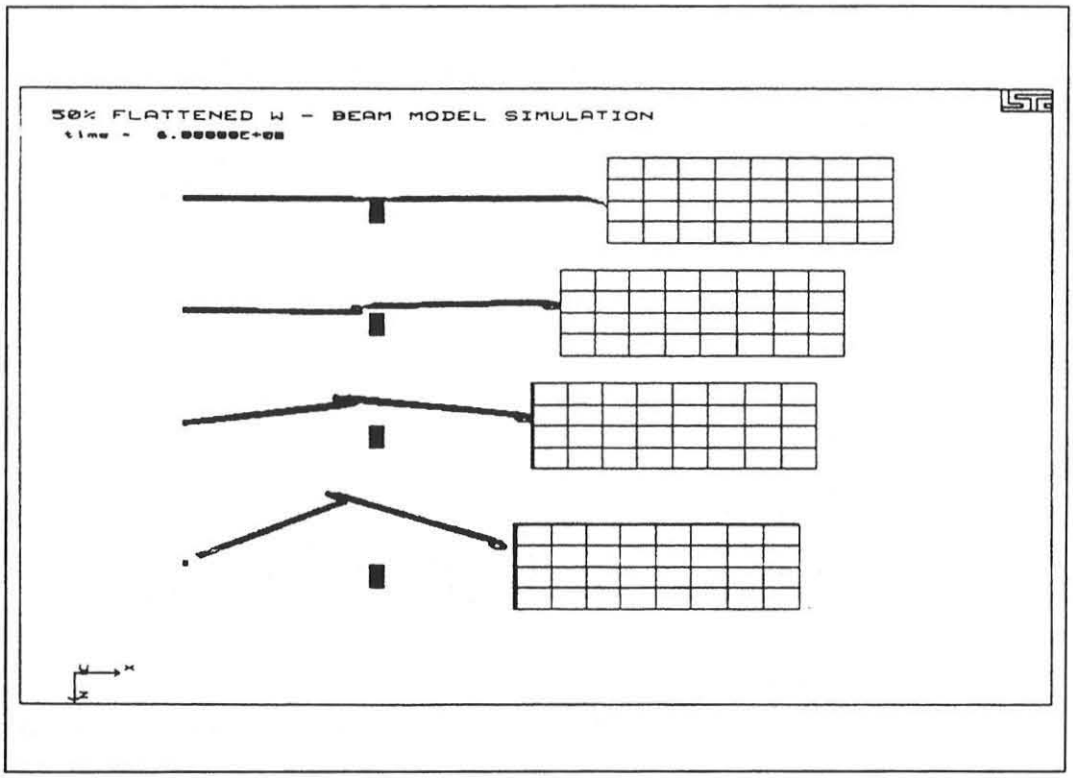

Figure 54. Impact stages at 60 ms intervals.

8.3.2 100% Flattening

The results of this simulation match the test results very closely. As seen in Figure 55, the velocity curves match closely in this simulation, as there is a decrease of just one mm/ms in the bogie's velocity. It is obvious from these results that there is very little energy absorbed in the buckling of a 100% flattened rail. An output graphic from the simulation is shown in Figure 56, which is compared to the actual test, shown in Figure 57.

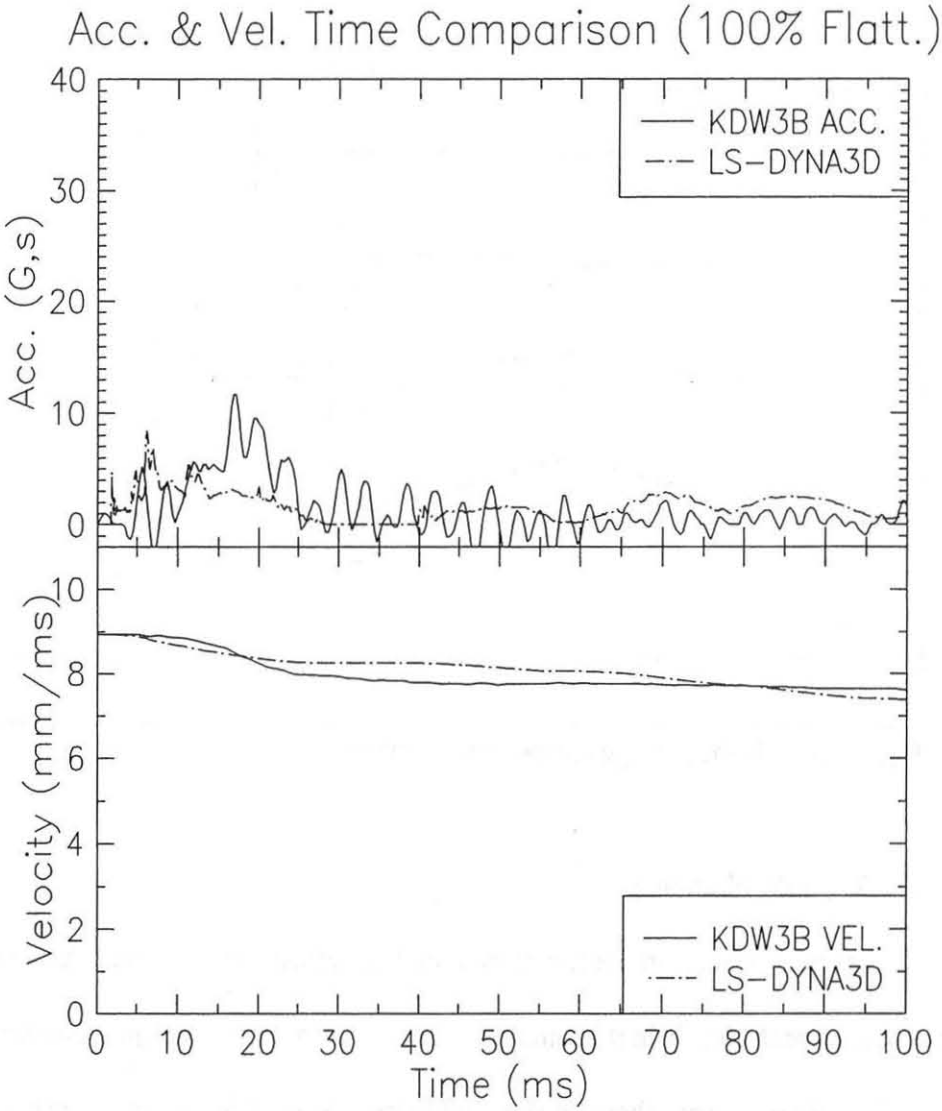

Figure 55. Accelerometer and velocity comparisons for 100% flattened W-beam.

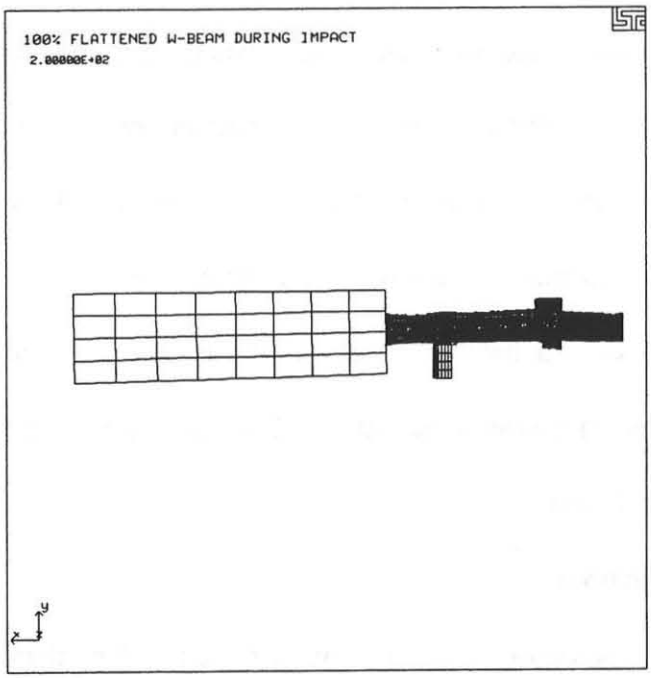

Figure 56. Simulated impact on 100% flattened beam.

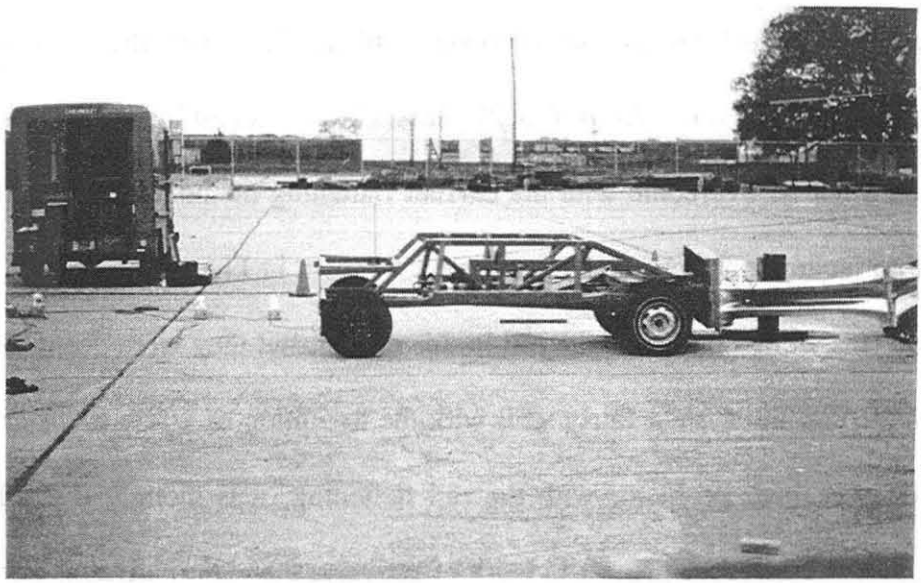

Figure 57. Test KDW3B during impact.

9 FULL-SCALE CRASH TESTING

Upon completion of the component testing and computer simulation which was performed during the course of the development of this system, one full-scale vehicle crash test was conducted to evaluate the performance of the overall system. This test consisted of a 1,863 lb (845 kg) small car impacting the terminal head-on at 100 km/h (62.1 mph). The vehicle was offset toward the roadway so that the impact with the system occurred at the driver's side quarter point. It was decided to conduct this test first because it was judged to be the most demanding test from the required matrix.

9.1 System Modifications

The flattening of a thrie beam rail is much more involved than the flattening of a W-beam rail, as the center corrugation causes many complications. When the 3.8 m (12 ft -6 in.) sections were flattened in the middle and tested dynamically, the flattening procedure worked fairly well, and the warpage of the beam was not a serious problem. However, the original design called for three flattened areas on the 7.6 m (25 ft) beam. This resulted in serious warpage of the beam which could not be overcome with the current flattening method. As a result, the design was modified to include only two flattened areas, as shown in Figures 58 and 59. There were still some problems with warpage of the rail in this design, but they were eventually overcome, and the beam fit into the system fairly well with the exception of a few small gaps at some of the posts. Despite these problems with the rail flattening, it is thought that this is still a viable concept. If this concept is proven to work effectively, then alternative methods of reducing the moment of inertia in key locations can be investigated if necessary.

9.2 System Details

The FRT (Flattened Rail Terminal) system tested utilized thrie beam installed at the same flare rate and post spacing as the current BCT system. Photographs of the system are presented in Figure 58 and 59, and a plan drawing is shown in Figure 60. As can be seen in the figures, the thrie beam was flattened 100% at the midpoint between post nos. 2 and 3, and again at post no. 4.

Foundation tubes were installed at the first two post locations. These tubes were different from the standard foundation tubes used in BCT installations in that they have been increased in length from 1.52 m (5 ft) to 1.98 m (6 ft - 6 in.), thereby allowing the soil plate to be removed.

The buffer section consisted of a standard wrap around thrie beam section, modified by bolting the standard MELT stiffening plates inside at the top and bottom of the piece. This was done to utilize the technology from the MELT system which inputs an eccentric load into the rail, causing it to buckle easier. The stiffener plates at the top and bottom also aid in capturing the front of the impacting vehicle. As the vehicle bumper penetrates the buffer head at the soft center, the stiffer top and bottom collapse in to wrap around the front end of the vehicle.

A 152 mm x 19 mm (6 in. x 3/4 in.) slot was placed in the thrie beam at the location where it was attached to the first post. This was done in an effort to reduce the initial force imparted into the vehicle by separating the two main energy absorbing events, the buckling of the rail and the breaking of the first post. The slot was designed to allow the rail to slide forward, so that buckling could be initiated before the first post was broken.

In order to further facilitate the buckling of the rail, it was not attached to the post at locations 2, 3, and 4. Instead, it was supported at these locations with a shelf bracket as shown

in Figure 61.

Post nos. 1 and 2 were 140 mm x 190 mm (5 ½ in. x 7 ½ in.) BCT type posts, modified to fit the thrie beam. Post nos. 3 through 7 were 152 mm x 203 mm x 1.98 m (6 in. x 8 in. x 6 ft -6 in.) CRT type posts which were specially made to fit the thrie beam rail.

The breakaway cable anchor system consisted of a standard BCT anchor box bolted to the lower corrugation of the thrie beam. The cable and related hardware were identical to those used in a standard BCT system.

A thrie beam to W-beam transition section was located at the end of the 7.6 m (25 ft) length of thrie beam, between post nos. 6 and 7. This was used to transition into the W-beam, which was used for the remainder of the system.

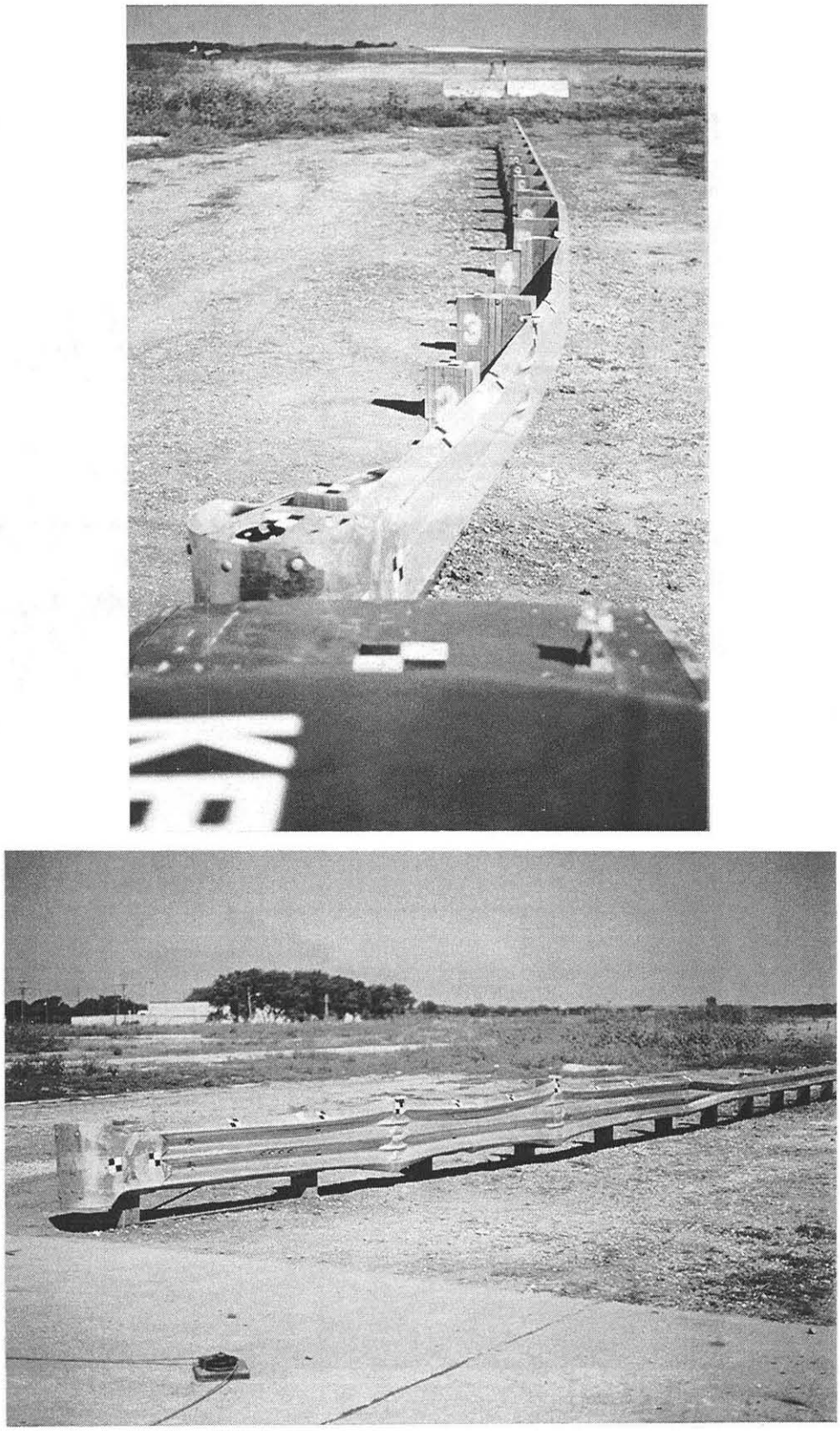

Figure 58. Photographs of the FRT system for Test KBCT-1.

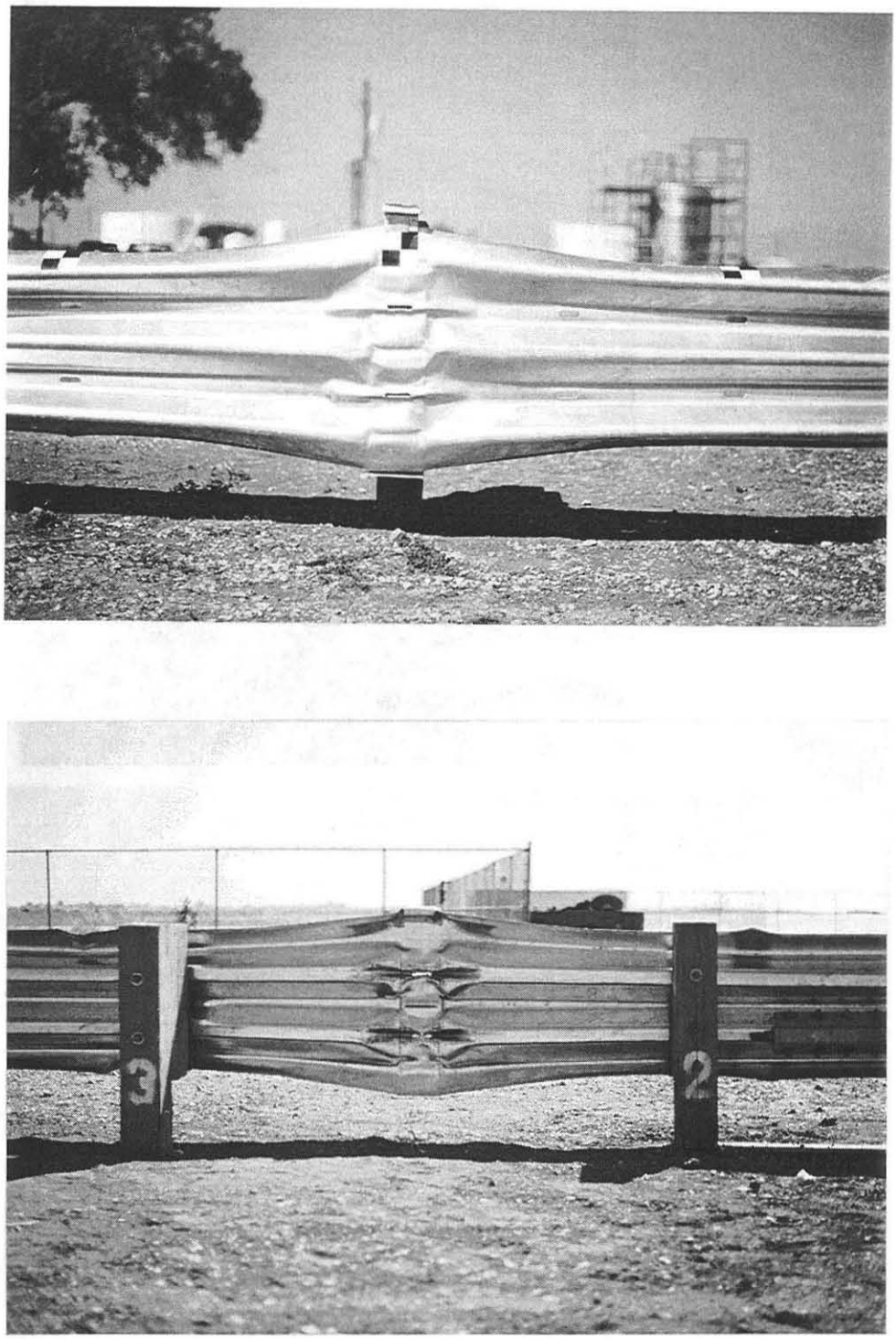

Figure 59. Photographs of the FRT system for Test KBCT-1 (continued).

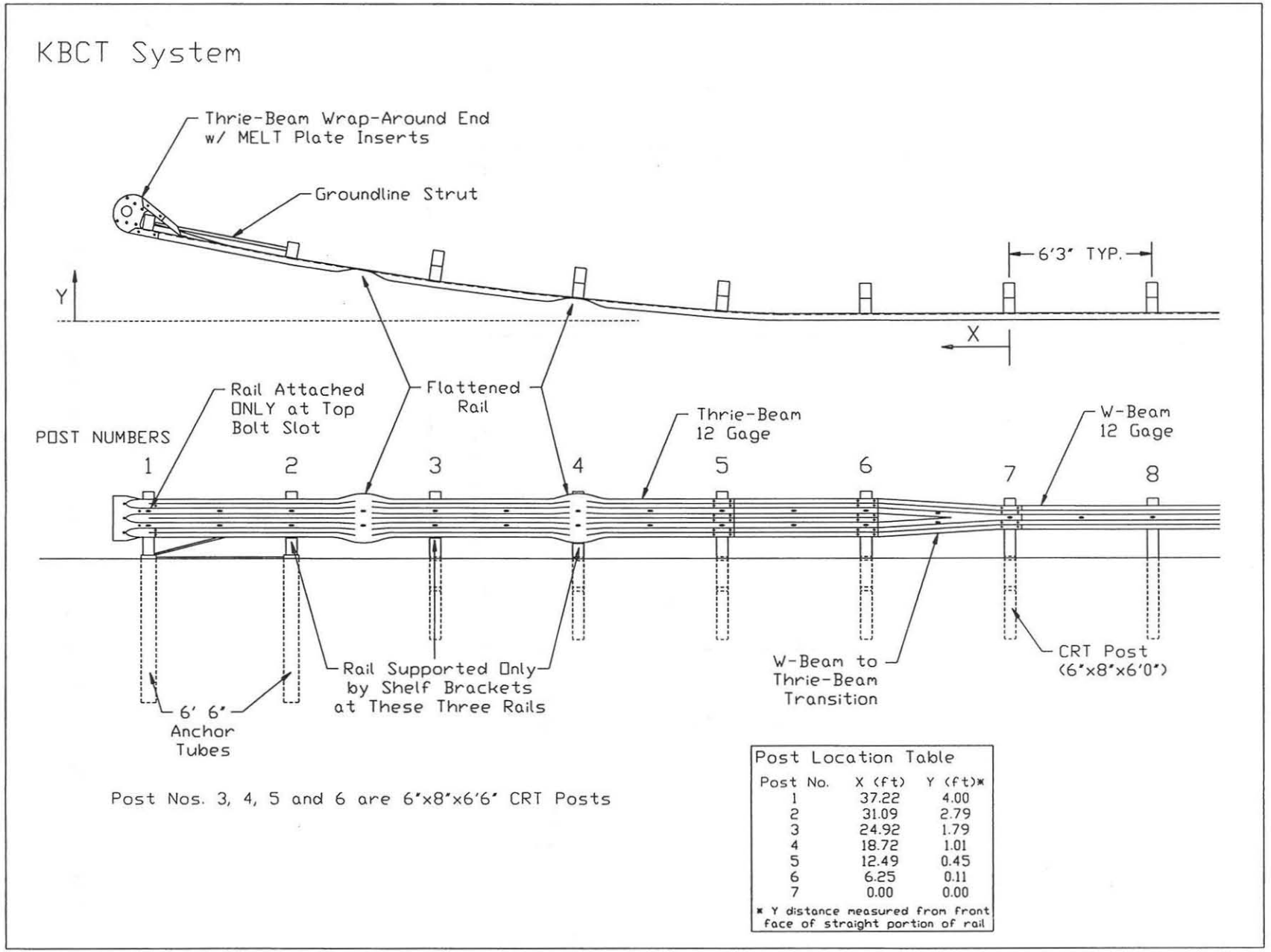

Figure 60. Plan drawing of the FRT for Test KBCT-1.

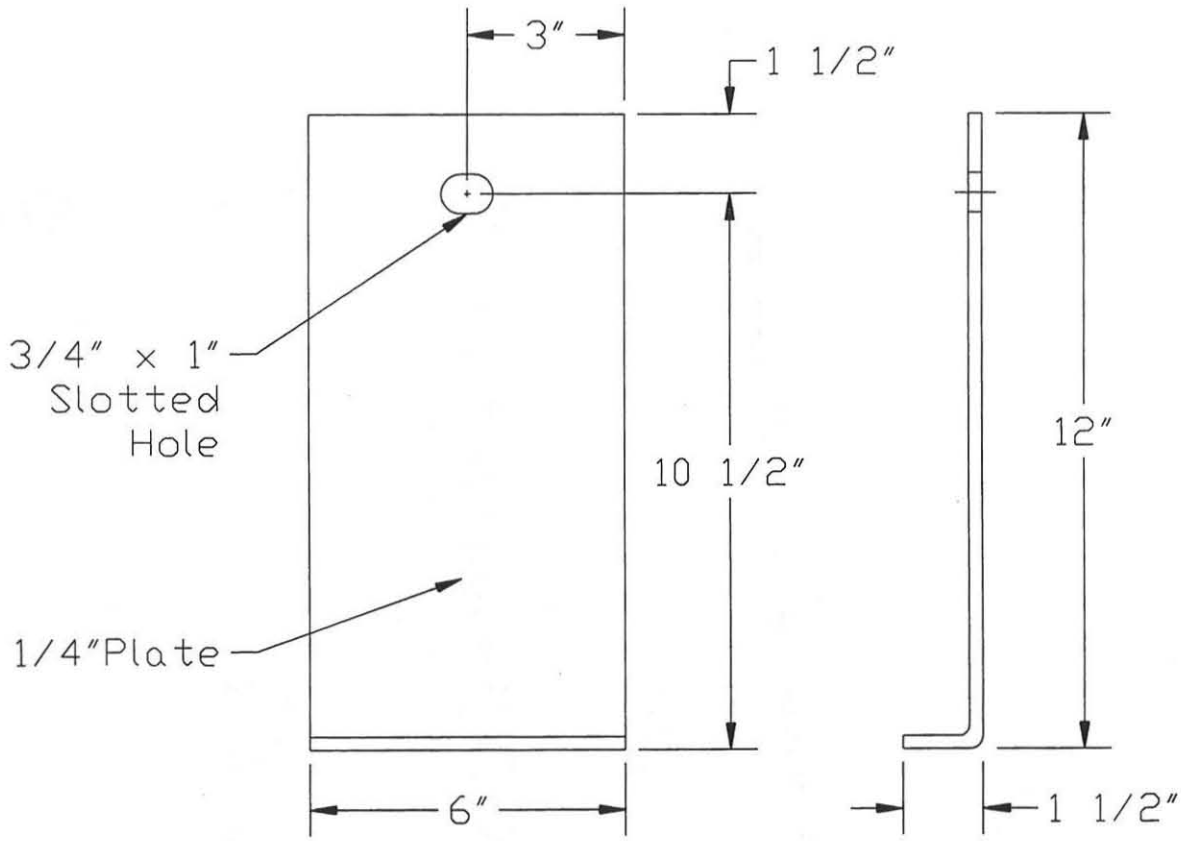

Figure 61. Shelf bracket used to support rail at post nos. 2, 3, and 4.

9.3 Test Conditions

9.3.1 Test Site

The Midwest Roadside Safety Facility's outdoor test site is located at the Lincoln Air-Park on the northwest end of the Lincoln Municipal Airport. The test facility is approximately 8 km (5 miles) northwest of the University of Nebraska-Lincoln. The site is surrounded and protected by an 2.4-m (8-ft) high chain-link security fence.

9.3.2 Vehicle Guidance System

A reverse cable tow system with a 1:2 mechanical advantage was used to propel the test vehicle. The distance traveled and the speed of the tow vehicle are one-half that of the test vehicle. The test vehicle was released from the tow cable before impact with the appurtenance. A fifth wheel, built by the Nucleus Corporation, was used in conjunction with a digital speedometer to increase the accuracy of the test vehicle impact speed.

A vehicle guidance system developed by Hinch (22) was used to steer the test vehicle. The guide-flag, attached to the front-left wheel and the guide cable, was sheared off before impact. The 95 mm (⅜-in.) diameter guide cable was tensioned to approximately 13.3 kN (3,000 lbs), and supported laterally and vertically every 30.5 m (100 ft) by hinged stanchions. The vehicle guidance system was 180 m (600 ft) long for this test.

9.3.3 Test Vehicle

A 1981 Dodge Champ, having a test inertial mass of 845 kg (1863 lbs), was used as the test vehicle for Test KBCT-1. Photographs of this test vehicle are shown in Figure 62, and vehicle properties are presented in Figure 63.

A number of square, black and white-checkered targets were placed on each test vehicle.

These targets were used in the high-speed film analysis. Two targets were located on the center of gravity, one on the top and one on the driver's side of the test vehicle. The remaining targets were strategically located such that they could be used in the film analysis of the tests.

The front wheels of the test vehicle were aligned for camber, caster, and toe-in values of zero so that the vehicle would track properly along the guide cable. Two 5B flash bulbs were mounted on the roof of the vehicle to pinpoint the time of impact with the bridge rail on the high-speed film. The flash bulbs were fired by a pressure tape switch mounted on the front face of the bumper.

9.3.4 Data Acquisition Systems

Accelerometers.

A triaxial piezoresistive accelerometer system with a range of ±200 G's was used to measure the acceleration in the longitudinal, lateral, and vertical directions at a sample rate of 3,200 Hz. The environmental shock and vibration sensor/recorder system, Model EDR-3, was configured with 256 Kb of RAM and a 1,120 Hz filter. Computer software, "DynaMax 1 (DM-1)" and "DADiSP" were used to digitize, analyze, and plot the accelerometer data.

This system was used in conjunction with a backup system, which consisted of two triaxial piezoresistive accelerometer systems with a range of ±200 g's (Endevco Model 7264). The accelerometers were rigidly attached to an aluminum block mounted near the vehicle's center of gravity. Accelerometer signals were received and conditioned by an onboard Series 300 Multiplexed FM Data System built by Metraplex Corporation. The multiplexed signal was then transmitted to a Honeywell 101 Analog Tape Recorder. In the event of a failure in the EDR-3 system, computer software "EGAA" and "DADiSP" would be used to digitize, analyze, and plot

the accelerometer data.

Rate Transducer.

A Humphrey 3-axis rate transducer with a range of 250 deg/sec in each of the three directions (pitch, roll, and yaw) was used to measure the rotational rates of the test vehicle. This data is not required by the current criteria, but is used to provide engineers with a better understanding of the dynamics of vehicle impacts with barriers. This information is also useful in verifying computer simulation results.

High Speed Photography.

Four high-speed 16-mm cameras operating at 500 frames/sec were used to film the crash test. A Red Lake Locam with a 12.5-mm lens was placed 21 m (69 ft) above the test installation to provide a field of view perpendicular to the ground. A Locam camera with a 76 mm lens was placed downstream from the impact point and had a field of view parallel to the barrier. A Locam camera with a 12.5 mm lens was placed on the traffic side of the terminal system and had a field of view perpendicular to the barrier. A Locam camera was also placed perpendicular to the system on the side opposite of the traffic. The film was analyzed using a Vanguard Motion Analyzer. Actual camera speed and camera divergence factors were considered in the analysis of the high-speed film.

Speed Trap Switches.

Five pressure tape switches, spaced at 1.52-m (5-ft) intervals, were used to determine the speed of the vehicle before impact. Each tape switch fired a strobe light and sent an electronic timing mark to the data acquisition system as the left-front tire of the test vehicle passed over it. Test vehicle speeds were determined from electronic timing mark data recorded on "EGAA"

software. Strobe lights and high-speed film analysis are used only as a backup in the event that vehicle speeds cannot be determined from the electronic data.

Figure 62. Test vehicle for Test KBCT-1.

Date: 8/25/95 Test Number: KBCT-1 Model: Champ

Make: Plymouth Vehicle I.D.#: JP3BE4438BU421725

Tire Size: P155/80R13 Year: 1981 Odometer: _____

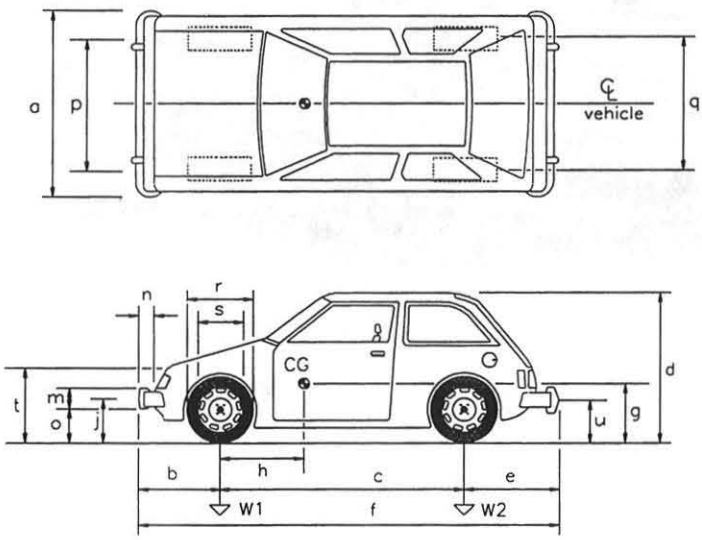

Vehicle Geometry - inches

a	59	b	33.5
c	90.5	d	50
e	32.5	f	156.5
g	22	h	32
j	17.5	m	4.75
n	6	o	15
p	55	q	54
r	22	s	14
t	29.5	u	19.5

height of wheel center 10.375"

Engine Type _____

Engine size _____

Transmission Type:

Automatic or (Manual)

FWD or (RWD) or 4WD

Weight - lbs	Curb	Test Inertial	Gross Static
W1	1250	1113	1198
W2	680	543	623
Wtotal	1930	1863	2028

Damage prior to test: _____

Figure 63. Vehicle dimensions, Test KBCT-1.

9.4 Performance Evaluation Criteria

The performance criteria used to evaluate this full-scale vehicle crash test was taken from NCHRP Report 350, *Recommended Procedures for the Safety Performance Evaluation of Highway Features* (14). The conditions for this test are shown in Table 10. The specific evaluation criteria are shown in Table 11.

The safety performance of the terminal was evaluated according to three major factors: (1) structural adequacy, (2) occupant risk, and (3) vehicle trajectory after collision. These three evaluation criteria are defined and explained in NCHRP Report 350 (14). After each test, vehicle damage was assessed by the traffic accident scale (TAD) (23) and the vehicle damage index (VDI) (24).

Table 10. NCHRP 350 Test Level 3 Crash Test Conditions.

Test Designation	Test Vehicle	Impact Conditions		Evaluation Criteria[1]
		Speed (km/h)	Angle (deg)	
3-30	820C	100	0	C,D,F,H,I,(J),K,N

[1] Evaluation criteria explained in Table 11, criteria in parenthesis are optional.

Table 11. Relevant NCHRP 350 Evaluation Criteria.

C.	Acceptable test article performance may be by redirection, controlled penetration, or controlled stopping of the vehicle.
D.	Detached elements, fragments or other debris from the test article should not penetrate or show potential for penetrating the occupant compartment, or present an undue hazard to other traffic, pedestrians, or personnel in a work zone. Deformations of, or intrusions into, the occupant compartment that could cause serious injuries should not be permitted.
F.	The vehicle should remain upright during and after collision although moderate roll, pitching and yawing are acceptable.
H.	Longitudinal and lateral occupant impact velocities should fall below the preferred value of 9 m/s (29.5 fps), or at least below the maximum allowable value of 12 m/s (39.4 fps).
I.	Longitudinal and lateral occupant ridedown accelerations should fall below the preferred value of 15 g's, or at least below the maximum allowable value of 20 g's.
J.	(Optional) Hybrid III dummy. Response should conform to evaluation criteria of Part 571.208, Title 49 of Code of Federal Regulation, Chapter V.
K.	After collision it is preferable that the vehicle's trajectory not intrude into adjacent traffic lanes.
N.	Vehicle Trajectory behind the test article is acceptable.

9.5 Test Results

In Test KBCT-1 the car impacted the end of the flared terminal head on at 93.8 km/h (58.3 mph). The vehicle was offset 381 mm (15 in.) toward the roadway, as specified in NCHRP Report 350 (14). Photos of the vehicle in its impact position are shown in Figure 63. A summary of Test KBCT-1, including vehicle trajectory and sequential photographs, is presented in Figure 64. Additional sequential photographs are shown in Figures 65 and 66.

Upon impact with the buffer end, the front of the vehicle began to crush inward, as did the buffer. At 30 ms after impact the vehicle began to yaw counter-clockwise as the rail started to buckle outward and downward at the first flattened rail section. At 62 ms after impact the rail contacted the ground at the point of buckling and began to gouge into the soil. The vehicle and buckled rail reached the second post at 92 ms, and by 126 ms after impact this post was completely fractured. The vehicle continued to yaw counter-clockwise while the point at which the buckling occurred reversed its direction of travel and began to come back toward the posts. At 250 ms after impact the vehicle and rail contacted post no. 3, and the vehicle continued to rotate until, at 276 ms, the passenger door impacted the buckled section of thrie beam. By 304 ms after impact the passenger side window was shattered, and the thrie beam began to buckle at the second flattened location. By 370 ms the rail has caused serious deformation to the vehicle and occupant compartment, and the vehicle was beginning to rebound to the side of the system. The vehicle continued to yaw, coming to a rest as shown in Figure 67.

Damage to the vehicle was extensive, as shown in Figure 68. Substantial occupant compartment deformation occurred when the vehicle yawed into the buckled thrie beam section. The passenger side door was completely caved in, and the roof was seriously buckled. The cable anchor

mechanism was fractured as shown in Figure 69.

The normalized longitudinal occupant impact velocity was 10.2 m/s (33.4 fps), which was above the preferred value of 9 m/s (29.5 fps) but below the maximum value of 12 m/s (39.4 fps). The maximum longitudinal ridedown deceleration of 8.3 G's was well below the design value of 15 G's. The normalized lateral occupant impact velocity of 2.6 m/s (8.5 fps) was well below the design value of 9 m/s (29.5 fps) and the maximum lateral ridedown deceleration of 15.5 G's was just above the preferred value of 15 G's, but well below the maximum value of 20 G's.

A summary of these test results is shown in Figure 64, as well as in Table 12. Plots summarizing the accelerometer data analysis are shown in Appendix B. Based on the results of this test, it was judged that this system does not pass the criteria set forth in NCHRP Report 350 (14) for test 3-30 because of the excessive occupant compartment deformation.

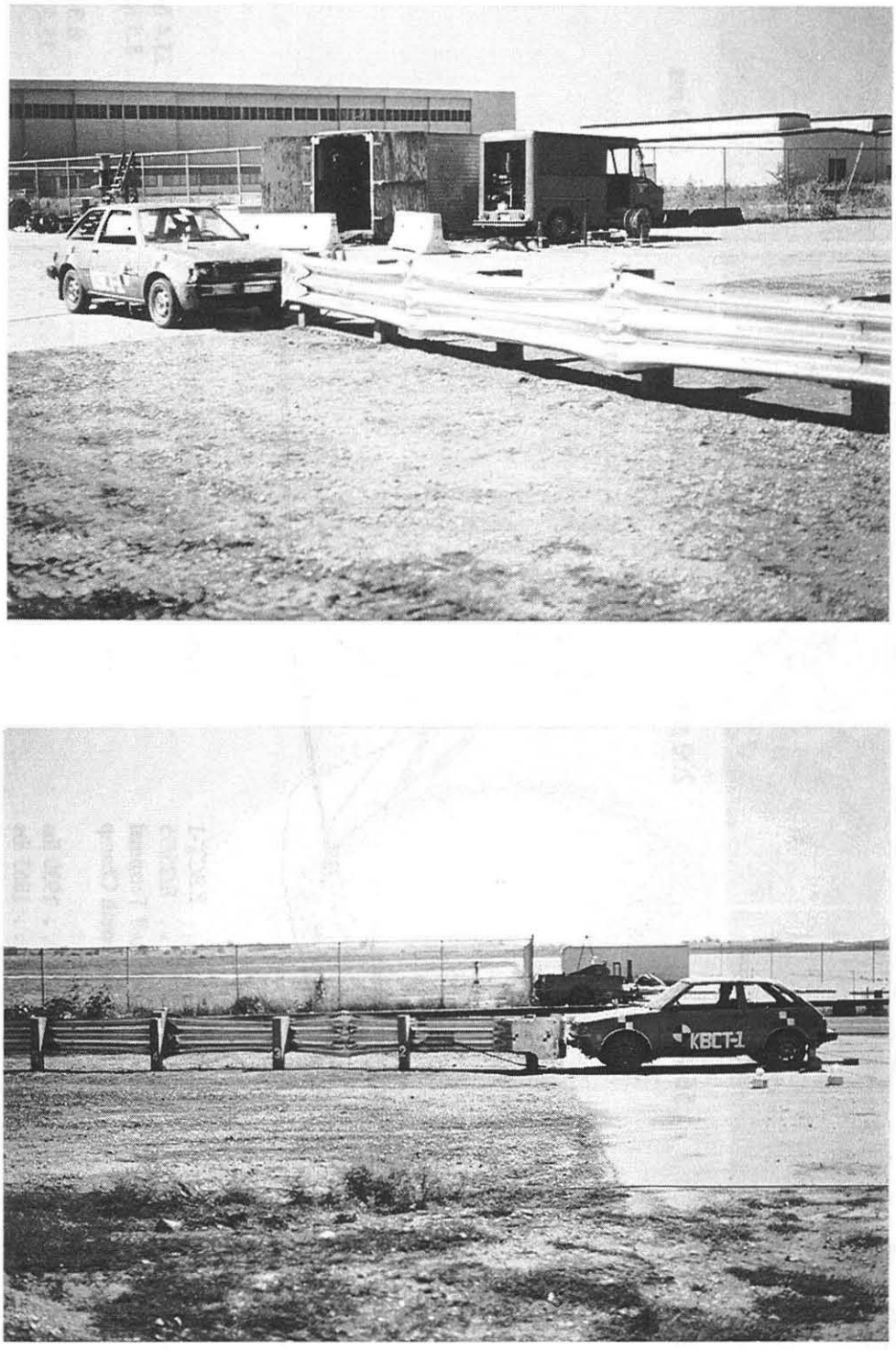

Figure 63. Vehicle and system prior to impact.

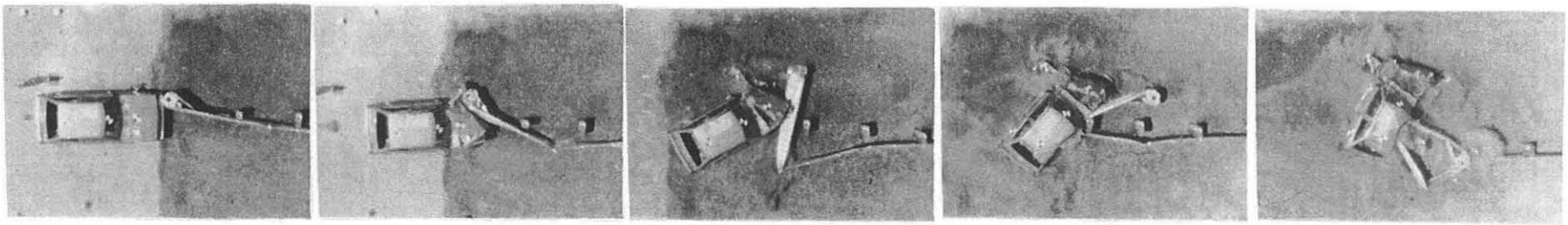

Impact 56 ms 200 ms 304 ms 500 ms

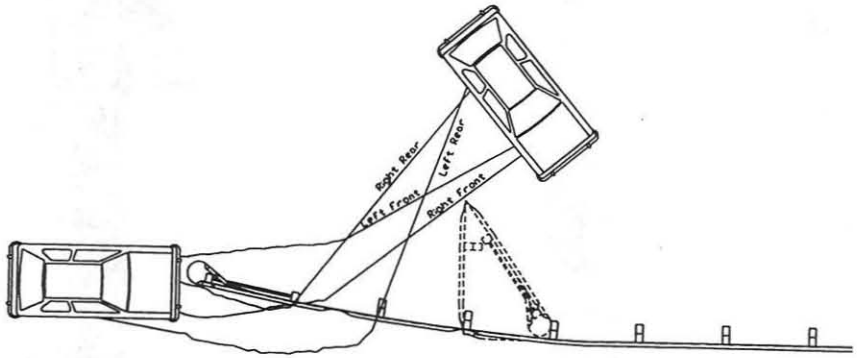

Test Number	KBCT-1
Date	8/25/95
Installation	Flattened Rail Terminal
Vehicle Model	1981 Plymouth Champ
Vehicle Weight	
Curb	1930 lbs
Test Inertial	1863 lbs
Gross Static	2028 lbs
Vehicle Impact Speed	58.3 mph
Vehicle Impact Angle	0 deg
Vehicle Impact Location	Head on, 15 in. to the left of center

Normalized Occupant Impact Velocity	
Longitudinal	33.4 fps
Lateral	8.5 fps
Occupant Ridedown Accelerations	
Longitudinal	8.3 g
Lateral	15.5 g
Vehicle Damage Classification	
TAD	12-FC-2, 3-RP-7
VDI	12FYEN1, 03RPAN3

Figure 64. Summary of Test KBCT-1.

Conversion Factors: 1 in.= 2.54 cm; 1 lb= 0.454 kg

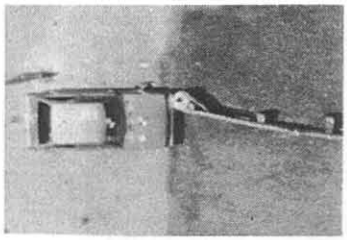

Impact

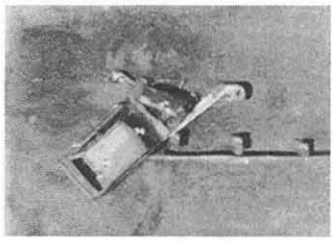

276 ms

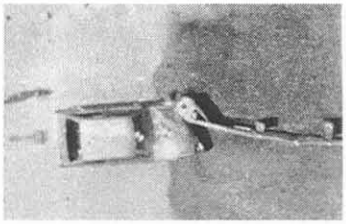

30 ms

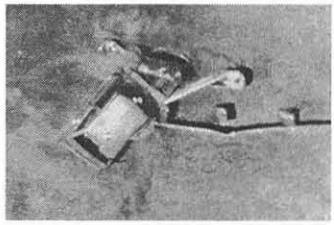

304 ms

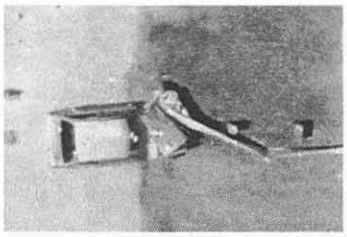

56 ms

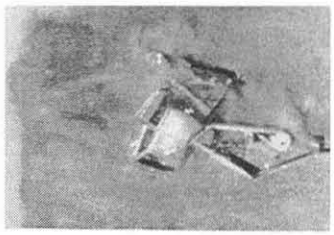

370 ms

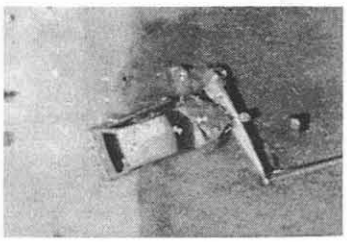

126 ms

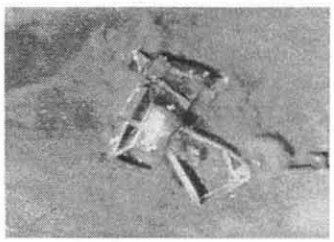

500 ms

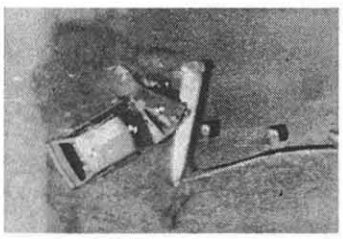

200 ms

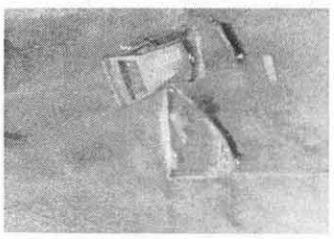

820 ms

Figure 65. Overhead sequential photos, Test KBCT-1.

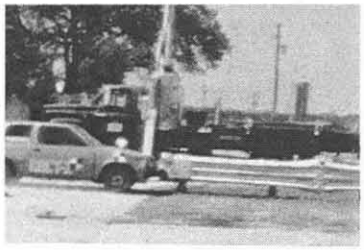

Impact

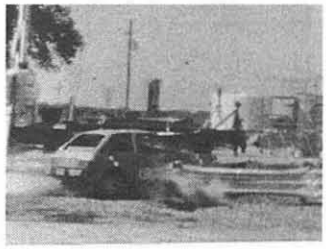

240 ms

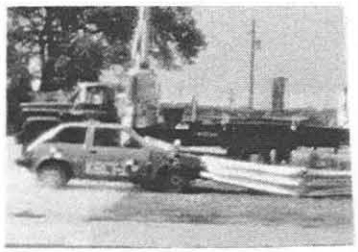

62 ms

300 ms

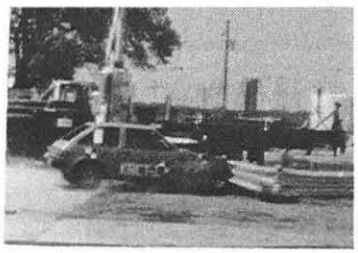

120 ms

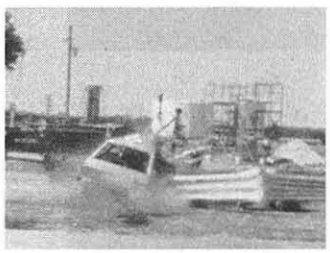

360 ms

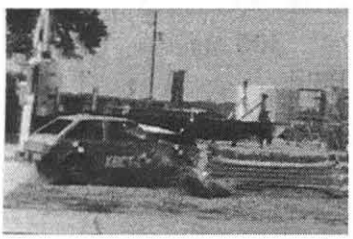

180 ms

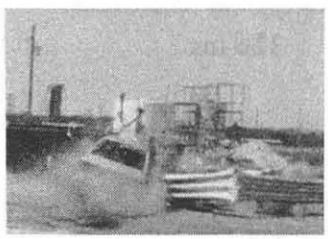

440 ms

Figure 66. Perpendicular sequential photos, Test KBCT-1.

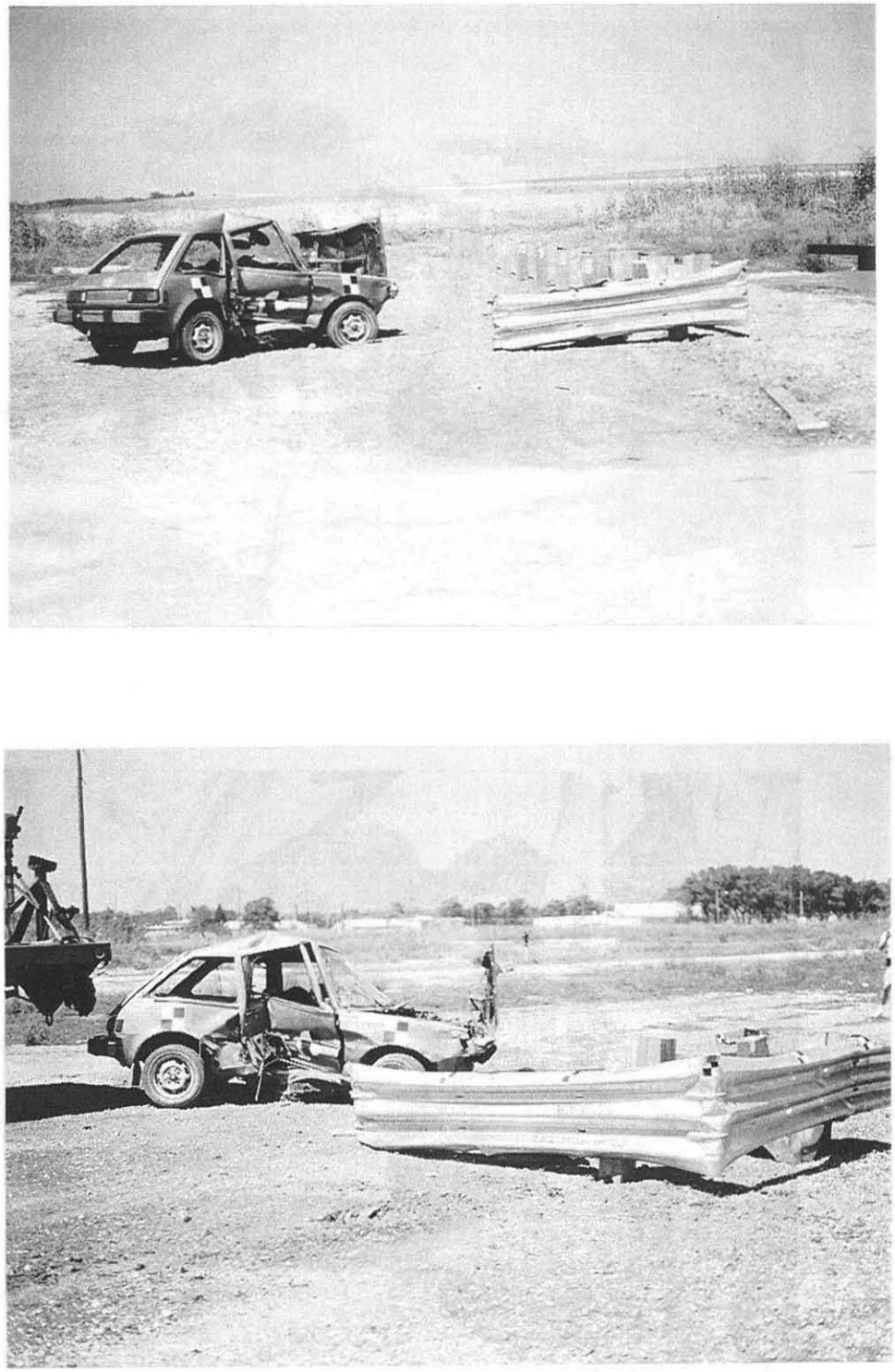

Figure 67. Vehicle trajectory, Test KBCT-1.

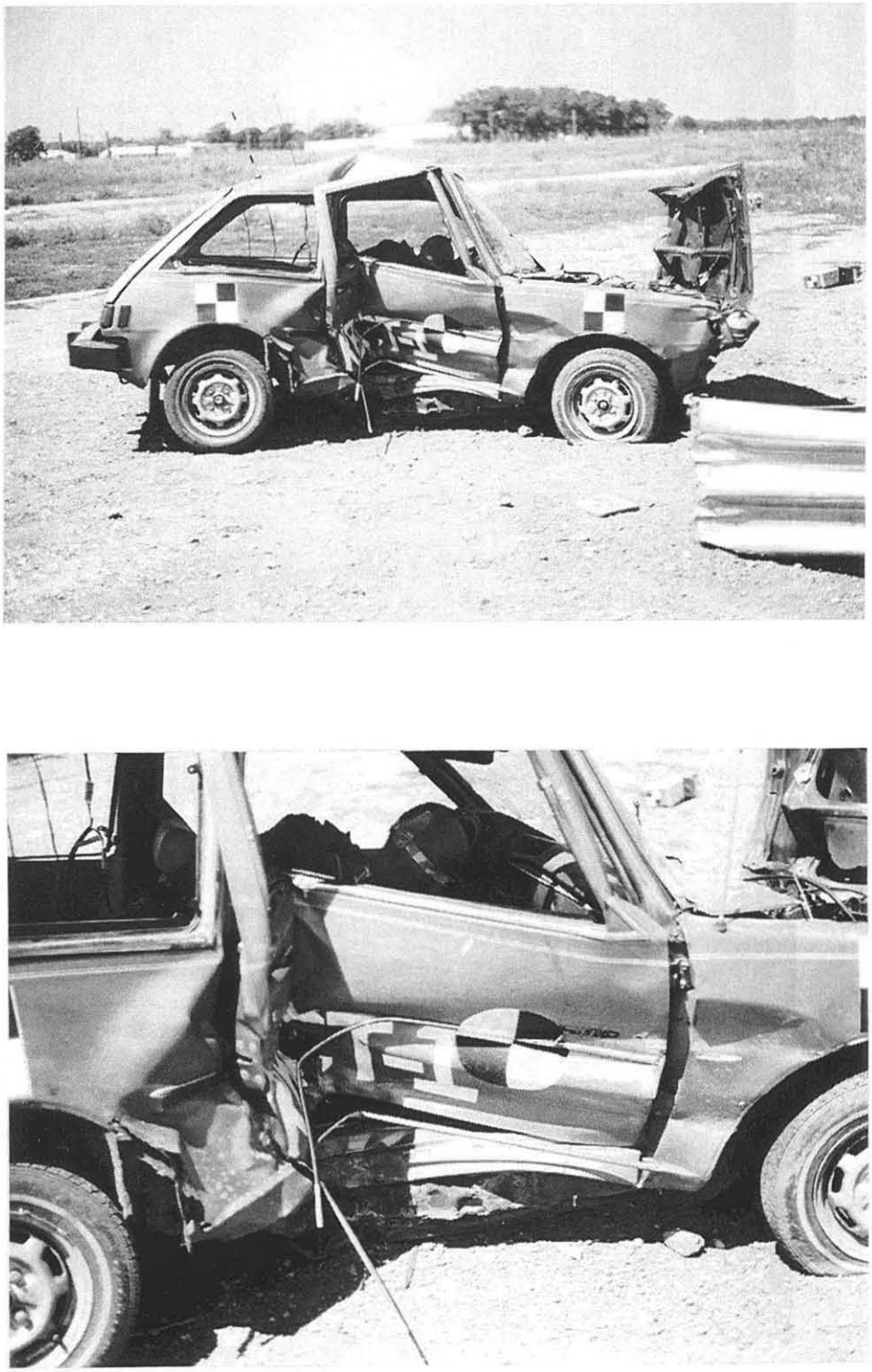

Figure 68. Vehicle damage, Test KBCT-1.

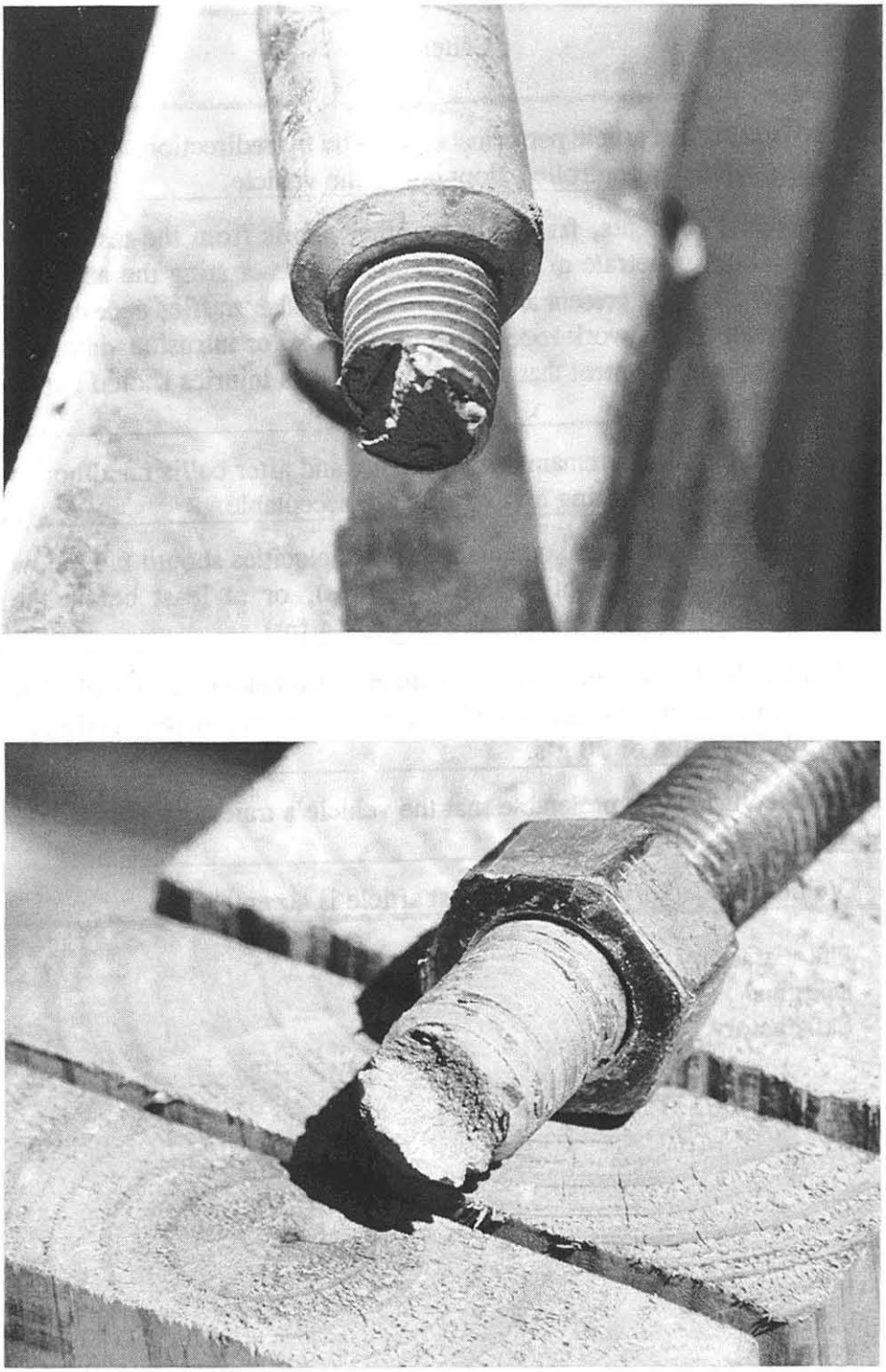

Figure 69. Failure of cable breakaway mechanism.

Table 12. Summary of Evaluation Results.

Criteria		Test KBCT-1 Results
C.	Acceptable test article performance may be by redirection, controlled penetration, or controlled stopping of the vehicle.	U
D.	Detached elements, fragments or other debris from the test article should not penetrate or show potential for penetrating the occupant compartment, or present an undue hazard to other traffic, pedestrians, or personnel in a work zone. Deformations of, or intrusions into, the occupant compartment that could cause serious injuries should not be permitted.	U
F.	The vehicle should remain upright during and after collision although moderate roll, pitching and yawing are acceptable.	S
H.	Longitudinal and lateral occupant impact velocities should fall below the preferred value of 9 m/s (29.5 fps), or at least below the maximum allowable value of 12 m/s (39.4 fps).	S
I.	Longitudinal and lateral occupant ridedown accelerations should fall below the preferred value of 15 g's, or at least below the maximum allowable value of 20 g's.	S
K.	After collision it is preferable that the vehicle's trajectory not intrude into adjacent traffic lanes.	S
N.	Vehicle Trajectory behind the test article is acceptable.	S

U - Unsatisfactory
M - Marginal
S - Satisfactory

10 ANALYSIS OF RESULTS

Following the crash test, an inspection of the damaged system revealed that the threaded rod end of the breakaway cable mechanism attached to the end post failed during impact, as shown in Figure 69. Upon further investigation, it was discovered that this problem had resulted from a design modification intended to improve the behavior of the system. As discussed previously, a 152 mm (6 in.) long slot had been located on the thrie beam where it was attached to the first post. The purpose of this slot was to allow the beam to slide forward, allowing buckling to initiate before the breaking of the first post. By separating these two events, the initial forces imparted into the vehicle would be minimized, thereby reducing both the occupant risk values and the amount of yaw moment induced in the car. Unfortunately this methodology did not work. As the thrie beam was pushed back to initiate the buckling, the cable anchor, still attached to the first post, tightened and imparted a load into the vehicle until it failed at the threaded rod section. As evidence of this high load being imparted into the post at ground level, the first post was broken off below the breakaway hole where the load was applied. The high load produced by this action caused the vehicle to yaw counterclockwise at a high rate, eventually impacting the buckled section with the passenger side door.

The next evaluation of this system should include a modification to the front of the system which will allow the post to break before the rail buckles. This will allow the cable mechanism to release as designed, eliminating the problem encountered in this test.

Another factor which may have contributed to the poor performance of this test was the change from three flattened sections to two, which was needed because of warping problems produced during the flattening procedure. With three flattened sections, the rail may have been able to buckle

out of the way without coming back in line with the vehicle and spearing into its side. Future evaluations of this system should investigate alternative flattening procedures that will accommodate three flattened sections in one 7.6 m (25 ft.) length.

11 CONCLUSIONS AND RECOMMENDATIONS

The objective of this research project was to design and develop an effective flared guardrail terminal. The one full-scale crash test which was conducted with a small vehicle was unsuccessful. However, it was shown that the concept of flattening the guardrail to produce regions of reduced stiffness was indeed feasible. Several ideas for correcting the problems encountered during this developmental effort have been identified. It is thought that if this concept is pursued further, it will result in an effective guardrail terminal.

12 REFERENCES

1. Michie, J.D. and M.E. Bronstad, *Guardrail Performance: End Treatments*, Southwest Research Institute, 1969.
2. Nordlin, E.F., R.N. Field, and J.J. Folsom, *Dynamic Tests of Short Sections of Corrugated Metal Beam Guardrail,* Highway Research Record 259, HRB, National Research Council, Washington, D.C., 1969.
3. Buth, C.E., and T.J. Hirsch, *Improved End Treatment for Metal Beam Guardrail,* Research Report 189-1, Texas Transportation Institute, Texas A&M University, College Station, Texas, 1977.
4. Hirsch, T.J., T.J. Dolf, and A. Arnold, *Maryland Turned-Down Guardrail Terminal*, Report FHWA-RD-83-02, Texas Transportation Institute, Texas A&M University, College Station, Texas, 1982.
5. Hinch, J.A., R.P. Owings, and G.A. Manhard, *Safety Modifications of Turned-Down Guardrail Terminals*, Report FHWA-RD-84-035, ENSCO, Inc., Springfield, Virginia, 1984.
6. Faller, R.K., J.C. Holloway, B.T. Rosson, and B.G. Pfeifer, *Safety Performance Evaluation on the Nebraska Turned-Down Approach Terminal Section*, Report TRP-03-32-92, Midwest Roadside Safety Facility, University of Nebraska-Lincoln, Lincoln, Nebraska, 1992.
7. Michie, J.D., *NCHRP Report 230: Recommended Procedures for the Safety Performance Evaluation of Highway* Appurtenances, TRB, National Research Council, Washington, D.C., 1981.
8. Michie, J.D., and M.E. Bronstad, *NCHRP Report 129: Guardrail Crash Test Evaluation:*

New Concepts and End Designs, HRB, National Research Council, Washington, D.C., 1972.

9. Pigman, J.G., and K.R. Agent, *Performance Evaluation of Breakaway-Cable-Terminal End Treatments*, Transportation Research Record 1198, TRB, National Research Council, Washington, D.C., 1988.

10. Kimball, C.E., Jr., M.E. Bronstad, and L.C. Meczkowski, *Evaluation of Guardrail Breakaway Cable Terminals*, Report FHWA-82-057, Southwest Research Institute, San Antonio, Texas, 1982.

11. Bronstad, M.E., J.B. Mayer, Jr., J.H. Hatton, Jr., and L.C. Meczkowski, *Crash Test Evaluation of Eccentric Loader Guardrail Terminals.* Transportation Research Record 1065, TRB, National Research Council, Washington, D.C., 1986.

12. Meczkowski, L.C., *Evaluation of Improvements to Breakaway Cable Terminals*, Federal Highway Administration Report No. FHWA-RD-91-065, McLean, VA, 1991.

13. Sicking, D.L., A.B. Qureshy, and H.E. Ross, Jr., *Development of a Slotted-Rail Breakaway Cable Terminal*, Transportation Research Record 1233, TRB, National Research Council, Washington, D.C., 1989.

14. Mak, K.K., R.P. Bligh, and W.L. Menges, *Crash Testing and Evaluation of Existing Guardrail Systems*, Volume XI: Appendix J, Draft Report to the Federal Highway Administration, Contract No. DTFH61-89-C-00089 "Testing of State Roadside Safety Systems", December 1995.

15. Ross, H.E. Jr, Sicking, D.L., Zimmer, R.A., Michie, J.D., *NCHRP Report 350: Recommended Procedures for the Safety Performance Evaluation of Highway* Features, TRB,

National Research Council, Washington, D.C., 1993.

16. *Annual Book of ASTM Standards*, Vol. 3.01, Designation: E8, E8M, American Society for Testing and Materials, 1993.
17. *Mechanical Metallurgy*, Dieter, G.E., McGraw Hill, New York. 1976.
18. *Mechanical Engineering Design*, Fifth Edition, Shigle J.E., and Mischke, C.R., McGraw-Hill.
19. *HyperMesh Version 1.30 User's Manual*, Altair Computing Inc., Troy, Michigan.
20. *LS-DYNA3D User's Manual Keyword Format, Version 930*, User's Manual Livermore Software Technology Corporation, Livermore, California, USA.
21. *LS-TAURUS User's Manual*, Hallquist, J.O., Livermore Software Technology Corporation, Livermore, California, USA.
22. Hinch, J., Yang, T-L, and Owings, R., *Guidance Systems for Vehicle Testings*, ENSCO, Inc., Springfield, VA, 1986.
23. *Vehicle Damage Scale for Traffic Investigators*, Traffic Accident Data Project Technical Bulletin No. 1, National Safety Council, Chicago, IL, 1971.
24. *Collision Deformation Classification, Recommended Practice J224 March 1980*, SAE Handbook Vol. 4, Society of Automotive Engineers, Warrendale, Penn., 1985.

Appendix A

Calculations

W-Beam

Beam specifications

Cross sectional area (A) . . . . . 1300 mm^2

Material Thickness (t) . . . . . 2.67 mm (12 gauge)

Length (L) . . . . . 1676 mm

Moment of Inertia for the buckling plane (I) . . . . . 1 x 10^6 mm^4

Radius of Gyration (K) . . . . . 27.7 mm

End condition constant (C) . . . . . 1.2 for fixed-pinned end conditions

Modulus of Elasticity for steel (E) . . . . . 207 GPa

Yield Strength (S_y) . . . . . 405.5 MPa

In order to calculate the critical load for global buckling, one must determine both the critical slenderness ratio, and the slenderness ratio for the given configuration. The slenderness ratio is defined as the length of the member divided by its minimum radius of gyration. The critical slenderness ratio is given as:

$$\left(\frac{L}{K}\right)_{critical} = \sqrt{\frac{2\pi^2 CE}{S_Y}}$$

Substituting the above values results in the following:

$(L/K)_{critical} = 110.0$

$(L/K) = 60.4$

Since the slenderness ratio is less than the critical ration, the Johnson's formula for short column buckling was used. According to Johnson's equation, the critical buckling load (P_{cr}) is given by:

$$\frac{P_{CR}}{A} = S_Y - \left[\frac{S_Y L}{2\pi K}\right]^2 \frac{1}{CE}$$

Which results in a predicted buckling load 447 kN.

Another possible mode of failure is the compressive failure of the material. The load required for this type of failure is given by:

$$P_{cr} = A \times S_y$$

substituting the values of the area and the yield strength results in a critical load of 527 kN.

Compressive bearing failure of the guardrail at the bolt locations was thought to be another possible failure mode. This critical load is determined by the formula:

$$P_{cr} = S_y \times t \times d \times N$$

Where

d = Bolt Diameter

N = Number of bolts

This calculation results in a critical load for this member of 138 kN.

A fourth possible mode of failure for this member is local buckling. Theoretical predictions of local buckling from the empirical point of view have been accomplished for columns with various cross sections for the peak force, the mean force and the variation of the force as the column collapse progresses. Most of these studies dealt with square, rectangular or circular cross sections only and are not suitable for the W-beam or thrie beam shapes which we are dealing with.

Thrie Beam

Beam Specifications

Cross-sectional area (A) ..... 2600 mm^2

Material thickness (t) ..... 3.42 mm

Length (L) ..... 1676 mm

Moment of Inertia along the buckling Plane (I) ..... 2.0 x 10^6 mm^4

Radius of Gyration (K) ..... 27.7 mm

End condition constant © ..... 1.2 for fixed-pinned end conditions

Modulus of Elasticity for steel (E) ..... 207 GPa

Yield Strength (S_y) ..... 405.5 MPa

Similar calculations to those for the W-beam sections result in values for the critical slenderness ratio and slenderness ratio of:

$(L/K)_{critical} = 110.0$

$(L/K) = 60.4$

Since the slenderness ratio is less than the critical ration, the Johnson's formula for short column buckling was used. According to Johnson's equation, the critical buckling load (P_{cr}) is given by

$$\frac{P_{CR}}{A} = S_Y - [\frac{S_Y L}{2\pi K}]^2 \frac{1}{CE}$$

Which results in a predicted buckling load 895 kN.

Another possible mode of failure is the compressive failure of the material. The load required for this type of failure is given by:

$$P_{cr} = A \times S_y$$

substituting the values of the area and the yield strength results in a critical load of 1054 kN.

Compressive bearing failure of the guardrail at the bolt locations was thought to be another possible failure mode. This critical load is determined by the formula:

$$P_{cr} = S_y \times t \times d \times N$$

Where

d = Bolt Diameter

N = Number of bolts

This calculation results in a critical load for this member of 265 kN.

APPENDIX B

ACCELEROMETER DATA ANALYSIS - TEST KBCT-1

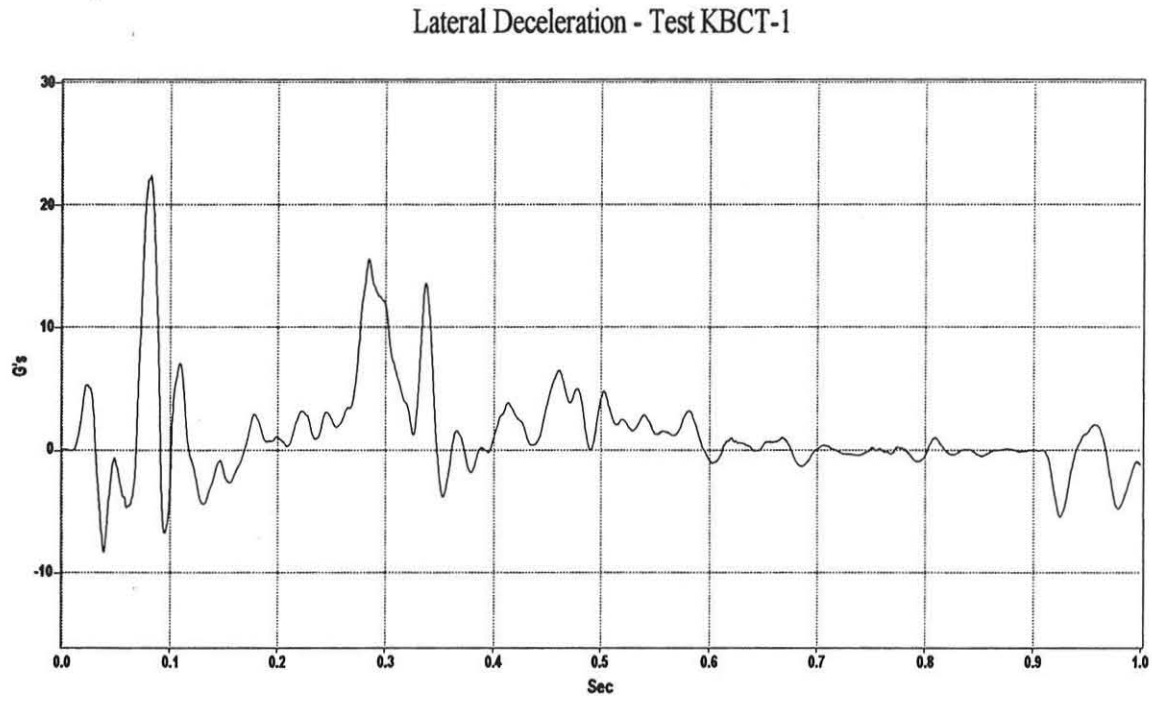

Figure B-1. Lateral Deceleration, Test KBCT-1.

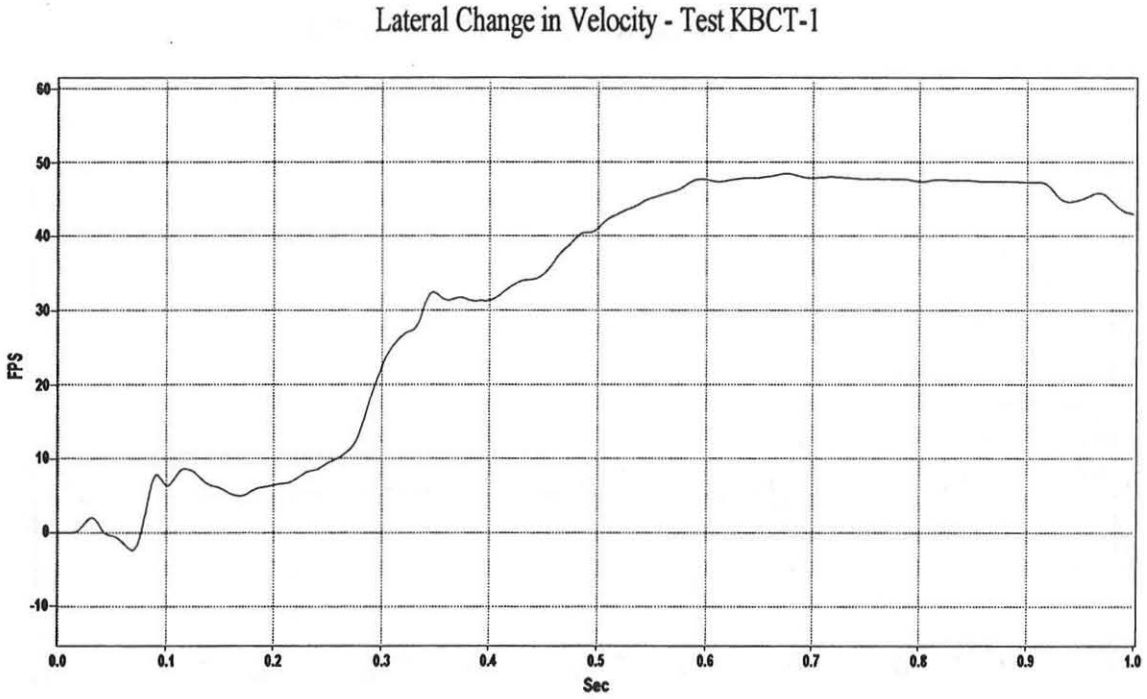

Figure B-2. Lateral Change in Velocity, Test KBCT-1.

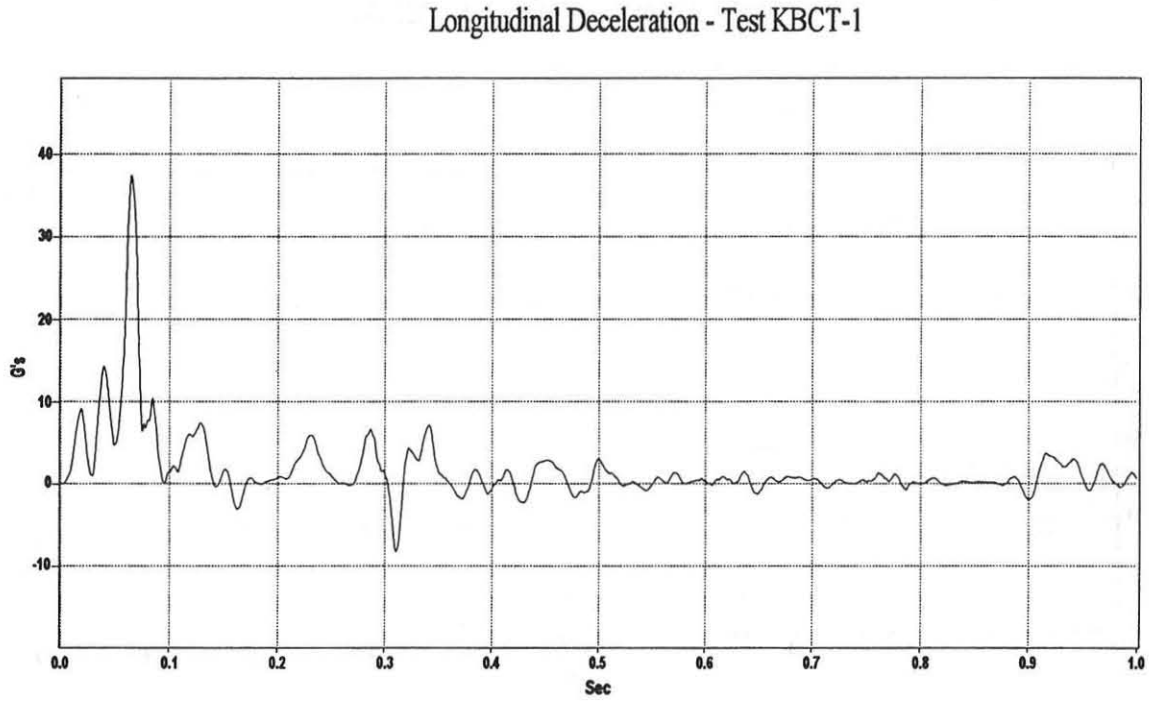

Figure B-3. Longitudinal Deceleration, Test KBCT-1.

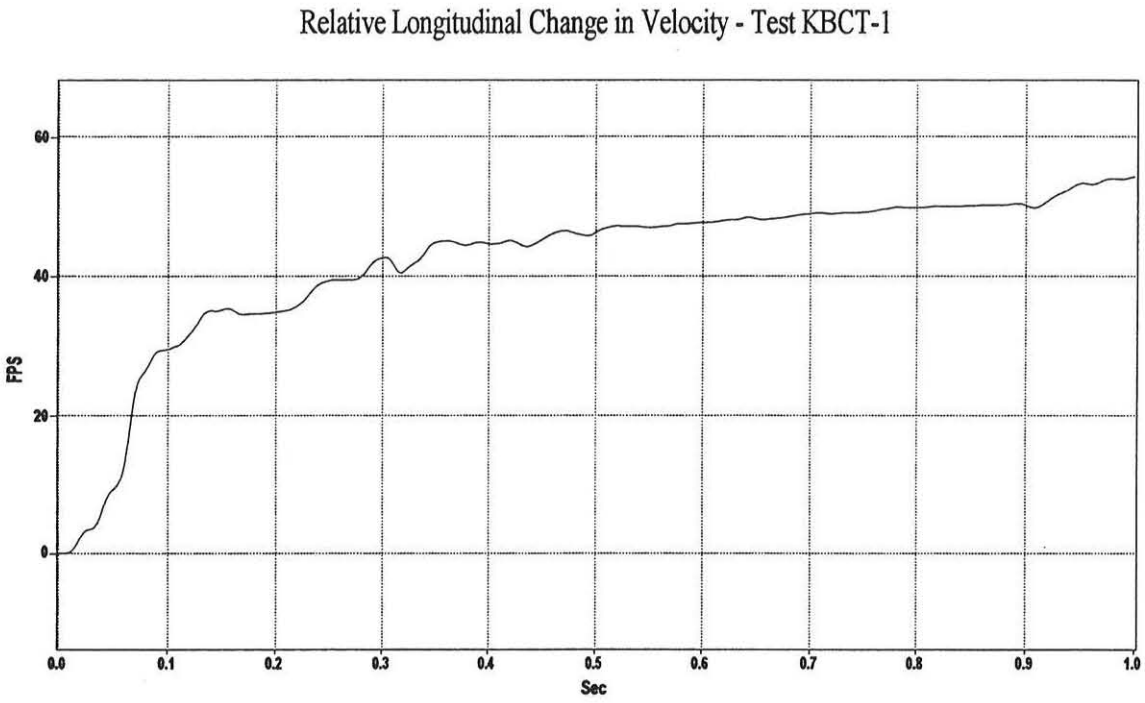

Figure B-4. Relative Longitudinal Change in Velocity, Test KBCT-1.